論文 / 著書情報
Article / Book Information

題目(和文)	
Title(English)	Study on magnetic porous hollow spheres with FePt netlike nanoshell
著者(和文)	渕上輝顕
Author(English)	Teruaki Fuchigami
出典(和文)	学位:博士(工学), 学位授与機関:東京工業大学, 報告番号:甲第9302号, 授与年月日:2013年9月25日, 学位の種別:課程博士, 審査員:北本 仁孝,和田 裕之,小田原 修,吉本 護,彌田 智一,松下 伸広
Citation(English)	Degree:Doctor (Engineering), Conferring organization: Tokyo Institute of Technology, Report number:甲第9302号, Conferred date:2013/9/25, Degree Type:Course doctor, Examiner:,,,,,
学位種別(和文)	博士論文
Type(English)	Doctoral Thesis

Study on magnetic porous hollow spheres with FePt netlike nanoshell

Teruaki Fuchigami

10D53328

Supervised by

Associate Professor Yoshitaka Kitamoto

Associate Professor Hiroyuki Wada

Department of Innovative and Engineered Materials

Tokyo Institute of Technology

September 2013

Contents

Chapter 1

Introduction

1.1 Development of magnetic particles and magnetic particles-assemblies

Magnetic particles have an attraction in biomedical and environmental applications because they show following unique properties by applying an external magnetic field. [1]

(1) Distribution and aggregation of magnetic particles can be controlled in solution.
(2) Magnetic particles can be transported by magnetic field gradient.
(3) Magnetic particles subjected to alternating magnetic fields generate heat.
(4) Magnetic particles generate magnetic fields by their magnetization.

These functions offer advanced technologies in biomedical and environmental fields. For example, an environmental pollutant and a target biomolecule can be recovered from contaminated solution by controlling distribution and aggregation of magnetic particles with some molecule which can adsorb specifically to the target molecule. Function (2) is used in magnetically guided drug delivery system (MG-DDS). Regarding (3), magnetic nanoparticles loaded with a medical agent can be accumulated to affected area by magnetic guidance. Magnetic hyperthermia has been studied as less-invasive therapy using the heat generation of the magnetic nanoparticles. Function (4) has been clinically used as a contrast agent in magnetic resonance imaging (MRI) already. Thus, the magnetic particles have been studied in various fields, and the control of their particle size, dispersibility and magnetic properties has been conducted.

Three-dimensional assemblies of magnetic nanoparticles may have advantages as compared with monodisperse magnetic nanoparticles for biomedical and environmental applications. For example, large surface area is required for improving molecular recognition in MG-DDS, magnetic separation and biosensor. The smaller the size of the magnetic particles, the specific surface area is increased. However, the magnetization response is reduced by decreasing particle size. Formula (1) expresses a force on magnetic nanoparticles given by external magnetic field. [1-3]

$$F_M = \frac{4}{3}\pi b^3 (M \cdot \nabla) H \quad (1)$$

Where b is the radius of the magnetic particles, M is magnetization of the magnetic particles and H is the applied magnetic fields strength. Magnetic particles in a solution under the magnetic field are attracted toward a magnet by the force F_M. The force decreases with decreasing particle size. Furthermore, the force needs to overcome a hydrodynamic drag force acting on the magnetic particle in flowing solution such as blood stream to transport the magnetic particles. Formula (2) expresses the hydrodynamic drag force F_D. [1-4]

$$F_D = 6\pi\eta b(V_f - V_p) \quad (2)$$

Where V_p is velocity of particles, V_f is that of the fluid and η is the viscosity of the fluid. In order to obtain high magnetic response with keeping a large surface area, three-dimensional assembly composed of magnetic nanoparticles of nanometer size is superior to monodisperse magnetic nanoparticles (Fig. 1.1). There are many kinds of structure in three-dimensional assembly. Figure 1.2 shows examples of the integrated structure and methods to fabricate them. In the form of magnetic nanoparticles-assembly, cluster structure simply made by aggregation of nanoparticles and a structure to form a magnetic shell by allowing accumulation of magnetic nanoparticles on the surface of template particles have been studied actively. In the latter structure, it is possible to make specific gravity close to water by using a material with a low density as a template particles or removing the template particles from the core-shell structure. Therefore, the core-shell structure with a magnetic shell has high versatility and utility. In addition, magnetic property can be combined to other functions such as optical and biological properties. For instance, Jin et al. obtained core-shell particles with magnetic property and optical property by using magnetic nanoparticles as a core particle and forming silica shell including fluorescent particle such as CdSe/ZnS and CdSeTe/CdS onto the magnetic core [5]. Furthermore, core-shell particle is applicable to DDS as a carrier for water-soluble drug because the water-soluble drug can be physically loaded to their hollow space formed by removing the template particles.

Thus, the composites and assemblies of particles have been studied to develop new functions and comprehensively superior properties and to create new materials. Especially, hollow structures using magnetic nanoparticles as a shell-material (magnetic capsule) have attracted attention in life science such as MG-DDS, magnetic separation

and biosensor because the magnetic capsules can load and release functional molecules and have a large surface area. In this thesis, I discuss fabrication and characteristics of magnetic hollow spheres with a nanosized porous shell from the viewpoint of its application to MG-DDS.

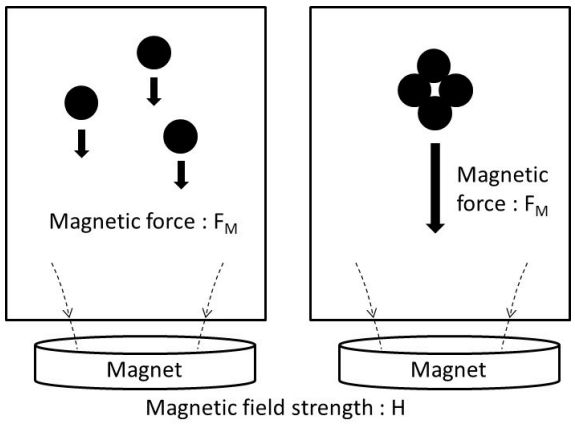

Figure 1.1 Magnetic attraction of magnetic nanoparticles in a solution

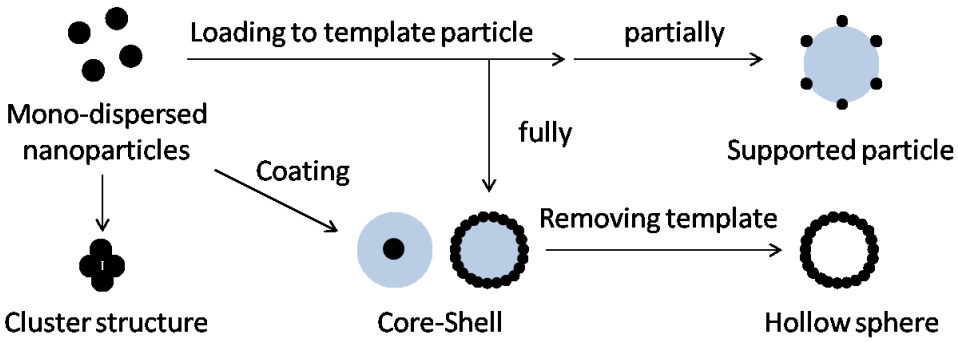

Figure 1.2 Structure and accumulation-method of nanoparticles-assembly

1.2 Magnetic capsule for magnetically guided drug delivery system

1.2.1 Feature and structure

Drug delivery systems (DDS) has been developed to control the accumulation of drugs at target lesions. In particular, for the treatment of cancer, the increment of the antitumor agent's concentration in tumor tissues without accumulation in normal tissues is important. However, it is difficult to control the delivery and release of drugs at tumor

sites by conventional passively targeted DDS. Actively targeted DDS has a potential to optimize therapeutic effects on tumors with both pinpoint precision and minimal invasion. Among such systems, the use of magnetic materials as the drug carrier is one of the most promising approaches because magnetic drug carriers can be attracted and manipulated by the gradient of external magnetic fields. Magnetic drug carriers injected into a blood vessel are accumulated in a diseased part by placing a permanent magnet near the part. There are two types of magnetic carrier. These are: 1) porous magnetic capsules filled with a drug and 2) magnetic particle(s) adsorbing the drug on the outside of the structure. Feature, superiority and problem of these drug carries are summarized in Table 1.1. The former method is superior to the latter as a method in terms of easy drug release along with the avoidance of any loss by elution in the bloodstream. This property is advantageous for the design of a DDS because the majority of intravenously injectable medicines are hydrophilic. Moreover, whereas it is relatively easy to encapsulate any kind of drugs in the hollow magnetic capsule through its porous wall, the latter method requires a complicated surface treatment of the magnetic particles in order to adsorb drugs to the surface.

Table 1.1 Feature, superiority and problem of drug carrier in MG-DDS

Carrier structure	Drug loading method	Feature and Problem
particle	Chemical adsorption	○It is easy to control carrier structure. △Complicated surface treatment is needed. ×Loss of drugs by elution in the blood stream
Porous hollow sphere	Concentration diffusion	△It is difficult to control carrier structure. ◎Any kind of drugs can be loaded.

Therefore, hollow magnetic capsules are more widely applicable as a magnetic carrier of therapeutic agents compared with solid magnetic particles. The following structure and properties are needed in magnetic capsules for MG-DDS targeted to deeply-placed cancer tumor.

(1) Whole diameter from several tens to 200 nm
(2) Nanosized thin shell
(3) Structure capable of loading and releasing drug agents
(4) Magnetic property which can be collected by magnetic field gradient
(5) Biocompatibility

(1), (2) Whole diameter and shell thickness

In nanoscale DDSs targeting cancer tissue, the size of the carrier is limited because small carriers (< 5 nm) are eliminated by renal excretion through the kidneys, and large size (> 200 nm) of foreign material are easily removed by the mononuclear phagocyte systems in the lungs, spleen and liver. Therefore, to avoid the elimination of carriers after intravenous administration, the total size of nanoscale drug capsules must be between several tens of nanometers and 200 nm [6-9]. Large space for medicine in capsules is required to increase the efficiency of delivery under the size limitation discussed above. The loading capacity for medicine was calculated from their whole diameter and shell thickness. Table 1.2 shows the volume ratio of hollow sphere for medicine to the volume of the whole capsule with various whole diameter and shell thickness. When using a magnetic capsule with a diameter of 100 nm and a shell thickness of 20 nm, the loading capacity for therapeutic agents is limited to only 22% of the capsule volume. Therefore, a thinner shell is required to increase the loading capacity for biomedical agents and to decrease the amount of magnetic components administered to human bodies under the size limitations applicable to nano-DDSs.

Table 1.2 Volume ratio of medicine in capsules with various whole diameter and shell thickness

Whole diameter / nm	Shell thickness / nm	Volume ratio of medicine / %
300	20	65
300	5	90
100	20	22
100	5	73

(3) Structure capable of loading and releasing drug agents

Porous structure is a famous as a structure which can load and release drug agent. As described above, drug agents can be loaded to hollow space through the pores by concentration diffusion. The control of the pore size is important to transport various drug agents such as anticancer drugs and nucleic acid medicine. Molecular mass of low molecular drugs is about 500, and that of large molecular drugs such as nucleic acid medicine is about 5,000-15,000. Considering a motion of the molecules, these pore size should be over 5 nm.

(4), (5) Magnetic property and biocompatibility

As described in Section 1.1, magnetic particles in flowing solution under magnetic fields are attracted toward a magnet by the force F_M, and the magnetic particles in the fluid are subjected to drag force F_D. In my strategy for MG-DDS, magnetic porous hollow spheres injected into a blood vessel are accumulated in the diseased part by placing a magnet near the part. Therefore, high magnetization required to be accumulated to the diseased part in a blood stream will be needed. Nishijima and Mishima reported the conditions of the magnetic field required for accumulation and navigation of magnetic particles in a blood capillary in an organ which is located deep in the body (25-50 mm). [2] They showed that magnetic field gradient should be 0.4 T/m in a fluid (flow velocity: 1mm/s) for the accumulation of magnetic particles which have 100 nm in size and 446 emu/cm^3 in saturation magnetization. High magnetic field gradient and magnetization are needed for the accumulation of magnetic particles. The volume of the magnetic shell (in other words, shell thickness) should be small in order to increase the loading capacity and decrease the amount of magnetic components administered to human bodies. Since the magnetic shell is a three-dimensional assembly of magnetic nanoparticles, the magnetic nanoparticles that consist of the shell should be small to satisfy the requirement regarding the loading capacity. Therefore, magnetic material which shows high magnetic response is required although the nanoparticles are in the nanometer range.

Iron oxides are often used for biomedical applications due to their high biocompatibility. Iron oxide particles have already clinically used as a contrast agent for MRI. Therefore, iron oxides were used in most of works related to magnetic hollow spheres. [10-16] The size of Fe_3O_4 nanoparticles forming the magnetic shell is required to be 20 nm so as to be magnetically directed by a rare-earth permanent magnet such as a NdFeB magnet, considering the magnetocrystalline anisotropy constant of Fe_3O_4 (~10^4 J m^{-3}). If a magnetic material with a magnetocrystalline anisotropy constant higher than that of Fe_3O_4 is applicable, the shell thickness and/or the nanoparticle size will be reduced without any inappropriate deterioration of the magnetic response. I summarized magnetocrystalline anisotropy, compatibility for human body and saturation magnetization of magnetic materials in Table 1.3. [17-25] FePt alloy and Co are suitable to make the nanosized thin shell because of their magnetocrystalline anisotropy higher than that of iron oxides. Additionally, their high chemical stability is interested in biomedical applications. However, Co is a material to cause metal allergy, so it should not be used for the material applying to human body. FePt is also a material to cause metal allergy originating in Pt, but it is relatively safe among the materials that cause metal allergy. I think it is possible to suppress the problem of metal allergy by reducing injected

quantity of the magnetic material. Therefore, I have focused on FePt alloy as a material for fabricating magnetic porous hollow spheres with the nanosized thin shell and high magnetic response in this thesis, and I have tried to construct a technology for fabricating the nanosized shell structure.

Table 1.3 Magnetocrystalline anisotropy, compatibility for human body and saturation magnetization of magnetic materials [17-25]

Material	M_s (emu/cm^3)	Magnetocrystalline anisotropy (kJ/m^3)	Compatibility for human body
Magnetite	446	9	○
Maghemite	414	4.7	○
fcc-FePt	-	206	△
fct-FePt	1140	7000	△
Co	1400	450	×
FeCo	1790	1.5	×

1.2.2 Ideal magnetic porous hollow spheres and reported magnetic capsule

Many kinds of magnetic capsule have been reported for various applications. I summarized the reported magnetic hollow spheres and compared them with ideal magnetic hollow spheres designed for MG-DDS in Table 1.4. Whole diameter was set considering elimination mechanism in a human body, and shell thickness was set considering loading capacity of drug agents. Magnetic property was evaluated based on the previously reported magnetite nanoparticles, which have 100 nm in size and 446 emu/cm^3. [2] Until now, there are no approaches to obtain the nanosized magnetic shell with high magnetic response considering loading capacity of drug agents and to obtain large pores for loading sterically-bulky substance such as nucleic acid medicine. Therefore, magnetic hollow spheres with the nanosized shell and large pores have not been reported. Porous hollow spheres with high magnetic response have been reported, but their shell thickness was too large to obtain high loading capacity of drugs. [15] Shell thickness can be tuned by decreasing accumulation amount of magnetic nanoparticles, but the magnetization will be decrease. A nanosized magnetic shell with high magnetic response have been reported by Katagiri et al., but the large pore (> 5 nm) was not obtained because they considered to load low molecular weight drug agents. [11] In this thesis, novel approach is proposed to obtain ideal porous hollow spheres designed for MG-DDS.

Table 1.4 Reported magnetic hollow spheres and their suitability for MG-DDS

Shell Material	Shell thickness (nm)	Whole diameter (nm)	Magnetic guidance	Pore size (nm)
Ideal porous hollow spheres	< 10	~ 200	233×10^{-5} (emu)	> 5
Fe_3O_4/silica [10]	×	×	×	-
Fe_3O_4/polymer [11]	○	×	Δ	-
NiZn-ferrite [12]	Δ	○	-	-
Fe_3O_4/silica [13]	○	×	×	○
Fe_3O_4 [14]	×	×	○	-
Fe_3O_4 [15]	×	×	○	Δ
Co-ferrite/SiO_2 [16]	×	×	○	-
$ZnFe_2O_4$ [26]	×	×	-	Δ
FePt [27]	Δ	Δ	-	○
$CoFe_2O_4$-Co_3O_4 [28]	×	×	Δ	○
Fe_3O_4 [29]	×	○	○	Δ

1.3 Magnetic capsule and Core-Shell particle

1.3.1 Fabrication strategy of magnetic capsule

So far, a number of approaches have been reported on the fabrication of magnetic capsules such as solvothermal route [30], reverse microemulsion method [31] and the most commonly employed template removal method [32-34]. In a typical sacrificial template step, the micro- or nano-structure hollow spheres can be obtained via depositing nanoparticles on the monodisperse template particles such as polymeric sphere, carbon sphere and silica sphere by controlled surface precipitation or direct surface reactions followed by selective removal of the template by thermal or chemical routes. Using template particles for fabricating capsular structure, it is easy to control the size of capsules by control of the size of template particles. In my research, control of the capsular size is extremely important as described above. Therefore, I focus on the template removal method for fabricating FePt porous hollow spheres.

Stability of the shell structure after removing the template particles is often problem. To obtain a stable shell, thermal fusion of magnetic nanoparticles or accumulation of magnetic nanoparticles onto polymer-multi-layer film are used [11, 26, 27]. Yong Lim

Foo et al. have fabricated FePt-nanoparticles/polymer/silica core-shell particles by reducing Fe and Pt precursors in the presence of silica template particles modified with a polymer-double layer composed of cationic polyelectrolyte, poly(ethyleneimine) (PEI) and anionic polyelectrolyte, poly(acrylic acid) (PAA). Then, they fabricated FePt hollow spheres by the calcination of FePt-nanoparticle/PAA/PEI/silica composite particles and dissolution of silica template particles. After the calcination, the crystallite size of FePt nanoparticles was increased and the magnetic property was improved. However, the size of FePt nanoparticles was also increased from ~15 nm to ~25 nm by a fusion of FePt nanoparticles. The calcination process is significantly important to obtain stable structure after removing template particles and high magnetization, but the calcination process makes the particle size large. It will induce an increase of shell thickness. The thickness of shell (particles size) fabricated by thermal fusion of magnetic nanoparticles are strongly related to thermal treatment conditions, accumulation density and size of magnetic nanoparticles. Therefore, these factors should be controlled to obtain the nanosized magnetic shell with large pores.

Then in another way, Katagiri et al. obtained a core-shell structure composed of Fe_3O_4 nanoparticles and melamin-formaldehyde spheres modified with a polymer-multilayer film of poly(allylamine hydrochloride) and Poly(sodium-p-styrenesulfonate) by deposition of Fe_3O_4 nanoparticles using Pd as a catalyst, then, they obtained Fe_3O_4 capsules by removing only the melamin-formaldehyde sphere using hydrochloric acid. In a hybrid shell composed of magnetic nanoparticles and polymer layer, shell thickness depends on the size of magnetic nanoparticles. Therefore, the shell thickness can be tuned by accumulation density of magnetic nanoparticles. The magnetic shell is stabilized by the polymer-multilayer film, but the hybrid shell composed of magnetic nanoparticles and polymer-multilayer will block loading sterically-bulky substance to hollow space and releasing of sterically-bulky substance from internal space if the shell structure is densely packed. Thus, the accumulation density of magnetic nanoparticles and polymer in the hybrid shell should be controlled to obtain porous hollow spheres as a carrier for sterically-bulky drug.

As described above, the shell thickness is strongly related to the accumulation density of magnetic nanoparticles in the magnetic shell. Therefore, first of all, it is necessary to fabricate the designed shell structure that a single-layer of magnetic nanoparticles is uniformly deposited onto a surface of template particles, and the accumulation density of nanoparticles onto the template particles must be controlled.

1.3.2 Fabrication strategy of core-shell particle

Composites made by accumulation of magnetic nanoparticles onto the template particles have been reported so far. There are two ways to accumulate magnetic nanoparticles onto the template particles. One is adsorption of monodisperse nanoparticles on the surface of the template particles and the other is growth of nanoparticles on the template particles. There are two ways to absorb nanoparticles on the template as follows: (1) aggregation of nanoparticles by electrostatic interaction between particles and (2) binding between nanoparticles and template particles with some molecules which can be bond to nanoparticles and the surface of the template. V. Salgueirino-Maceira et al. obtained a core/shell silica/FePt sphere by electrostatic adsorption of monodisperse FePt nanoparticles onto polymer layers on the surface of silica particles [35]. Jinwoo Cheon et al. integrated silica particles modified with an amino group and monodisperse Fe_3O_4 particles modified with a thiol group using sulfosuccinimidyl-(4-N-maleimidomethyl)cyclohexane-1-carboxylate as a binding molecule [36]. In these methods, it is difficult to accumulate nanoparticles with a high density on the surface of core particles because the nanoparticles are well dispersed by electrostatic interaction or coating with dispersant. When these nanoparticles accumulate on the surface of core particles, additional accumulation of nanoparticles is blocked by primarily accumulated nanoparticles because of the electrostatic repulsion and/or steric effects of capping agents.

Generally, the growth of nanoparticles occurs though a process shown in Fig. 1.3. Firstly, metal atoms are supplied by reduction of metal ion or decomposition from metal precursor, then the nucleation of nanoparticles occurs when the concentration of metal atoms exceeds a specific value. Nanoparticles grow up by supply of metal ions or atoms to the nuclei. The atom concentration in the solution during the growth of particles changes with time as shown in Fig. 1.3. The atom concentration increases without the nucleation, and then the concentration decreases from nucleation period to particles growth period. If the atom concentration increases uniformly in the solution, the nucleation can occur all over the solution. This nucleation is called homogeneous nucleation. On the other hand, it is also possible to make nucleation in specific area in the solution by adding impurities which can be nucleation site or raising the metal salt concentration locally in the solution. This nucleation is called heterogeneous nucleation, and electrostatic interaction and coordinate interaction are used to obtain heterogeneous nucleation. For example, when making the nanoparticles by reducing metal ions, polymer as a dispersant in the solution forms coordination bond with the metal ions, and the metal ions are condensed around the polymer (Fig. 1.4). Finally, the nucleation occurs selectively around the polymer. Jun

Ren et al. accumulated Fe or Mn metal cation onto polystyrene (PS) particles via carboxyl groups on the PS surface by electrostatic interaction, and then, they obtained core-shell structure by reducing of the metal cations near the surface of the PS particles [37]. In such method, nanoparticles can be accumulated with a high density on the core particles compared with the adsorption process. It is significantly important to prepare nucleation sites on the core particles for the uniform accumulation of the nanoparticles with high density.

In this thesis, I have tried to accumulate FePt nanoparticles by growing FePt nanoparticles on the surface of template particles in order to the uniform accumulation of the nanoparticles with high density and control the accumulation density.

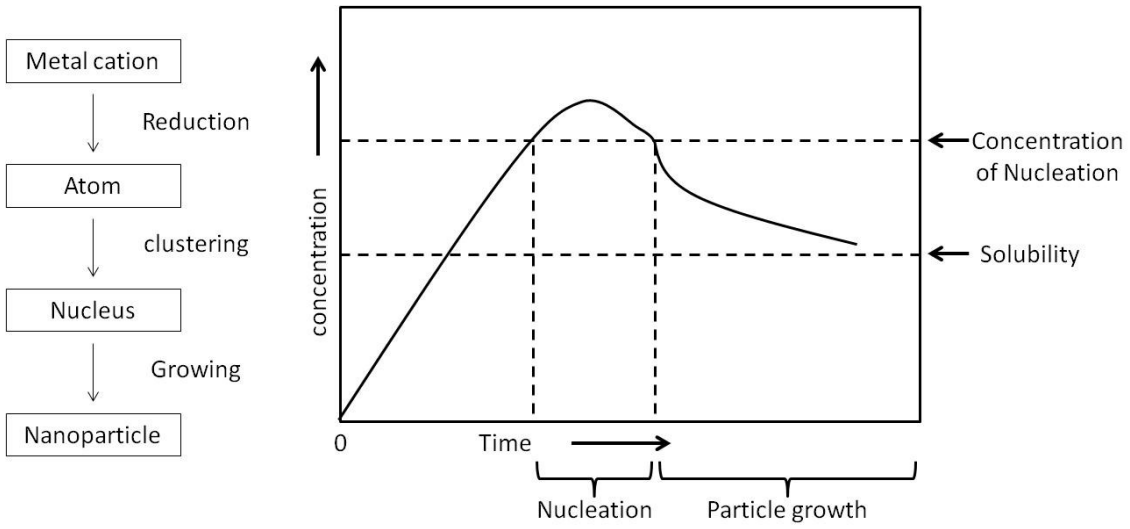

Figure 1.3 Formation-process of metal nanoparticles and temporal change of solute concentration in liquid phase

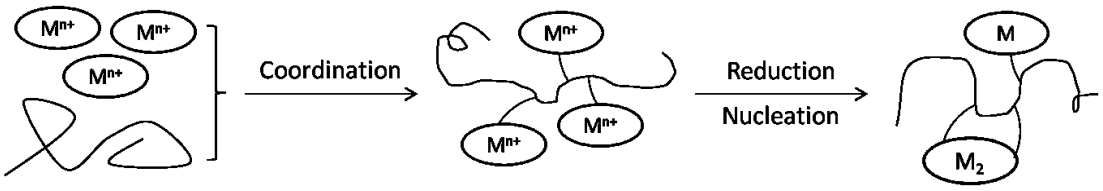

Figure 1.4 Formation scheme of metal-polymer complex

1.4 Objectives, motivation and outline of thesis

The most important aim of this study is to establish a fabrication method of magnetic porous hollow spheres with the nanosized thin shell and high magnetic response.

I propose two types of porous hollow sphere composed of FePt alloy. [38, 39] Figure 1.5 shows a fabrication scheme of the porous hollow spheres. Firstly, negatively charged silica template particles are modified with a single polymer layer of cationic polyelectrolyte. FePt nanoparticles are accumulated onto the polymer-modified silica template particles by reducing Fe and Pt precursors, obtaining FePt-nanoparticle/polymer/silica core-shell particles. FePt-nanoparticle/polymer hybrid capsules can be obtained by dissolving silica template particles from FePt-nanoparticle/polymer/silica core-shell particles. Using template particles, whole diameter of the hollow spheres can be tuned. Pore size and shell thickness of the hybrid shell mostly depend on morphologies of the nanoparticle assembly such as the size and the density of the accumulated FePt nanoparticles on the polymer layer; nanosized thin shell and large pores can be obtained by decreasing the size and the density. However, stability of the hollow spheres may also depend on the morphologies of the accumulated FePt nanoparticles and polymer layer. Thus, I have tried to accumulate FePt nanoparticles onto various kinds of polymer layer and controlled the accumulation density of FePt nanoparticles in order to investigate an interaction between accumulated FePt nanoparticles and the hybrid structure by controlling an accumulation density of FePt nanoparticles onto polymer-layer.

As the second type of porous hollow structure, I fabricate an FePt netlike nanoshell by thermal treatment of FePt-nanoparticle/polymer/silica core-shell particles in supercritical fluid. In the supercritical fluid treatment, adjacent FePt nanoparticles are fused in the plane of the assembly on the template particles. As a result, the netlike structure composed of FePt alloy is obtained. The shell thickness is equal to the size of the FePt nanoparticles of FePt-nanoparticle/polymer/silica core-shell particles because the sintering of FePt nanoparticles is progressed preferentially in the plane direction, not in the thickness direction. A lot of factors such as accumulation density, size of FePt nanoparticles on the template particles and thermal-treatment conditions (temperature, pressure and time) will affect the structure of netlike nanoshell. Especially, the accumulation density of FePt nanoparticles will strongly related to the structure such as shell thickness and pore size. It is necessary to evaluate accumulation density required to obtain stable nanosized thin shell with large pores. In two types of porous hollow sphere, the accumulation density of FePt nanoparticles was controlled to porous hollow spheres. In thermal treatment, various conditions were examined to fabricate porous hollow spheres with the nanosized thin

shell and high magnetic response, and the formation mechanism of netlike structure was proposed.

In this thesis, I list two important points to be discussed as follows; 1) controlled accumulation of FePt nanoparticles onto polymer layer on the silica template particles and 2) formation of porous hollow spheres composed of FePt netlike nanoshell based on thermal fusion by supercritical fluid treatment. First, FePt-nanoparticles/polymer/silica core-shell particles are fabricated in various conditions, and the accumulation of FePt nanoparticles onto polymer layer are discussed in Chapter 2. Secondly, porous hollow spheres with FePt netlike nanoshell are fabricated by thermal treatment of FePt-nanoparticles/polymer/silica core-shell particles, and morphological microstructure, physical properties, and formation mechanism of the porous hollow spheres with FePt netlike nanoshell are discussed in Chapter 3. Application of the porous hollow spheres with netlike nanoshell to MG-DDS is demonstrated in Chapter 4. General conclusion is described in Chapter 5.

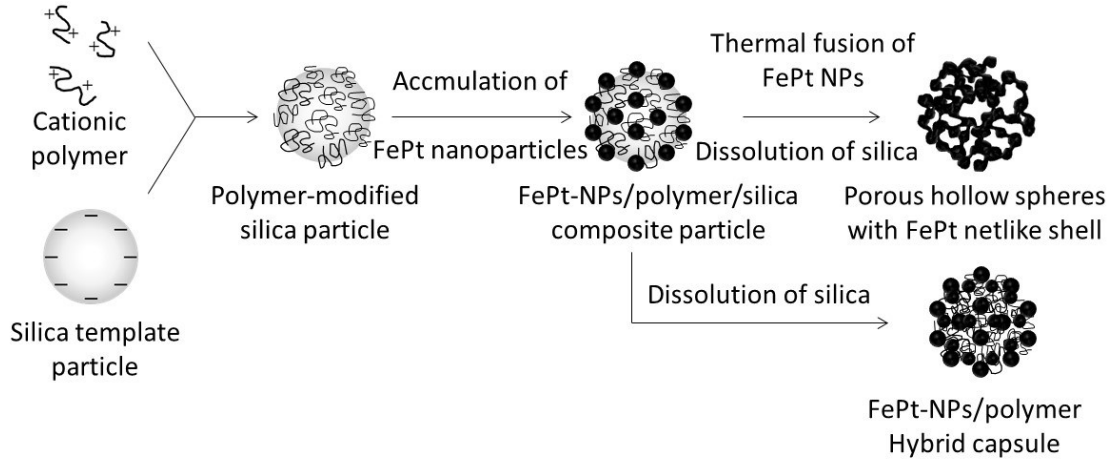

Figure 1.5 Fabrication scheme and TEM images of FePt-NPs/Polymer hybrid capsule and porous hollow spheres with FePt netlike shell [38, 39]

Reference

[1] Pankhurst, Q. A.; Connolly, J.; Jones, S. K.; Dobson, J J. Phys. D: Appl. Phys. 2003, 36, 167–180.
[2] S. Nishijima and F. Mishima, Magnetics Jpn. Vol. 4, No. 11, 2009
[3] J. Dobson, Drug. Dev. Res., 67:55-60 (2006)
[4] Y. Hirota et al., Physica C, 469, 2009, 1853–1856
[5] Q. Ma et al., Biomaterials, 33, 2012, 8486-8494
[6] K. Miyata et al., React Funct Polym 71, 2011, 227-34
[7] M. Yokoyama et al., J. Control Release, 55, 1998, 219-29
[8] N. Nishiyama et al., Drug Discov Today, 2, 2005, 21-26
[9] DC. Litzinger., Biochim Biophys Acta, 1190, 1994, 99-107
[10] Lu, Z.; Qin, Y.; Fang, J.; Sun, J.; Li, J.; Liu, F.; Yang, W. Nanotechnology 2008, 19, 055602–055606.
[11] K. Kumoto et al., J. colloid and Inter. Sci., 341, 2010, 64-68
[12] Abe, M.; Nishio, N.; Hatakeyama, M.; Hanyu, N.; Tanaka, T.;Tada, M.; Nakagawa, T.; Sandhu, A.; Handa, H. J. Magn. Magn. Mater.2009, 321, 645–649.
[13] Liu, J.; Deng, Y.; Liu, C.; Sun, Z.; Zhao, D. J. Colloid Interface Sci. 2009, 333, 329–334.
[14] Shen, S.; Wu, W.; Guo, K.; Meng, H.; Chen, J. Colloids Surf., A 2007, 311, 99–105.
[15] Xia, H.; Foo, P.; Yi, J. Chem. Mater. 2009, 21, 2442–2451.
[16] Wang, C.; Chen, I.; Lin, C. J. Magn. Magn. Mater. 2006, 304, 451–453.
[17] E.Nesbitt et al., Appl Phys.Lett. 1968, 11, 12
[18] K. Inomata, T. Sawa, S. Hashimoto, J. Appl. Phys., 1988, 64, 2537
[19] R. E. Rosensweig, J. Magn. Magn. Mater., 2002, 252, 370
[20] R. C. O'Handley, Modern Magnetic Materials., New York: Wiley, 2000
[21] R. V. Major, V. Mehrotra, M. W. Russell, E. P. Giannelis, R. D. McMicheal, R. D. Shull, R. F. Ziolo, J. Appl. Phys., 1993, 73, 5109
[22] R. V. Major, C. M. Orrock, IEEE Trans. Magn., 1988, 24, 1856
[23] R. Kuentzler, Phys. Stat. Sol. B, 1973, 58, 519
[24] G. Hausch, J. Magn. Magn. Mater., 1990, 92, 87
[25] D. Weller, A. Moser, L. Folks, M. E. Best, W. Lee, M. F. Toney, M. Schwickert, J. U. Thiele, M.F. Doener, IEEE Trans. Magn., 2000, 36, 10
[26] D. Wang et al., J. Phys. Chem. C, 2009, 113, 2792-2797
[27] J. Wang et al., Chem. Mater. 2007, 19, 2566-2572

[28] Zhang C, Zhang H, Du B, Hou R, Guo S. J Colloid Interface Sci 2012; 368:97-106
[29] J. Yuan, X. Zhang and H. Qian, J. MMM, 322, 2010, 2172–2176
[30] L.P. Zhu et al., Cryst. Growth, Des. 8, 2008, 957
[31] D. Zhang et al., Mater. Lett. 62, 2008, 4053
[32] X.W. Lou et al., Adv. Mater., 20, 2008, 1
[33] F. Caruso et al., Science, 282, 1998, 1111
[34] S. Ding et al., Polymer, 47, 2006, 8360
[35] V. Salgueirino-Maceira et al., small 2005, 1, 11, 1073-1076
[36] J. Lee et al., Angew. Chem., 2006, 118, 8340-8342
[37] J. Ren et al., Thin Solid Films, 515, 2006, 2555-2561
[38] T. Fuchigami, et.al. Langmuir 2011, 27, 2923-2928
[39] T. Fuchigami et al., Biomaterials, 33, 2012, 1682-1687

Chapter 2

FePt-nanoparticle/polymer/silica core-shell particle

2.1 Introduction

To prepare FePt nanoparticles, polyol processes [1-7] are extensively used. I fabricated FePt nanoparticles by an improved polyol process. The use of diol or polyalcohol (polyol) to reduce and/or decompose metallic salts to metallic particles referred to as the polyol process [1]. The polyol acts first as a solvent for precursors. Then the metal salts are reduced by the polyol, and the polyol are oxidized. In ethylene glycol, for instance, a duplicative oxidation of acetaldehyde that is produced by dehydration of ethylene glycol occurrs with the reduction of metal ions. To take a direct synthesis of FePt nanoparticles with the chemically ordered phase, the reduction temperature must be very high since a heat treatment over 823 K is required for the phase-transformation from fcc structure to fct structure in the case of FePt nanoparticles [1]. In this study, I used a tetraethylene glycol (TEG) as a polyol because it has a high boiling point (600 K).

Figure 2.1 shows the fabrication strategy of FePt core-shell particles and the structure of Fe and Pt precursors used in this study. Silica spherical particles are used as a core particle because silica particles have high thermal stability and they can be easily dissolved in an aqueous solution such as aqueous sodium hydroxide and ammonia solution. Acetylacetonate complexes are used as metallic precursors which are solved in an organic solvent. To accumulate FePt nanoparticles onto silica particles, FePt nanoparticles are synthesized in the presence of polymer-modified silica particles by the polyol process.

In my previous report, FePt nanoparticles were accumulated uniformly onto PDDA-modified silica particles with high deposition density, and FePt-nanoparticle/PDDA/silica core-shell particles were obtained [8]. There are two ways to accumulate metal nanoparticles onto polymer molecules. One is the adsorption of metal nanoparticles to polymer molecules with chemical or physical bonds after growing of metal nanoparticles in a solution. The other is growing of metal nanoparticles on the polymer. Figure 2.2 shows schematic illustrations of accumulation of metal nanoparticles onto the polymer layer that modifies the silica particle. In this chapter, I demonstrated FePt-nanoparticle/polymer/silica core-shell particles fabricated with five types of polymers, which are anionic polyelectrolyte poly(acrylic acid sodium salt) (PAA), non-electrolyte

poly(N-vinyl-2-pyrrolidone) (PVP), non-electrolyte poly(vinyl alcohol) (PVA), and cationic polyelectrolyte poly(ethyleneimine) (PEI) and PDDA. I discuss crystal structures and magnetic properties of FePt-nanoparticles/polymer/silica composites for investigating effects of polymer on the growth of FePt nanoparticles. In addition, I fabricated FePt-nanoparticle/PDDA/silica core-shell particles by changing ratio of Fe to Pt precursor in the synthesis to investigate the accumulation and growth of FePt nanoparticles on PDDA-modified silica particles.

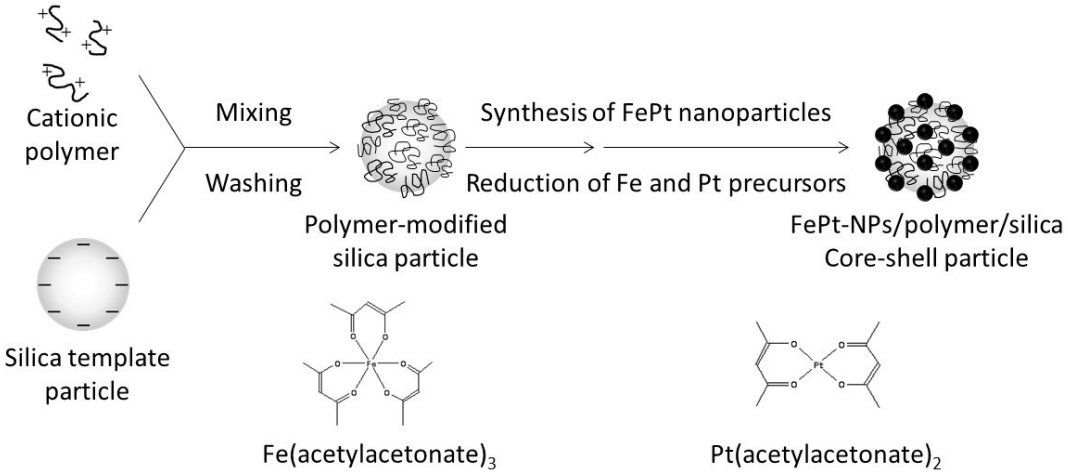

Figure 2.1 Fabrication scheme of FePt-nanoparticle/polymer/silica core-shell particle and structure of Fe and Pt precursors

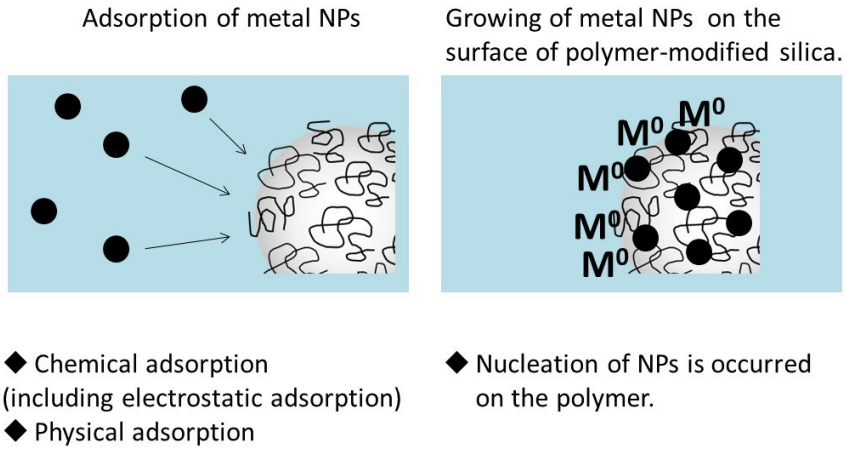

Figure 2.2 Schematic illustrations of accumulation of metal nanoparticles onto polymer layer

2.2 Experimental

To modify silica template particles with a polymer, an aqueous dispersion (5 mL) of amorphous silica particles (80 mg, Nippon Shokubai, KE-P30, average diameter = 0.32μm) was mixed with 7 wt.% of an aqueous solution (24 mL) of each polymer. I have tried to accumulate FePt nanoparticles onto the silica particles treated with 1 wt.% of polymer solution, but the polymer-modified silica particles were not uniformly and densely covered with FePt nanoparticles. Therefore, I tried to fabricate the FePt-nanoparticle/polymer/silica composite particles with silica template particles treated with higher concentration of polymer solution. This mixture was stirred for 10 min at 298 K in an ultrasonic bath. Excess polymer molecules were removed by washing three times by means of centrifugation with deionzed water, removal of supernatant, and redispersion using an ultrasoic bath. In addition, unmodified silica particles were also used as template particles of the composite particles. Polymer-modified silica template particles (mass of adding silica particles: 40 mg) were dispersed in tetraethylene glycol (TEG) (50 mL) after solvent exchange by dehydration at 353 K under vacuum. Then FePt nanoparticles were synthesized through the following polyol method. A mixture of Fe (III) acetylacetonate ($Fe(acac)_3$) (0.21 mmol, 75 mg), Pt (II) acetylacetonate ($Pt(acac)_2$) (0.19mmol, 76mg), silica template particles (40mg), and TEG (50 mL) was placed in a 100 mL three-necked, round-bottom flask. The reaction flask was placed on a mantle heater. The mixture was stirred for 24 hours and then heated with stirring from 300 K at a heating rate of 10 K min^{-1} and kept at 503 or 533 K by refluxing for 2 hours in an inert gas (Ar/H_2). Fe (III) acetylacetonate and Pt (II) acetylacetonate as metallic precursors were reduced in TEG as a reducing reagent. After the reaction, the solution was allowed to cool to room temperature. The composite silica particles were precipitated by centrifugation. After discarding the light yellow supernatant, the precipitate was washed several times with ethanol. The composite silica particles were obtained by centrifuging and drying in air at 333 K as powder samples.

Properties of FePt-nanoparticle/polymer/silica core-shell particles were investigated in the following methods. The structure and morphology were investigated by powder x-ray diffraction (XRD) and transmission electron microscopy (TEM). The elemental composition measurement of FePt alloy was carried out by an inductively coupled plasma (ICP) atomic emission spectrometer. Electron excitation in metallic complex was analyzed by ultraviolet-visible (UV-vis) spectroscopy. Gravimetric change of the composite particles was examined by a thermogravimetric (TG) analysis and chemical reaction in a thermal treatment was examined by a differential thermal analysis (DTA).

Fourier transform infrared (FT-IR) spectroscopy was conducted to investigate the interaction between ligands and nanoparticles. Zeta potentials of polymer-modified silica particles and unmodified silica particles were measured using a zetasizer nano (Malvern) **and a nano Partica (Horiba)**. Magnetic properties were measured by a physical property measurement system (Quantum Design Corp. PPMS).

2.3 Dependence on species of polymer

Figure 2.3 shows the structure of the polymer used in this study. Adsorption of polymers on the surface of silica template particles was confirmed from their zeta potentials. The charge of the silica particle was changed after polymer-modification as shown Table 2.1. Anionic polyelectrolyte such as PAA could not be directly adsorbed onto the surface of silica particles by electrostatic repulsion between the polymer and silica particles. Therefore, silica particles were modified with cationic polyelectrolyte, PDDA, before modification of anionic polyelectrolyte.

FePt nanoparticles were synthesized at 503 K in the presence of polymer-modified silica particles with an average diameter of 320 nm. Figure 2.4 shows TEM images of FePt nanoparticles synthesized in the presence of unmodified silica particles. FePt nanoparticles were accumulated on silica particles, but the silica particles were not entirely covered with FePt nanoparticles and coagulated FePt nanoparticles that were not adsorbed on silica particles were observed. These results suggested FePt nanoparticles were grown in TEG solution, then adsorbed onto the surface of unmodified silica particles.

Figure 2.5 shows TEM images of FePt nanoparticles synthesized on five types of silica template particles, which were PDDA-modified silica particles, PEI-modified silica particles, PVP-modified silica particles, PVA-modified silica particles and PAA/PDDA-modified silica particles. These polymer-modified silica particles were entirely covered with FePt nanoparticles as shown in Fig. 2.5 although the surface charge depends on the species of polymer as shown in Table 2.1. These results suggest that the accumulation of FePt nanoparticles and polymers on the surface of silica particles was not elicited by electrostatic adsorption. Zeta potential of FePt nanoparticles synthesized without polymer and silica particles was about -40 mV. Since the polarity of polymer-modified silica template particles did not influence the morphology of accumulation of FePt nanoparticles on them, electrostatic interaction was not probably the main reason of the accumulation. Therefore, FePt nanoparticles were probably grown on the polymer layer. Accumulation of FePt nanoparticles onto PDDA- or PEI-modified silica particles was more uniform than the others. Figure 2.6 shows XRD patterns of the FePt-nanoparticle/silica composite particles and the FePt-nanoparticle/polymer/silica core-

shell particles. Whereas 111 diffraction peak with the strongest intensity at 2 $\theta = 41^{\circ}$ and diffraction peaks at 2 $\theta = 24^{\circ}$ and 33° are observed for an ordered-alloy fct (face-centered tetragonal) FePt, 111 diffraction peak with the strongest intensity at 2 $\theta = 40^{\circ}$ is observed without diffraction peaks at 2 $\theta = 24^{\circ}$ and 33° for a disordered-alloy fcc (face-centered cubic) FePt; the 111 diffraction peak shifts from 40° to 41° with the increase of the ordered-alloy phase [9]. The six types of the composite particles containing FePt nanoparticles and silica particles shown in Fig. 2.4 and Fig. 2.5 exhibited a typical XRD pattern of fcc-FePt, and there was no significant difference. Their 111 diffraction peaks were at around 40.5°. On the other hand, there was a difference in their magnetic properties. Figure 2.7 shows the temperature dependence of the imaginary part of AC magnetic susceptibility χ'' measured at 10 kHz of the FePt-nanoparticle/polymer/silica core-shell particles. χ'' takes a maximum value at a certain temperature, which is defined as blocking temperature related to a thermal relaxation of magnetization. The blocking temperature of magnetic nanoparticles is strongly reflecting a magnetic anisotropic energy. Magnetic anisotropic energy is the product of magnetocrystalline anisotropy (K_u) and particle volume. The blocking temperature of the core-shell particles and crystallite size calculated from XRD patterns as shown in Fig. 2.6 are summarized in Table 2.2. The crystallite size of FePt nanoparticles synthesized with unmodified silica particles was larger than that of the others. There was no significant difference in their crystallite sizes of FePt nanoparticles grown on the polymer-modified silica particles. On the other hand, interestingly, the FePt nanoparticles on polymer-modified silica particles exhibited to have different blocking temperatures depending on the species of polymer even though the difference of their crystallite size was small. Especially, FePt-nanoparticle/PEI/silica and FePt-nanoparticle/PDDA/silica had the same morphology as shown in Fig.2.5, and their composition of FePt was the same (Fig. 2.8), but they exhibited different blocking temperatures. The composition ratio was investigated by an ICP atomic emission spectrometer. The composition of FePt is strongly related to the magnetic properties. Therefore, the difference of the blocking temperature was attributed to the difference of magnetic anisotropic energy. These results clearly showed the polymers have an effect on the magnetic properties. The blocking temperature of the FePt nanoparticles on the PDDA-modified silica particles was approximately 1.4 times as large as that of FePt nanoparticles on unmodified silica particles. PDDA would have a significant effect on promoting the atomic ordering in the FePt nanoparticles compared with PVP, PVA, PEI and PAA. Regarding the FePt nanoparticles formed on the PVP-modified silica particles, their magnetic properties were probably not uniform because there were two peaks in the temperature dependence of χ'' as shown in Fig. 2.7.

FePt-nanoparticle/polymer/silica core-shell structure has already been reported by Yong Lim Foo et al. [10]. They used bi-layer of polymer to accumulate FePt nanoparticles with high deposition density on silica particles. My results demonstrated polymer-multi-layer was not necessary for the accumulation of FePt nanoparticles with high deposition density, and the five types of polymer can be used for the accumulation of FePt nanoparticles in the polyol process. A system for loading and releasing drugs from the shell composed of metal nanoparticles and polymer multi-layer is needed. I think the shell composed of polymer single-layer is advantageous for loading and releasing of drugs. It has been already reported PEI can bond to the FePt nanoparticles through electron donation from the nitrogen atom of the NH_2 group [10, 11]. Also, PVP can bond to metal cations or metal nanoparticles through electron donation from their O and N atoms [12, 13]. PAA can bond to the FePt nanoparticles with its carboxylate group (COO) in both monodentate and bidentate forms [11]. However, the accumulation mechanism of FePt nanoparticles to PDDA has not been reported and was not clear yet. I have tried to investigate the accumulation mechanism of FePt nanoparticles on PDDA-modified silica particles.

Table 2.1 Zeta potentials of polymer-modified silica template particles in water.

Material	Zeta-potential (mV)
Silica particles	- 41
PDDA-modified silica particles	+55
PEI-modified silica particles	+40
PVP-modified silica	+4
PVA-modified silica	-34
PAA/PDDA-modified silica particles	-58

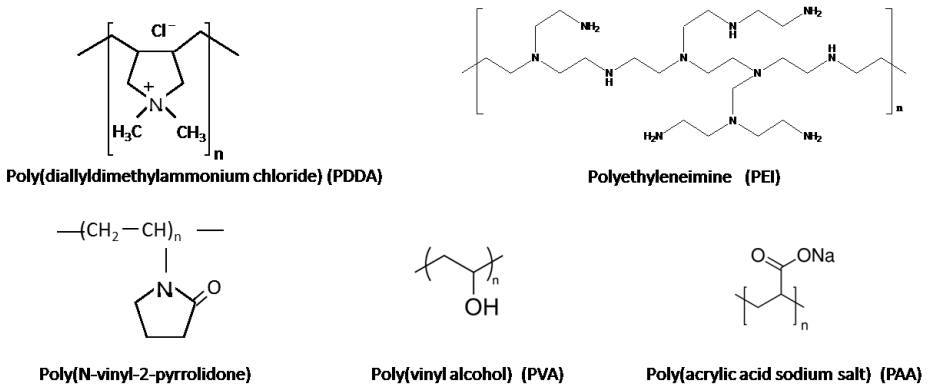

Figure 2.3 Structure of polymers used in this study

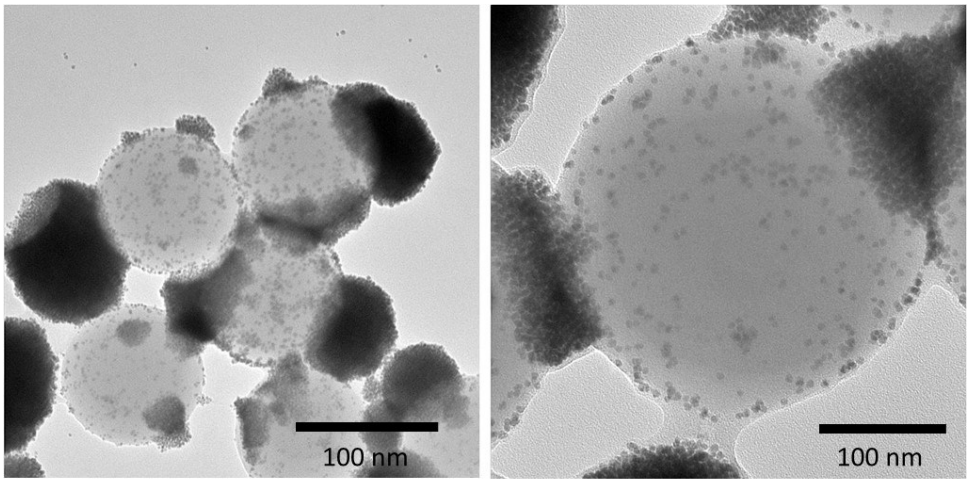

Figure 2.4 TEM images of FePt nanoparticles synthesized in the presence of unmodified silica particles.

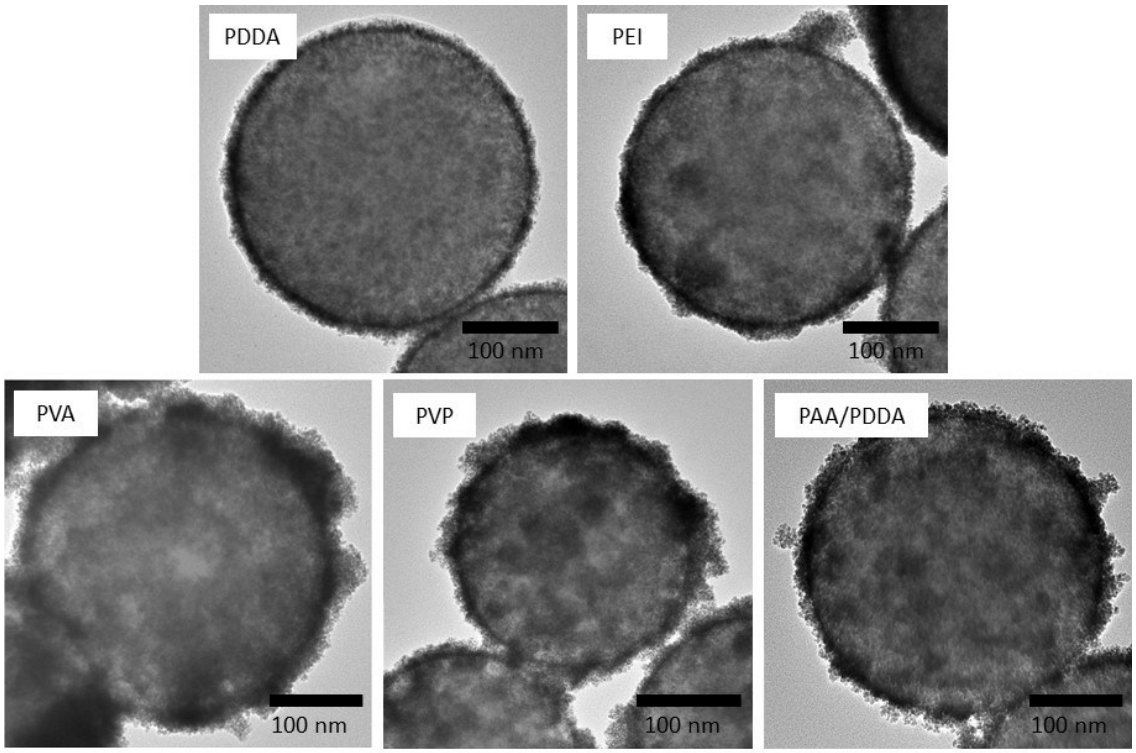

Figure 2.5 TEM images of FePt nanoparticles synthesized in the presence of polymer-modified silica template particles.

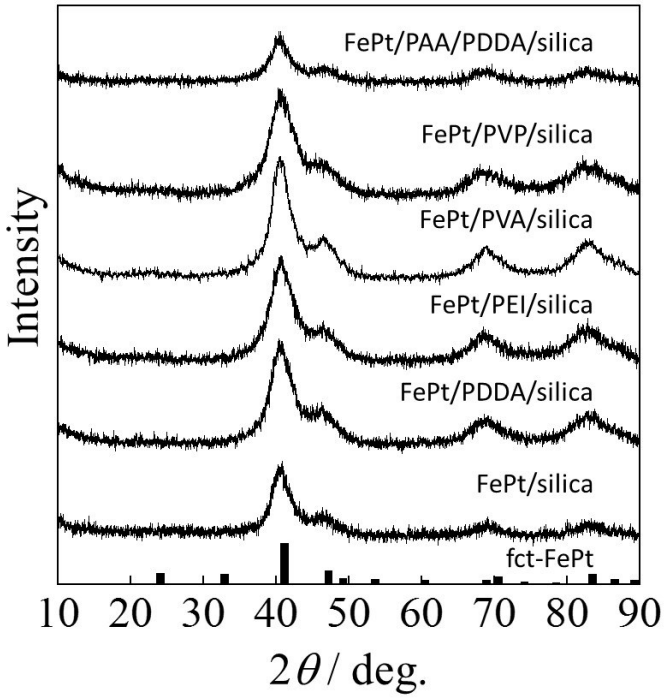

Figure 2.6 XRD patterns of FePt nanoparticles on unmodified silica particles and FePt nanoparticles on polymer-modified silica particles

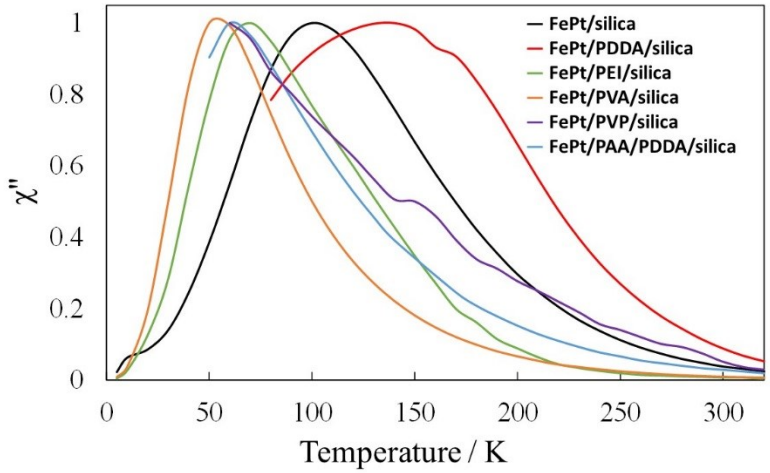

Figure 2.7 Temperature dependence of AC magnetic susceptibility χ" measured at 10 kHz of FePt nanoparticles formed on PDDA-modified silica particles, PEI-modified silica particles, PVA-modified silica particles, PVP-modified silica particles and PAA/PDDA-modified silica particles are shown in Figs. 2.5. The core-shell particles were prepared at 503 K. All the plots were normalized by the maximum χ" of each temperature dependence.

Table 2.2 Crystallite size calculated from XRD patterns and blocking temperature of FePt nanoparticles on the surface of various polymer-modified silica particles

Material	Crystallite size (nm)	Blocking temperature (K)
FePt/Silica	2.4	110
FePt/PDDA/silica	2.2	140
FePt/PEI/silica	2.1	80
FePt/PVP/silica	2.0	<70
FePt/PVA/silica	2.2	50
FePt/PAA/PDDA/silica	2.1	70

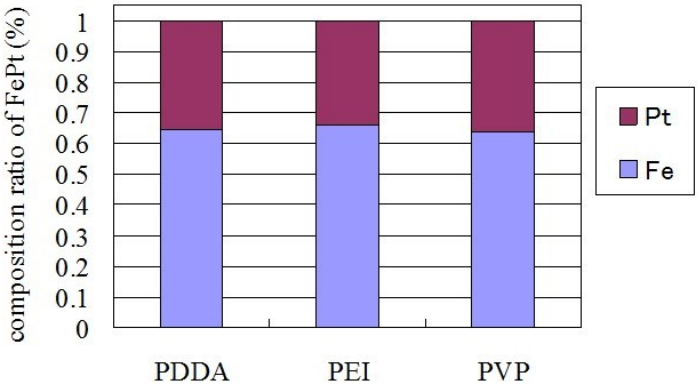

Figure 2.8 Composition of FePt nanoparticles on the PDDA-modified silica particles, PEI-modified silica particles and PVP-modified silica particles

2.4 Dependence on molar ratio of Fe precursor and Pt precursor

FePt nanoparticles, Fe nanoparticles and Pt nanoparticles were synthesized by changing the molar ratio of $Pt(acac)_2$ and $Fe(acac)_3$ in the polyol method explained in Section 2.2. For solvent exchange, these particles were dialyzed with water for 3 days. Figure 2.9 shows TEM images of the nanoparticles synthesized in the presence of PDDA-modified silica particles. When the Pt ratio in the reaction solution was 0–0.30, many particles were observed not only on the PDDA-modified silica particles but also around the PDDA-modified silica particles. In contrast, when the Pt ratio in the reaction solution was 0.47–0.70, uniform shell was observed on the composite particles, and nanoparticles that were not accumulated onto the PDDA-modified silica particles were not observed, However, when the Pt ratio was higher than 0.90, nanoparticles that were not accumulated on the PDDA-modified silica particles were observed, and when the Pt ratio was 1.0, the

PDDA-modified silica particles were not covered completely. Figure 2.10 shows TEM images of the composite particles for the Pt ratio of 0 and 0.1 precipitated by centrifugation, then washed three times with ethanol. After the purification, the amount of the nanoparticles accumulated on the silica particles decreased. These results suggest that iron or iron oxide nanoparticles were just adsorbed on the PDDA-modified silica particles, and that Fe cannot bond directly to PDDA molecules, and FePt nanoparticles were probably accumulated via bonding with Pt on PDDA molecules.

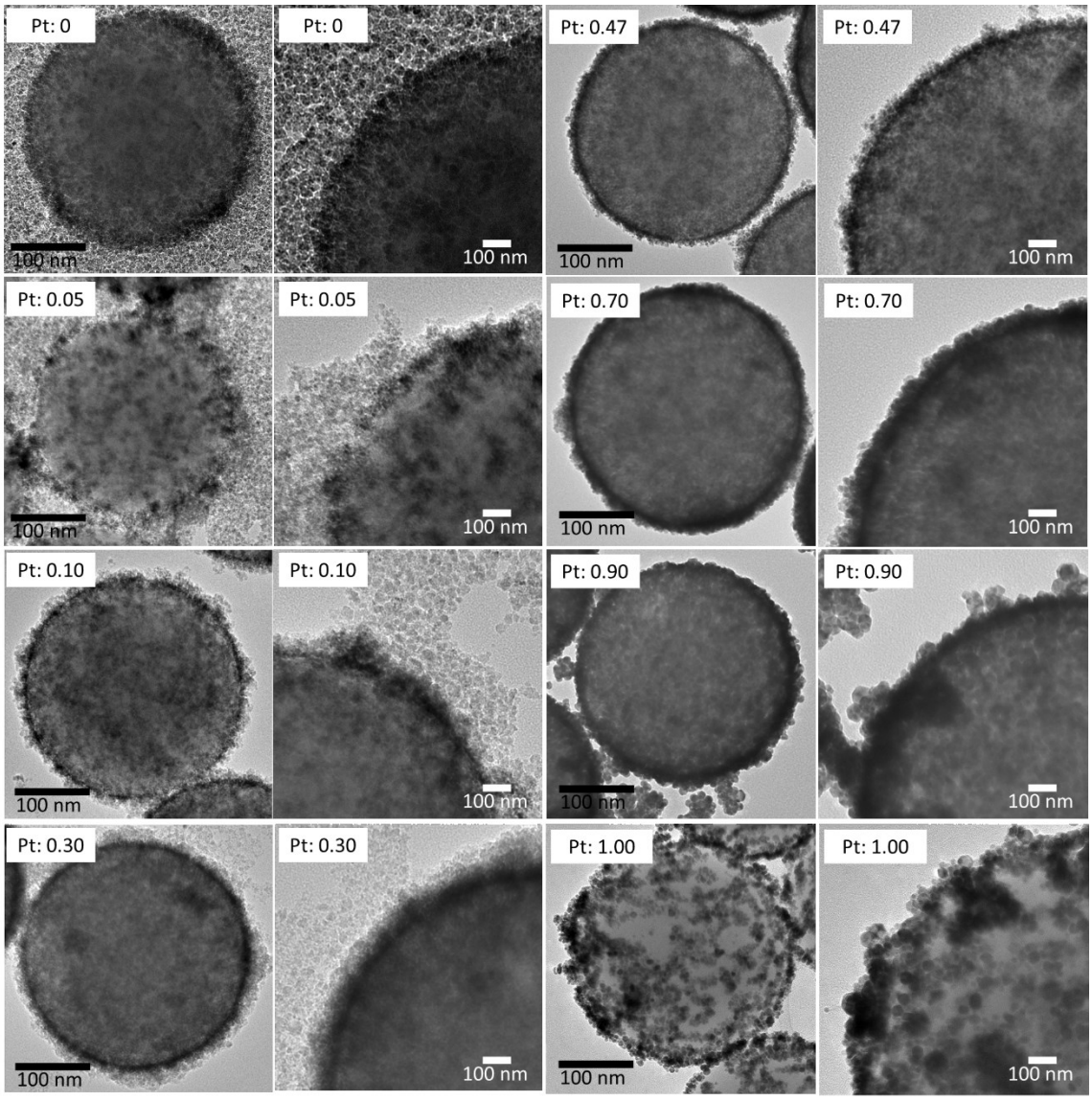

Figure 2.9 TEM images of the nanoparticles by changing the ratio of Pt precursor from 0 to 1.

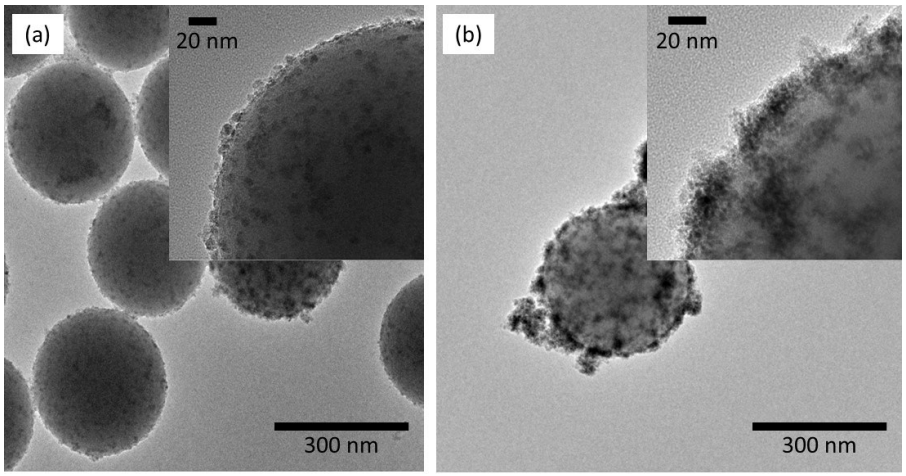

Figure 2.10 TEM images of the composite particles fabricated with the Pt ratio of (a) 0 and (b) 0.1. These composite particles were precipitated by centrifugation, then washed several times with ethanol.

2.5 Formation mechanism of FePt nanoparticles on PDDA-modified silica particles

To investigate the formation of FePt nanoparticles on the PDDA-modified silica particles, a mixture of $Fe(acac)_3$ (0.21 mmol, 75 mg), $Pt(acac)_2$ (0.19mmol, 76mg), PDDA-modified silica template particles, and TEG was heated at 323, 353, 383, 413, 443 and 473 K for 5 min. In all the cases, the reaction was quenched by using an ice bath, allowed to cool to room temperature, and purified. Figures 2.11(a) and 2.11(b) show TEM images of the surface of PDDA-modified silica particles after stirring with Fe and Pt precursors in TEG and the composite particles synthesized at 323 K, respectively. Hemispherical particles were observed on the surface of PDDA-modified silica particles after heating with precursors at 323 K for 5 min as shown in Fig. 2.11(b). These hemispherical particles ware not observed on the PDDA-modified silica particles mixed with the metal precursors in TEG as shown in Fig. 2.11(a). Figures 2.12(a)-2.12(d) show TEM images of the composite particles synthesized at 353, 383, 413 and 443 K. Hemispherical particles were also observed in TEM images of the composite particles at 353 K. Spherical particles were observed on the surface of PDDA-modified silica particles in TEM images of the composite particles synthesized at 383 K. The amount of particles was increased after increasing synthesis temperature from 383 K to 413 K as shown in Figs. 2.12(b) and 2.12(c). The composite particles synthesized at 443 K were completely covered with FePt nanoparticles. Large particles were observed in the TEM images of the composite particles synthesized at 323, 353 and 413 K as shown in Figs. 2.13. These particles would be formed in this quenched method. Fe and Pt atoms formed

by reduction of FePt precursors and reducing agents (TEG) were remained in a process of purification. The large particles would be formed in the process of purification such as washing and centrifugation process. Therefore, I thought these particles were not formed in the standard reaction method at 503 K.

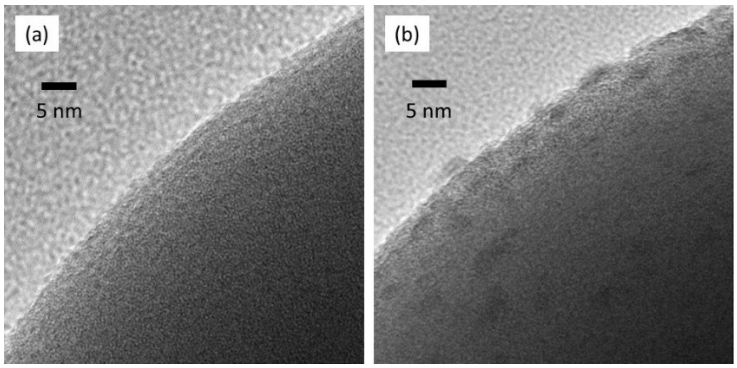

Figure 2.11 TEM images of the surface of (a) PDDA-modified silica particles after stirring with Fe and Pt precursors in TEG and (b) the surface of the composite particles synthesized at 323 K.

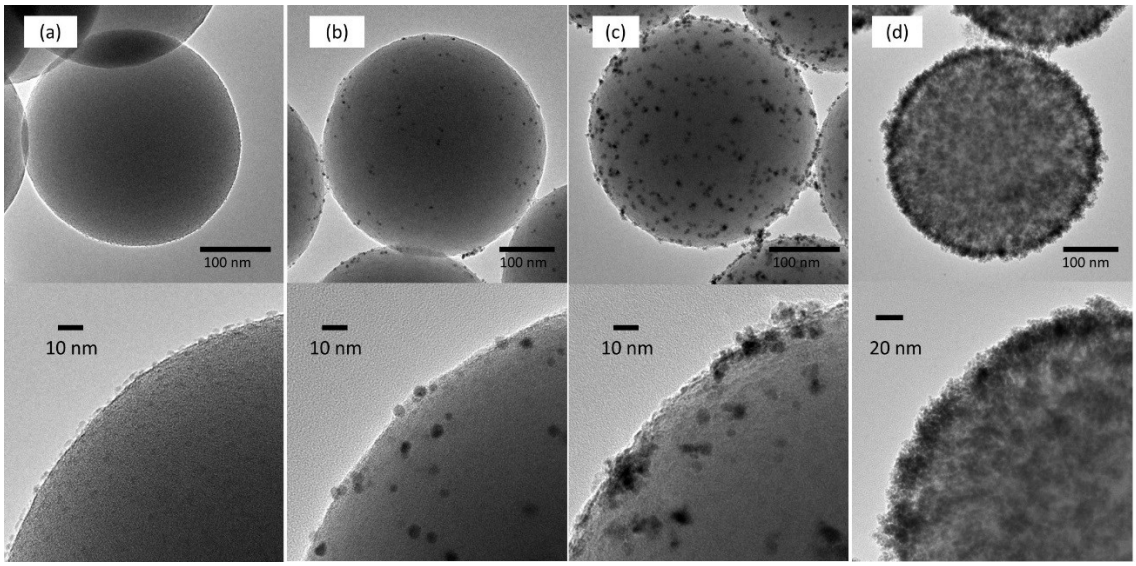

Figure 2.12 TEM images of composite particles synthesized at (a) 353, (b) 383, (c) 413 and (d) 443 K

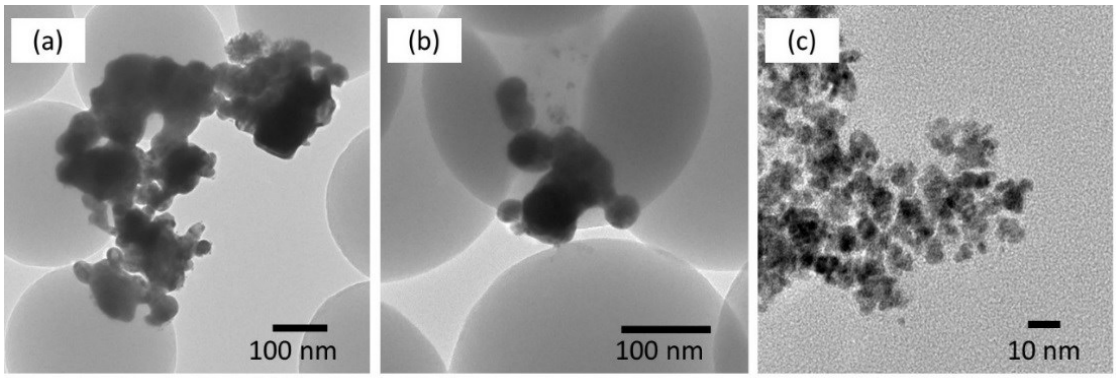

Figure 2.13 TEM images of composite particles synthesized at (a) 323, (b) 353 and (c) 413 K

Figure 2.14 shows XRD patterns of the composite particles synthesized at 323-473 K. A sharp peak was observed around at 39.8° in XRD patterns of the composite particles synthesized at 323, 353 and 413 K. The sharp peak was probably related to the large particles observed in Figs. 2.13, and the XRD patterns indicated the large particles as shown in Figure 2.13 (a) and (b) were Pt particles. This result suggested Pt atoms were formed by a reduction of $Pt(acac)_2$ at low temperature and Pt atoms were continuously supplied during elevated temperature process by gradual reduction of $Pt(acac)_2$. Therefore, when only Pt precursor was used for the synthesis, slowly-supplied Pt atoms were used for not only nucleation of Pt but also growing of Pt particles, and the size of Pt particles was not uniform as shown in Fig. 2.9. Broad peak was observed around at 40° in XRD pattern of the composite particles synthesized at 383 K, and higher angle shift of the broad peak was observed in XRD patterns of the samples synthesized at 383 K, 413 K and 443 K. XRD patterns of the composite particles synthesized at 413 K showed two peaks at least. I thought one was a 111 diffraction peak of $FePt_3$ and the other was that of fcc-FePt. XRD patterns of iron oxide or iron were not observed in XRD patterns of the composite particles. Fe atoms formed by a reduction of $Fe(acac)_3$ during elevated temperature process were adsorbed to Pt nuclei and/or Pt particles formed on the PDDA molecules and FePt nanoparticles were formed by atomic diffusion of Fe atoms and Pt atoms, but all of $Fe(acac)_3$ was not completely reduced at 413 K. Therefore, FePt nanoparticles which have a different composition ratio were formed at 413 K.

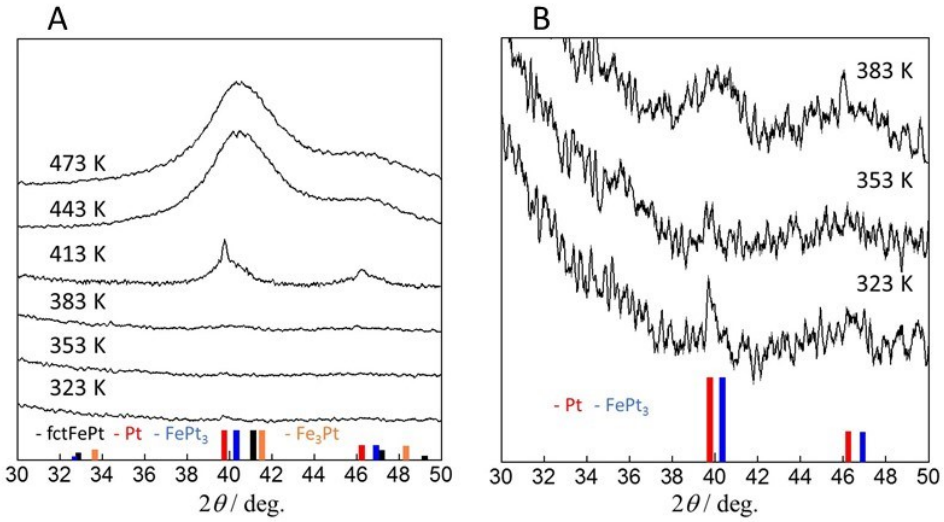

Figure 2.14 XRD patterns of (A) composite particles synthesized at 323, 353, 383, 413, 443 and 473 K, (B) composite particles synthesized at 323, 353 and 383 K.

To investigate nucleation of Fe on the Pt nuclei and/or Pt particles, $Fe(acac)_3$ was reduced in the presence of Pt-nanoparticle/PDDA/silica composite particles. Firstly, Pt-nanoparticles/PDDA/silica composite particles were fabricated in the polyol method explained in Section 2.2. Then, the Pt-nanoparticle/PDDA/silica composite particles were purified by centrifugation and washing with ethanol. A mixture of the Pt-nanoparticle/PDDA/silica composite particles, 75.0 mg of $Fe(acac)_3$ and TEG were placed in a 100 mL three-necked, round-bottom flask. The reaction flask was placed on a mantle heater. The mixture was stirred for 24 hours and then heated with stirring from 300 K at a heating rate of 10 K min^{-1} and kept at 503 K by refluxing for 2 hours in an inert gas (Ar/H_2). Finally, the samples were purified by centrifugation and washing with ethanol. Figures 2.15 show XRD patterns of the Pt-nanoparticle/PDDA/silica composite particles and a sample fabricated by reducing of $Fe(acac)_3$ in the presence of the Pt-nanoparticle/PDDA/silica composite particles, and TEM images of the sample. 111 diffraction peak of Pt was observed in both of XRD patterns, and there was no significant difference. XRD patterns of iron oxide were observed in XRD pattern of the sample fabricated by reducing of $Fe(acac)_3$ in the presence of the Pt-nanoparticle/PDDA/silica composite particles. Many particles were observed not only on the Pt-nanoparticle/PDDA/silica composite particles but also around the composite particles. These results suggested that Fe nuclei was not formed on Pt particles which have already formed on the PDDA-modified silica particles.

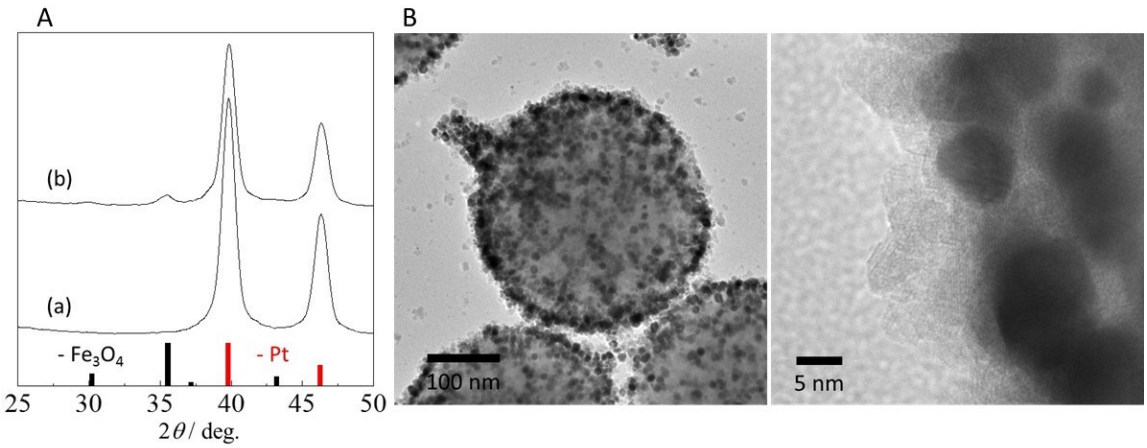

Figure 2.15 (A) XRD patterns of (a) the Pt-nanoparticle/PDDA/silica composite particles and (b) the sample fabricated by reducing of $Fe(acac)_3$ in the presence of the Pt-nanoparticle/PDDA/silica composite particles, and (B) TEM images of the sample fabricated by reducing of $Fe(acac)_3$ in the presence of the Pt-nanoparticle/PDDA/silica composite particles

I thought the formation mechanism of FePt nanoparticles from these results in the following (Figure 2.16). Firstly, Pt atoms formed by reduction of $Pt(acac)_2$ were adsorbed to PDDA moleculefes on the silica template particles, and Pt nuclei were formed on the PDDA molecules in the temperature range of room temperature to 353 K. FePt nanoparticles were formed by atomic diffusion of Fe and Pt atoms between the Fe nuclei and Pt nuclei at temperature of 353 K and higher. The formation of FePt nanoparticles was dominated by nucleation of Pt, followed by a slow growth process of Fe atoms. Pt atoms were continuously supplied during elevated temperature process by gradual reduction of $Pt(acac)_2$, and the Pt atoms were adsorbed to the PDDA molecules which were not adsorbed to FePt nanoparticles. Thus, Fe and Pt nucleation was also occurred during the formation of FePt nanoparticles by gradual reduction of FePt precursors. The detailed formation mechanism is not clear, but these results clearly show Pt nuclei were formed on the PDDA layer on the silica particles.

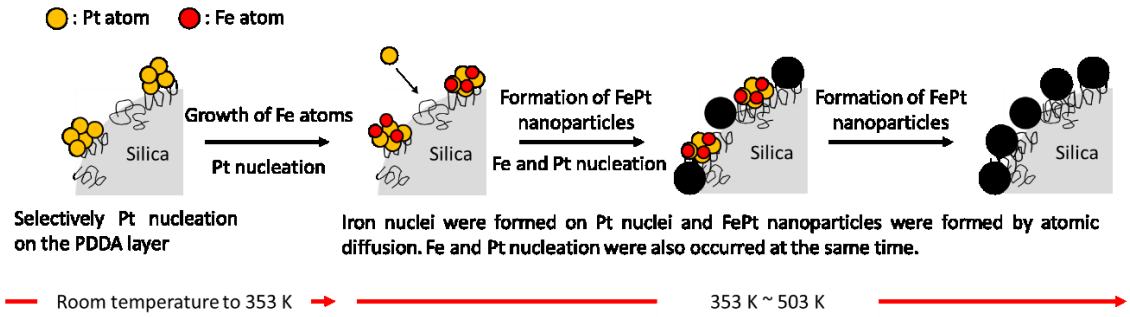

Figure 2.16 Schematic illustration of formation mechanism of FePt nanoparticles on PDDA-modified silica particles

2.6 Conclusion

In this chapter, I demonstrated the formation of FePt-nanoparticle/polymer/silica core-shell structure. FePt nanoparticles of 3-5 nm were accumulated to five types of polymer, PDDA, PEI, PVA, PVP and PAA. A uniform shell composed of FePt nanoparticles was obtained using PDDA- and PEI-modified silica particles. FePt-nanoparticle/polymer hybrid shells were obtained independently of electrostatic properties of these polymers. Their crystallite size did not depend on the species of polymer, but their blocking temperature depended on it. I found polymer layers on silica particle played an important role in the growth of FePt nanoparticles, and PDDA would have a significant effect on promoting the atomic ordering in the FePt nanoparticles compared with PVP, PVA, PEI and PAA. It was found that FePt nanoparticles were selectively grown on PDDA modifying silica template particles with a help of Pt nuclei.

Reference

[1] S. Sun, C. B. Murray, D. Waller, L. Folks, A. Moser, Science, 287, 2000, 1989
[2] S. Sun, E. E. Fullerton, D. Waller, C. B. Murray, IEEE Trans. Magn. 37, 2001, 1239
[3] B. Jeyadevan, K. Urakawa, A. Hobo, N. Chinnasamy, K. Shinoda, K. Tohji, D. D. J. Djayaprawira, M. Tsunoda, M. Takahashi, J.Appl. Phys., 42, 2003, 350–352
[4] K. Sato, B. Jeyadevan, K. Tohji, J. Magn. Magn. Mater., 289, 2005, 1 –4
[5] Y. Kitamoto, J. He, Electrochim. Acta, 54, 2009, 5969–5972
[6] T. Iwamoto, K. Matsumoto, Y. Kitamoto, N. Toshima, J. Colloid Interface Sci., 308, 2007, 564–567
[7] T. Iwamoto, Y. Kitamoto, N. Toshima, Phys. B, 404, 2009, 2080–2085
[8] T. Fuchigami, et.al. Langmuir 2011, 27, 2923-2928
[9] H. Sakuma, T. Taniyama, K. Ishii, Y. Kitamoto, Y. Yamazaki, J. Magn. Magn. Mater. 2006, 300, 284-292.
[10] J. Wang et al., Chem. Mater. 2007, 19, 2566-2572
[11] N. Shukla, C. Liu, P. M. Jones, D. Weller, J. MMM, 266, 2003, 178-184
[12] M. Liu, X. Yan, H. Liu, W. Yu, Reactive and Functional polymers 44, 2000, 55-64
[13] M. T. Salehi, M. Nasr-Esfahani, A. Sharifian-Esfahani, E. Ekramian, IPCBEE, 14, 2011, 174-177.

Chapter 3

Porous hollow sphere with FePt nanoshell

3.1 Introduction

Porous hollow spheres have attracted attention as a catalyst because of their large surface area. Also, porous hollow spheres can be used as a carrier for various functional materials such as anticancer agents, protein with molecular recognition property and photocatalyst because a porous structure is useful for coming and going of the materials and a hollow structure can load large amount of materials. FePt alloy has attracted attention in fuel cell as low-platinum catalysts. [1] FePt has two crystal structures. One is a face-centered cubic (fcc) structure and the other is face-centered tetragonal (fct) structure. FePt alloy which has fct structure (fct-FePt) show higher magnetocrystalline anisotropy than that has fcc structure (fcc-FePt), and the fct-FePt nanoparticles are more stable than fcc-FePt nanoparticles and catalytically active for an oxygen reduction reaction (ORR) in acidic environment [2]. Catalytic ability strongly depends on a surface area of particles. Therefore, porous capsules composed of FePt alloy are useful for not only MG-DDS but also catalysts for fuel cell.

In this chapter, I demonstrated the fabrication of two types of porous hollow spheres with a FePt shell. Figure 3.1 shows the fabrication process for these two types of porous hollow spheres. The first type of FePt porous hollow spheres is an inorganic-organic hybrid capsule that is fabricated by dissolution of silica template particles from FePt-nanoparticle/PDDA/silica core-shell particles by using NaOH aqueous solution. The second type of FePt porous hollow spheres are composed of FePt netlike structure fabricated by thermal treatment of the FePt-nanoparticle/PDDA/silica core-shell particles. The core-shell particles will be accumulated in a solid-state calcination. Avoiding the agglomeration is needed to apply the hollow spheres to MG-DDSs because large size (> 200 nm) of foreign materials are removed by the mononuclear phagocyte systems in the lung, spleen and liver, and also the large materials will clog the blood vessels during delivery of drugs. Therefore, thermal treatment of the FePt-nanoparticle/PDDA/silica core-shell particles should be conducted in a fluid to avoid the agglomeration. However, thermal treatment with higher temperature than the synthesis temperature (503 K) in a fluid is difficult because boiling point of most of fluid is lower than 573 K. Therefore, I decided to use a supercritical fluid treatment. Supercritical fluid treatments reported

previously are often used for nanoparticle synthesis, especially the crystallization of metal particles and increasing the particle size [3,4]. A supercritical fluid is substance at a temperature and pressure above its critical point, where distinct liquid and gas phases do not exist. It can effuse through solids (like a gas), and dissolve materials (like a liquid). The most important thing is that the FePt-nanoparticle/PDDA/silica core-shell particles can be thermally treated in a fluid. Critical temperature, critical pressure and critical density for H_2O and C_2H_5OH of supercritical fluid were summarized in Table 3.1. I used two kinds of supercritical fluid for the thermal treatment of the core-shell particles because critical temperatures of water and ethanol were higher than the synthesis temperature, and these fluids are safe for human body. I treated the core-shell particles with these fluids by changing temperature, pressure and treatment time to control their structure for applying them to MG-DDSs and fuel cell as a catalyst.

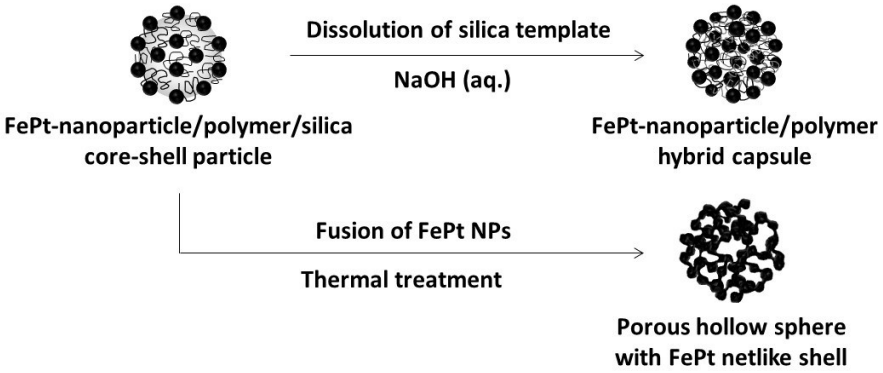

Figure 3.1 Fabrication process for two types of porous hollow spheres with FePt nanoshell

Table 3.1 Critical temperature, critical pressure and critical density for H_2O and C_2H_5OH of supercritical fluid

fluid	Critical temperature (K)	Critical pressure (MPa)	Critical density (g/cm^3)
H_2O	647.1	22.1	0.32
C_2H_5OH	512.4	8.1	0.27

3.2 Experimental

3.2.1 Modification of silica template particles with PDDA

PDDA-modified silica particles were fabricated by mixing an aqueous dispersion (5 mL) of amorphous silica particles (80 mg; average diameter: 100 nm) with various concentrations (1–7 wt.%) of PDDA aqueous solution (25 mL). The PDDA modified silica particles were purified to remove excess PDDA by washing with water. The PDDA-modified silica template particles (40 mg) were then dispersed in TEG (50 mL) after solvent exchange by centrifugation.

3.2.2 Synthesis of FePt-nanoparticle/PDDA/silica core-shell particles

The details of the synthesis method are described in chapter 2. FePt-nanoparticle/PDDA/silica core-shell particles were synthesized the following method. $Fe(acac)_3$ and $Pt(acac)_2$ were used as precursors of the FePt alloy. A mixture of $Fe(acac)_3$ (0.212, 0.106 or 0.053 mmol), $Pt(acac)_2$ (0.192, 0.096 or 0.048 mmol), silica template particles (40 mg) and TEG (50 mL) was added to a 100 mL three-necked, round-bottom flask and the mixture heated with stirring at 503 K by refluxing for 2 h in an inert gas (Ar/H_2). After the reaction, the core-shell particles were precipitated by centrifugation and washing with ethanol.

3.2.3 Fabrication of FePt-nanoparticle/PDDA hybrid capsules

The FePt-nanoparticle/PDDA/silica composite particles were stirred with 3 mol dm^{-3} NaOH aqueous solution at 343 K for 1 h to dissolve the silica template particles. The FePt-nanoparticle/PDDA hybrid capsules were then purified several times by centrifugation and redispersion using an ultrasonic bath in deionized water.

3.2.4 Fabrication of porous hollow spheres with a netlike nanoshell

Porous hollow spheres with FePt netlike nanoshell were fabricated by a supercritical liquid treatment of the FePt-nanoparticle/PDDA/silica core-shell particles. The aqueous dispersion of the composite particles was put into a reaction cell. The reaction cell of 11 cm^3 was heated in an electric furnace and kept at 473-673 K for 0.5-12.5 h. The pressure in the reaction cell was controlled by the volume of the reaction aqueous dispersion and temperature. After rapid cooling to room temperature, in which the reaction cell was put into a large water bath, samples were obtained as powder samples by centrifuging and drying procedures.

3.2.5 Cross-section observation

FePt-nanoparticle/PDDA/silica composite particles were treated with supercritical ethanol at 673 K and 10 MPa for 1.5 h. 10 mg of the treated sample was embedded in 1mL of an epoxy resin (Epok-812, Oken-shoji). Epoxy resin curing agents (0.5 mL of MNA and 0.5 mL of DDSA, Oken-shoji) were added to the resin. Then, 7.5 μL of polymeric initiator (DMP-30, Oken-shoji) was added to the mixture of resin and curing agents. The epoxy resin was cured at 60 °C for 12 h. The samples embedded cured resin was sliced in half by ion milling system (E-3500, Hitachi High-Technologies Corporation, Japan). The cross-section of the sample was observed by using a Scanning Electron Microscope (SEM, S-4800, Hitachi, Japan).

3.2.6 Dry sintering of the FePt-nanoparticle/PDDA/silica particles

30 mg of FePt-nanoparticle/PDDA/silica core-shell particles were dispersed in 1 mL of water. Then, 1 mL of the suspension of the FePt-nanoparticle/PDDA/silica core-shell particles were put on a porcelain plate and dried at 333 K in air for removing water. Then, the porcelain plate was put in an electronic furnace, and the FePt-nanoparticle/PDDA/silica core-shell particles were sintered in at 573 K for 1.5 h under Ar/H_2 gas flow of 190 ml/min. After sintering process, the sample was cooled down to room temperature naturally. The sample was dispersed in water for fabricating TEM sample.

3.2.7 Liquid phase sintering of the FePt-nanoparticle/PDDA/silica particle

30 mg of FePt-nanoparticle/PDDA/silica core-shell particles were dispersed in 5 ml of water. 5 ml of the suspension was put in a flask. 50 ml of polyethylene glycol (PEG) was added to the flask, and the water was evacuated from a mixture of PEG and the suspension of FePt-nanoparticle/PDDA/silica core-shell particles by heating under vacuum at 353 K. A mixture of PEG and FePt-nanoparticle/PDDA/silica core-shell particles was put in a 100 mL there-necked, round-bottom flask, and the reaction flask was placed on a mantle heater. The mixture was heated with stirring from 300 K at a heating rate of 10 K min^{-1} and kept at 573 K by refluxing for 1.5 hours in an inert gas (Ar/H_2). After the sintering in PEG, the solution was allowed to cool to room temperature. The composite silica particles were precipitated by centrifugation. After discarding the light brown supernatant, the precipitate was washed several times with ethanol. The composite silica particles were obtained by centrifuging and drying in air at 333 K as powder samples.

3.3 FePt-nanoparticle/PDDA hybrid capsules

FePt nanoparticles were synthesized at 503 K in the presence of silica particles treated with various concentrations of PDDA aqueous solution (1–7 wt%) by reduction of $Fe(acac)_3$ (0.106 mmol) and $Pt(acac)_2$ (0.096 mmol) [5-8]. The modification of negatively charged silica template particles with a cationic polymer resulting in the change of zeta potential of the silica template particles from negative to positive. The adsorption of PDDA molecules on the surface of silica particles was confirmed by measuring their zeta potentials. Increasing the concentration of the PDDA solution used to treat the silica particles, there was no significant difference in their zeta potentials (Table 3.2). Figure 3.2 shows XRD patterns of the composite particles fabricated with silica template particles treated with various concentrations of PDDA aqueous solutions, 1 wt%, 5 wt% and 7 wt%. All of the samples showed typical XRD pattern of FePt. In contrast, the morphologies of the composite particles fabricated with these PDDA-modified silica particles were slightly different (Fig. 3.3a–c). FePt nanoparticles accumulated on the surface of the PDDA-modified silica particles, and there was no difference in the size and shape of these FePt nanoparticles; the diameter of the FePt nanoparticles was between 3 and 5 nm. However, silica template particles treated with lower concentrations of PDDA solution (1 or 5 wt%) were only partially covered with FePt nanoparticles, whereas silica particles treated with 7 wt% PDDA solution were entirely covered with FePt nanoparticles (Fig. 3.3a–c). In chapter 2, I demonstrated that FePt nanoparticles accumulate on the PDDA layer adsorbed on the surface of silica particles confirming that the surface of the silica template particles treated with 1 or 5 wt% PDDA solution were not entirely covered with PDDA molecules, and that FePt nanoparticles accumulated only at the PDDA molecules adsorbed on the silica surface. This means that the FePt nanoparticles were selectively grown on the PDDA layer. Figure 3.3d–f shows TEM images of FePt-nanoparticle/PDDA hybrid capsules fabricated by dissolution of the silica template particles from the composite particles shown in Figure 3.3a–c. Complete FePt-nanoparticle/PDDA hybrid capsules were successfully obtained by dissolving the silica template particles from the composite particles entirely covered with FePt nanoparticles (Fig. 3.3f). In contrast, most of the FePt nanoparticle/PDDA aggregates were broken and dispersed after dissolution of the silica template particles from the composite particles partially covered with FePt nanoparticles (Fig. 3.3d and e).

Table 3.2 Zeta-potentials of silica particles treated with various concentrations of PDDA aqueous solution.

Concentration of PDDA aq. (wt. %)	Zeta potential (mV)
0 (unmodified silica particles)	− 70.2
1	+ 69.8
5	+ 65.1
7	+ 72.4

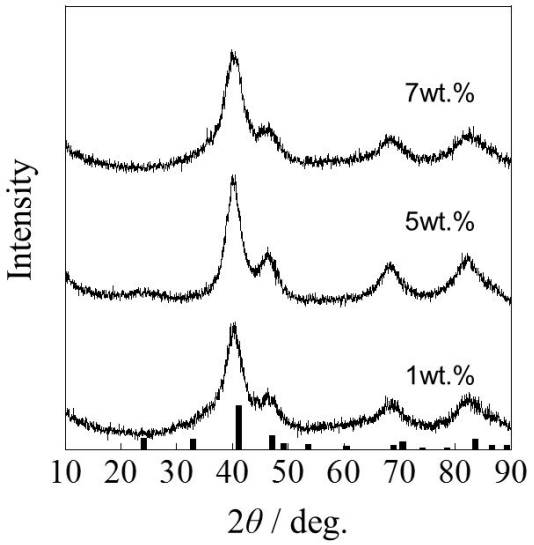

Figure 3.2 XRD patterns of FePt-nanoparticle/PDDA/silica composite particles fabricated with silica template particles treated with various concentrations of PDDA aqueous solutions, 1 wt%, 5 wt% and 7 wt%.

Table 3.3 Crystallite size of FePt-nanoparticle/PDDA/silica composite particles fabricated with silica template particles treated with various concentrations of PDDA aqueous solutions, 1 wt%, 5 wt% and 7 wt%.

Concentration of PDDA aq. (wt. %)	Crystallite size (nm)
1	2.0
5	2.5
7	2.1

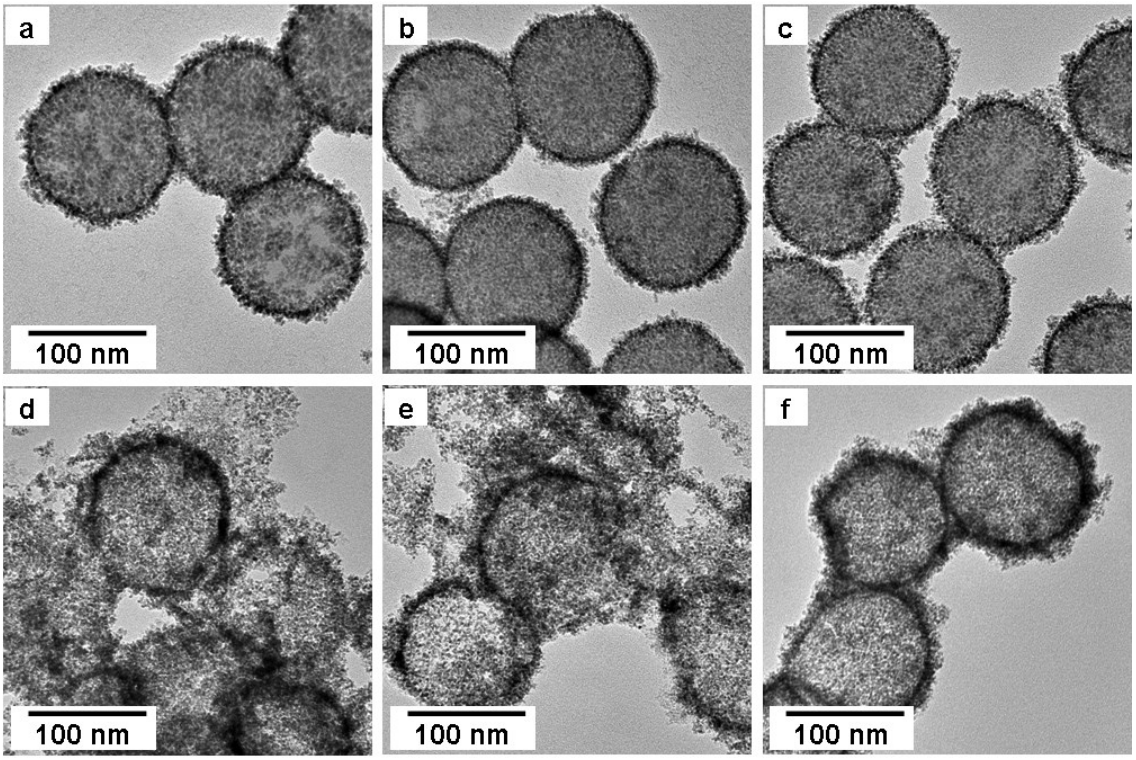

Figure 3.3 TEM images of FePt-nanoparticle/PDDA/silica composite particles fabricated with silica template particles treated with various concentrations of PDDA aqueous solutions, (a) 1 wt%, (b) 5 wt% and (c) 7 wt%, and FePt-nanoparticle/PDDA hybrid capsules fabricated by dissolution of the silica template particles from the composite particles. (d–f) are images of the hybrid capsules fabricated from a–c respectively.

Figure 3.4 shows XRD patterns of FePt-nanoparticle/PDDA/silica composite particles fabricated by using weight ratios of FePt precursors to silica particles of 4, 2 and 1, and the crystallite size was summarized in Table 3.4. All of the samples showed typical a XRD pattern of FePt, and there was no difference in their crystallite sizes. Figures 3.5a–c show TEM images of FePt-nanoparticle/PDDA/silica composite particles fabricated by using weight ratios of FePt precursors to silica particles of 4, 2 and 1, respectively, and by using silica template particles treated with 7 wt% of PDDA solution. The size of the FePt nanoparticles was not affected by changing the amount of precursors used in their synthesis; only the amount of FePt nanoparticles accumulated on the surface of the PDDA-modified silica particles changed, and a thinner shell was obtained by decreasing the weight ratio. Occupancy of FePt nanoparticles on the surface of silica particles was calculated from contrast in the TEM images. The occupancy of FePt nanoparticles was summarized with the weight ratio of FePt precursors to silica particles in Table 3.5.

Figures 3.5d–f show TEM images of FePt-nanoparticle/PDDA hybrid capsules fabricated by dissolution of the silica template particles from the composite particles shown in Figures 3.5a–c. Decreasing the occupancy of FePt nanoparticles on the surface of silica particles resulted in the increase of rupturing capsules. Few magnetic capsules were obtained after dissolving the template particles from the composite particles fabricated by using a weight ratio of FePt precursors to silica particles of 1 (Fig. 3.5f). Using a weight ratio of FePt precursors to silica particles of 4, I obtained FePt-nanoparticle/PDDA hybrid capsules that had an average diameter of 120 nm. The thickness of the hybrid shell was 10 nm at the maximum. These hybrid shells had many pores ($d < 6$ nm) and were stable in water.

Figure 3.6 shows a proposed model of the morphology of the FePt-nanoparticle/PDDA hybrid capsules in water. PDDA, a water-soluble polymer, adsorbed on the surface of the silica particles is dispersed again after dissolution of the silica template particles. My results show that when the occupancy of FePt nanoparticles on the surface of silica particles was about 50%, most of the hybrid capsules rupture. FePt nanoparticles and PDDA molecules were connected each other, and the amounts of FePt nanoparticles and PDDA molecules were important factors to maintain the three-dimensional (3D) structure of the hybrid capsules. It is hypothesized that the FePt nanoparticles anchor the PDDA molecules so that they are not dispersed in water despite their water-solubility, and that this combination of FePt nanoparticles and PDDA molecules accounts for the 3D structure being retained. Therefore, the decrease of the FePt nanoparticles resulted in a decrease of the mechanical strength of the magnetic capsules, because the strength of their three-dimensional structure depended on the binding force between PDDA and the FePt nanoparticles; thus, magnetic capsules with a pore larger than 6 nm could not be obtained. For these reasons, I decided to fabricate mechanically stronger FePt hollow capsules by fusion of the FePt nanoparticles.

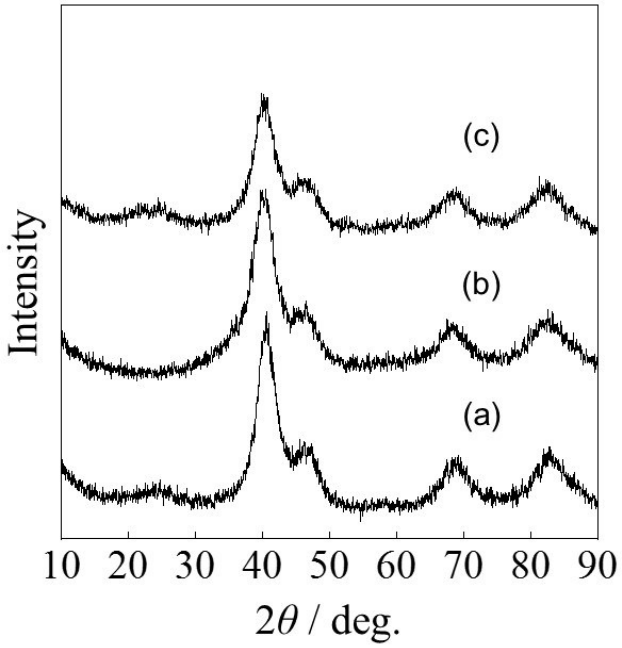

Figure 3.4 XRD patterns of FePt-nanoparticle/PDDA/silica composite particles fabricated by changing the weight ratio of FePt precursors to silica particles to (a) 4, (b) 2 and (c) 1 using silica template particles treated with 7 wt% of PDDA solution.

Table 3.4 Crystallite size of FePt-nanoparticle/PDDA/silica composite particles fabricated by changing the weight ratio of FePt precursors to silica particles to (a) 4, (b) 2 and (c) 1 using silica template particles treated with 7 wt% of PDDA solution.

weight ratio of FePt precursors to silica particles	Crystallite size (nm)
4	2.0
2	2.0
1	2.2

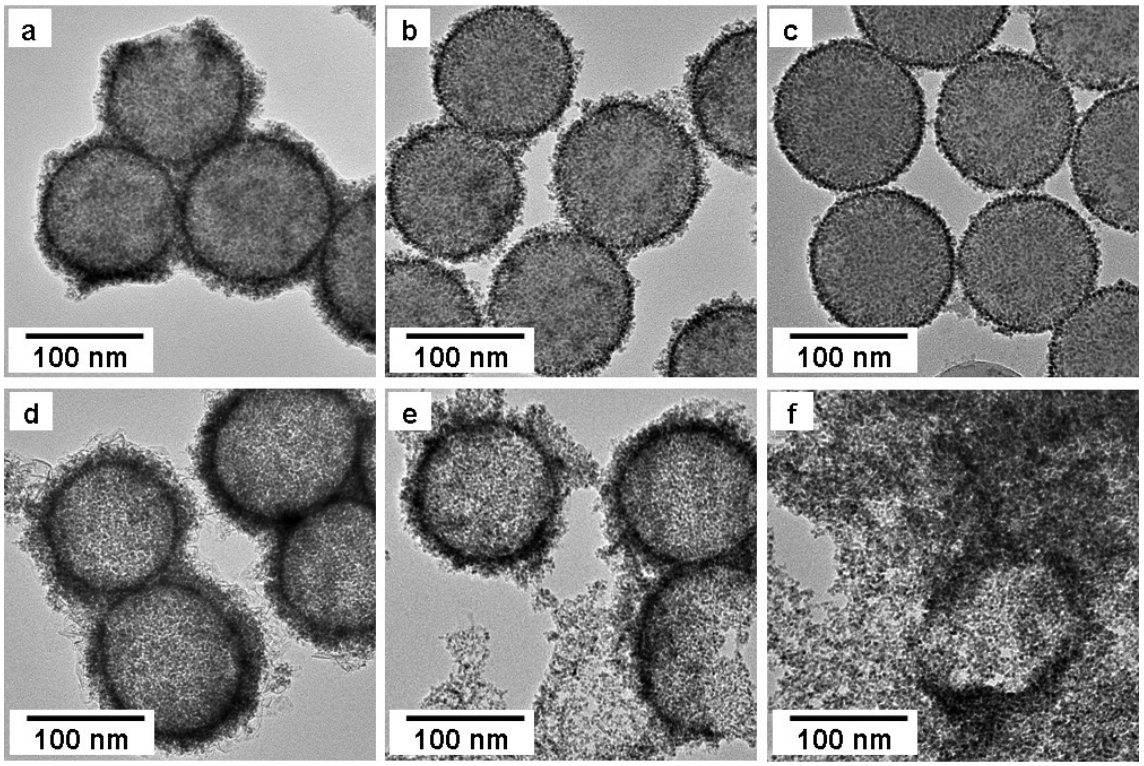

Figure 3.5 TEM images of FePt-nanoparticle/PDDA/silica composite particles fabricated by changing the weight ratio of FePt precursors to silica particles to (a) 4, (b) 2 and (c) 1 using silica template particles treated with 7 wt% of PDDA solution, and FePt-nanoparticle/PDDA hybrid capsules fabricated by dissolution of silica template particles from the composite particles. (d−f) are images of hybrid capsules fabricated from a–c, respectively.

Table 3.5 Occupancy of FePt nanoparticles on the surface of silica particles

Weight ratio of FePt precursors to silica particles	4	2	1
Occupancy of FePt nanoparticles	93 ± 8 %	70 ± 10 %	50 ± 10 %

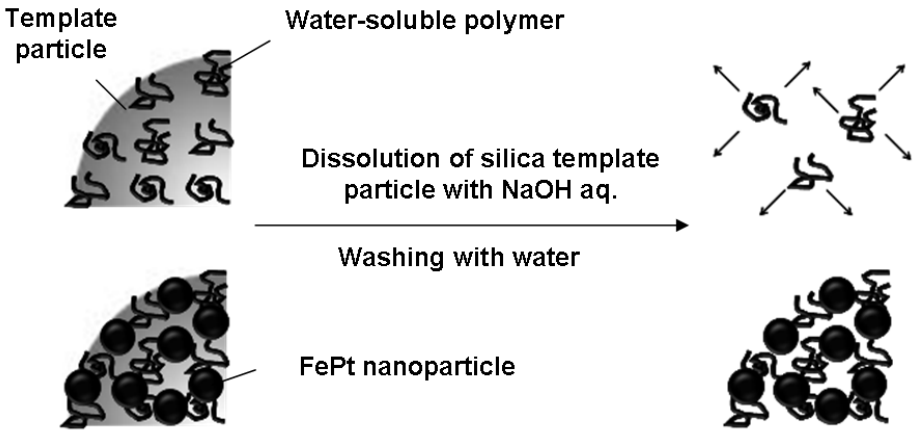

Figure 3.6 Proposed model of the morphology of FePt-nanoparticle/PDDA hybrid capsules.

3.4 Supercritical fluid treatment of core-shell particles

3.4.1 Supercritical water treatment of core-shell particles

Figure 3.7 shows TEM images of the FePt-nanoparticle/PDDA/silica core-particles and the core-shell particles treated with supercritical water at 673 K and 37 MPa for 3.5 hours. The FePt-nanoparticle/PDDA/silica core-shell particles were fabricated with 320 nm of silica particles treated with 7 wt% of PDDA solution. After the supercritical water treatment, particle-shaped FePt and silica particles were not observed (Fig. 3.7(b) and (c)), and there were a lot of pores on the shell. Maximum pore size was 10 nm in a diameter. It has been reported that SiO_2 (the quartz form) was dissolved in a supercritical water at 673 K [9]. These results suggested the silica particles were dissolved during the supercritical water treatment and FePt nanoparticles were fused together. Figure 3.8 shows TG-DTA curves of a PDDA aqueous solution (Mw < 100,000) measured in air atmosphere. Weight loss started from 298 K to 423 K was attributed to a loss of water. These results showed the decomposition of PDDA molecules started from 553 K in air atmosphere, and the PDDA molecules were decomposed during the supercritical water treatment.

Figure 3.9 shows XRD patterns of FePt-nanoparticle/PDDA/silica core-shell particles fabricated with 320 nm of silica particles treated with 7 wt% of PDDA solution and the FePt-nanoparticle/PDDA/silica particle treated with supercritical water at 673 K and 37 MPa for 3.5 hours. Their crystallite size calculated from their XRD patterns was summarized in Table 3.6. The porous hollow spheres exhibited a typical XRD pattern

of FePt. Crystallite size increased from 2.6 to 7.9 nm after the supercritical water treatment. However, diffraction peaks from iron oxide were observed in the XRD pattern of the porous hollow spheres fabricated by the supercritical water treatment. Supercritical water has high oxidizability and is used to oxidize organic compounds. Therefore, either iron oxide was formed on the surface of the FePt shell or Fe was dissolved out into the supercritical water and then oxidized during the supercritical water treatment.

Figure 3.10 shows magnetization curves of the core-shell particles and the porous hollow spheres were measured at 300 K in applied magnetic fields from 9 to 0 T, and their blocking temperature is summarized in Table 3.6. Magnetization per weight at 9 T increases after dissolution of the silica template particles from the core-shell particles due to the removal of the non-magnetic silica particles [6]. However, magnetization at 9 T of the porous hollow spheres was smaller than that of the FePt-nanoparticle/PDDA/silica core-shell particles. The reason of the decrease of the magnetization was that iron oxide was formed on the surface of the FePt netlike shell or Fe was dissolved out into the supercritical water and then oxidized during the supercritical water treatment. To inhibit the oxidation or dissolution and increase magnetization, Ar/H_2 (H_2: 3%) gas was introduced in an aqueous dispersion of the FePt-nanoparticle/PDDA/silica core-shell particles and in a reaction cell.

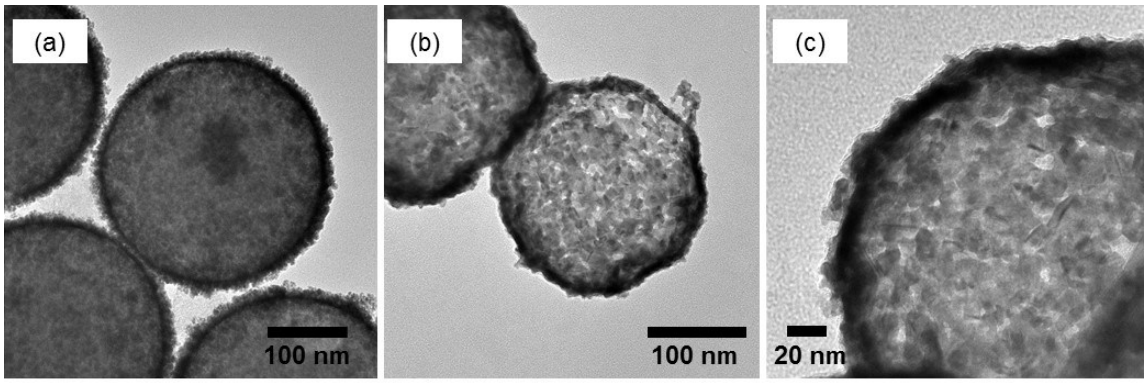

Figure 3.7 TEM images of (a) FePt-nanoparticle/PDDA/silica core-shell particles fabricated with 320 nm of silica particles treated with 7 wt% of PDDA solution, (b) and (c) the porous hollow spheres fabricated by supercritical water treatment at 673 K and 37 MPa for 3.5 hours

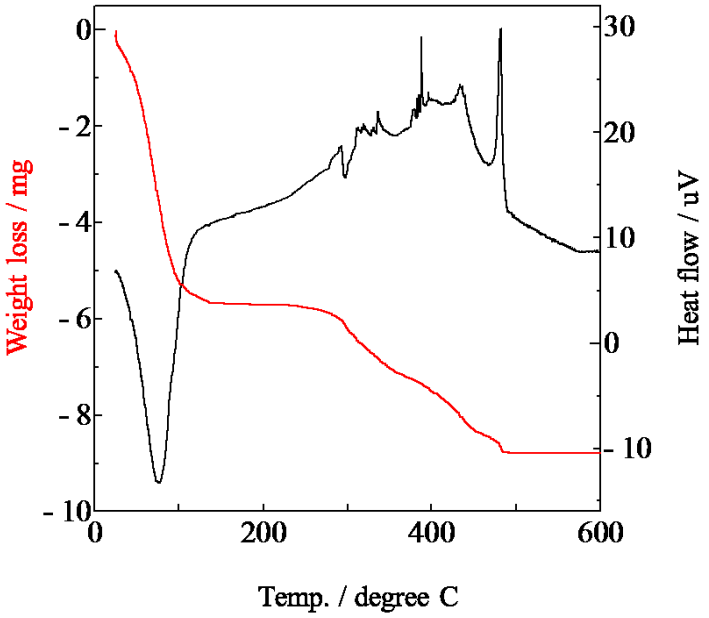

Figure 3.8 TG-DTA curves of PDDA aqueous solution (Mw < 100,000, 10mg) measured in air atmosphere

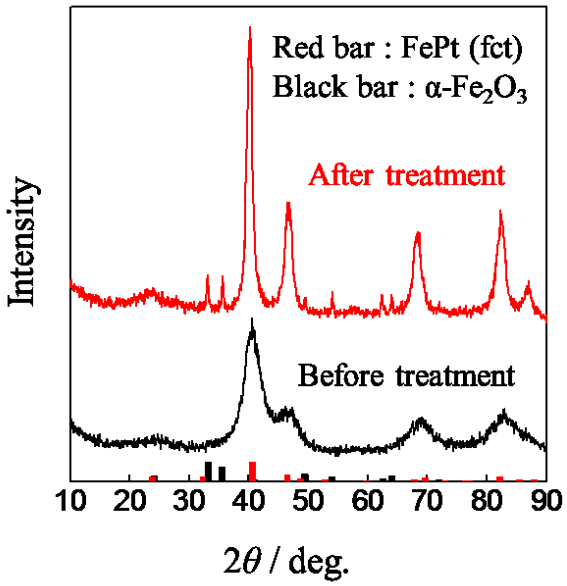

Figure 3.9 XRD patterns of FePt-nanoparticle/PDDA/silica core-shell particles fabricated with 320 nm of silica particles treated with 7 wt% of PDDA solution and the porous hollow spheres fabricated by the supercritical water fluid at 673 K and 37 MPa for 3.5 hours

Table 3.6 Crystallite size and blocking temperature of FePt-nanoparticle/PDDA/silica core-shell particles fabricated with 320 nm of silica particles treated with 7 wt% of PDDA solution and the porous hollow spheres fabricated by the supercritical water treatment at 673 K and 37 MPa for 3.5 hours

sample	Crystallite size (nm)	Blocking temperature (K)
Before treatment	2.6	95
After treatment	7.9	160

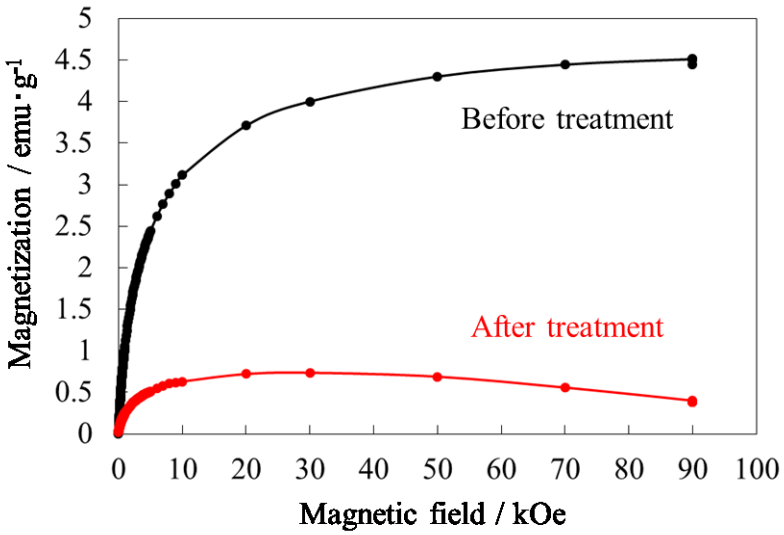

Figure 3.10 Magnetization curves of FePt-nanoparticle/PDDA/silica core-shell particles fabricated with 320 nm of silica particles treated with 7 wt% of PDDA solution and the porous hollow spheres fabricated by the supercritical water treatment at 673 K and 37 MPa for 3.5 hours. These curves were measured at 300 K in applied magnetic fields from 9 to 0 T.

3.4.2 Supercritical water treatment in Ar/H_2 (H_2: 3%) atmosphere

5 ml of the suspension of FePt-nanoparticle/PDDA/silica core-shell particles was put into the reaction cell. Then the Ar/H_2 (H_2: 3%) gas was introduced into the aqueous solution for 30 min, and the reaction cell was sealed. After that, the reaction cell was heated in an electric furnace and kept at 673 K for 3.5 h. After rapid cooling to room temperature samples were obtained as powder samples by centrifuging and drying procedures. Figure 3.11 shows TEM images of the porous hollow spheres fabricated by the supercritical water treatment at 673 K and 37 MPa in Ar/H_2 atmosphere. The morphology of the porous hollow spheres fabricated by the supercritical water treatment in Ar/H_2 atmosphere was similar to that of the porous hollow spheres fabricated by the supercritical water treatment in air atmosphere. A few FePt nanoparticle which was not fused was observed in the shell. Figure 3.12 shows XRD patterns of the FePt-nanoparticle/PDDA/silica core-shell particles fabricated with 320 nm of silica particles treated with 7 wt% of PDDA solution and the porous hollow spheres fabricated by the supercritical water treatment at 673 K and 37 MPa in Ar/H_2 atmosphere. Diffraction peaks from iron oxide were also observed in the XRD pattern of the core-shell particles treated with supercritical treatment in Ar/H_2 atmosphere. However, the peak intensity of the porous hollow spheres fabricated by the supercritical water treatment in Ar/H_2 atmosphere was weaker than that of the core-shell particles treated with supercritical treatment in air as shown in Fig. 3.13. Crystallite size and blocking temperature of FePt-nanoparticle/PDDA/silica core-shell particles and the porous hollow spheres fabricated by the supercritical water treatment in Ar/H_2 atmosphere were summarized in Table 3.6. The crystallite size increased from 2.2 nm to 7.7 nm and the blocking temperature of the core-shell particles treated with supercritical water in Ar/H_2 atmosphere was higher than that of the porous hollow spheres fabricated by the supercritical water treatment in air. Figure 3.14 shows magnetization curves of the core-shell particles and the porous hollow spheres measured at 300 K in applied magnetic fields from 9 to 0 T. The magnetization at high magnetic field slightly increased after supercritical treatment, but these results showed Ar/H_2 atmosphere was not much effective to inhibit the oxidation or dissolution of Fe in FePt alloy during the supercritical water treatment.

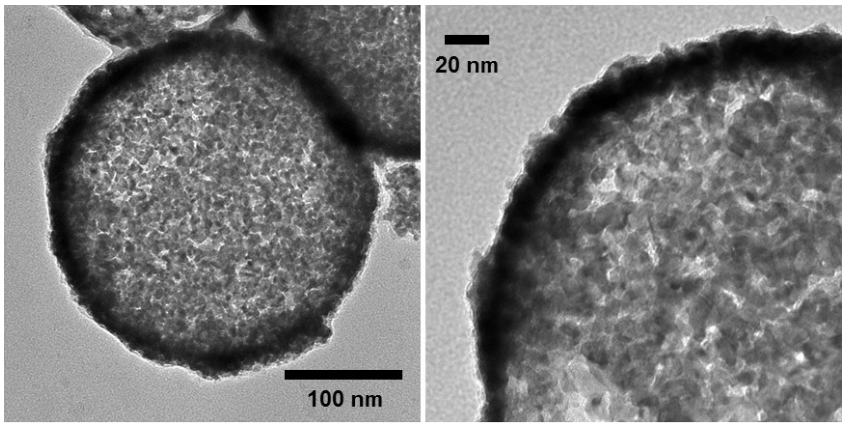

Figure 3.11 TEM images of the porous hollow spheres fabricated by the supercritical water treatment at 673 K and 37 MPa in Ar/H_2 (H_2: 3%) atmosphere

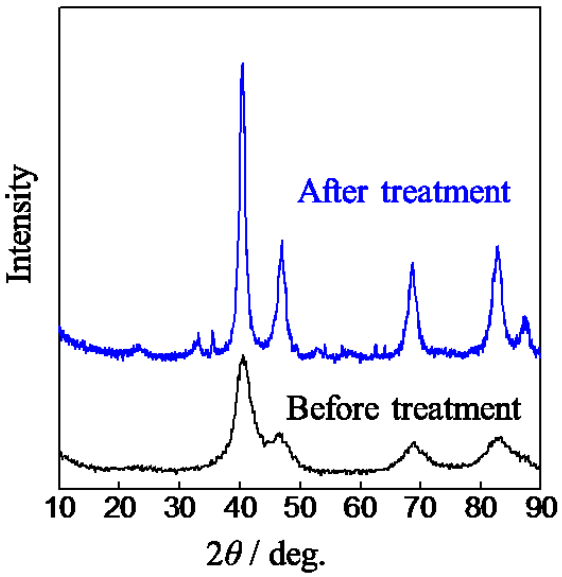

Figure 3.12 XRD patterns of the FePt-nanoparticle/PDDA/silica core-shell particles fabricated with 320 nm of silica particles treated with 7 wt% of PDDA solution and the porous hollow spheres fabricated by the supercritical water treatment at 673 K and 37 MPa in Ar/H_2 (H_2: 3%) atmosphere

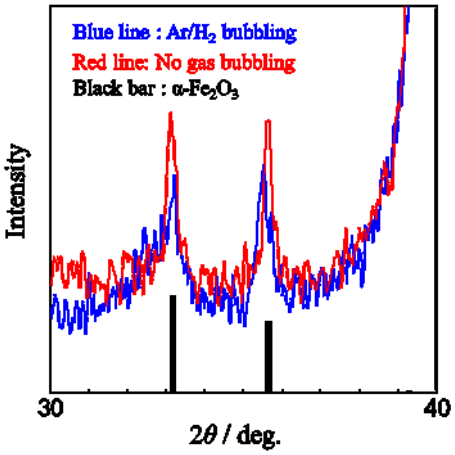

Figure 3.13 XRD patterns of the porous hollow spheres fabricated by the supercritical water treatment at 673 K and 37 MPa for 3.5 h. in (red line) air and (blue line) Ar/H_2 (H_2: 3%) atmosphere

Table 3.7 Crystallite size of the FePt-nanoparticle/PDDA/silica core-shell particles fabricated with 320 nm of silica particles treated with 7 wt% of PDDA solution and the porous hollow spheres fabricated by the supercritical water treatment at 673 K and 37 MPa in Ar/H_2 (H_2: 3%) atmosphere.

sample	Crystallite size (nm)	Blocking temperature (K)
Before treatment	2.2	70
After treatment	7.7	220

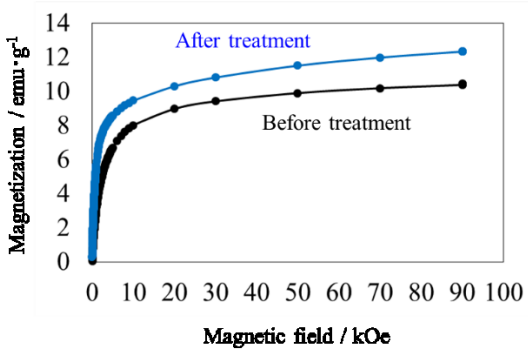

Figure 3.14 Magnetization curves of FePt-nanoparticle/PDDA/silica core-shell particles fabricated with 320 nm of silica particles treated with 7 wt% of PDDA solution and the porous hollow spheres fabricated by the supercritical water treatment at 673 K and 37 MPa for 3.5 hours in Ar/H_2 (H_2: 3%) atmosphere. These curves were measured at 300 K in applied magnetic fields from 9 to 0 T.

3.4.3 Influence of occupancy of FePt nanoparticles on netlike structure

Figure 3.15 shows TEM images of FePt-nanoparticle/PDDA/silica composite particles and the porous hollow spheres with a FePt netlike shell fabricated by supercritical water treatment at 673 K and 37 MPa in Ar/H_2 atmosphere for 3.5 h. The composite particles were fabricated with silica particles treated with 7 wt% of PDDA solution and a weight ratio of FePt precursors to silica particles of 4 and 1 (Figs. 3.13a and b). The occupancy of FePt nanoparticles in the core-shell particle fabricated with a weight ratio of FePt precursors to silica particles of 4 was 93 ± 8%, which was larger than that in the core shell particles fabricated with a lower weight ratio. Changing the occupancy of FePt nanoparticles, the morphology of the shell was changed as shown in Figs. 3.15a and b. After supercritical water treatment, when the occupancy of FePt precursors to silica particles was 93 ± 8%, their pores were so small and low, and the morphology was membranal. When the occupancy of FePt precursors to silica particles was 50 ± 10 %, FePt-nanoparticle/PDDA hybrid capsules could not be obtained (Fig. 3.5c); however, porous hollow spheres could be successfully obtained (Fig. 3.15c). Despite the ratio of FePt precursors to silica particles being too low to obtain hybrid capsules after dissolution of the silica particles, supercritical water treatment fused the FePt nanoparticles resulting in porous capsules being produced from the 3D netlike structure of the FePt alloy. The total diameter of the porous hollow spheres with FePt netlike shell was about 90 nm and the shell thickness was about 3 nm. In addition, there were large pores in the shell of the FePt porous hollow spheres that had a diameter up to 10 nm. A magnetic capsule with a diameter of 90 nm and a shell thickness of 3 nm has a loading capacity for therapeutic agents of 80% of the capsule volume. The larger internal capacity and larger pores in the porous hollow spheres with netlike shell are advantageous for carrying and releasing larger amounts anti-cancer drugs [10-13]. Additionally, the large pores are useful for loading sterically-bulky molecules such as therapeutic agents.

XRD patterns of the FePt-nanoparticle/PDDA/silica core-shell particles and the porous hollow spheres are shown in Fig. 3.16. The FePt-nanoparticle/PDDA/silica core-shell particles exhibited a typical XRD pattern of FePt, and there was no marked difference in their crystalline structure. Crystallite sizes were calculated by using Scherrer's formula (Table 3.8). Crystallite size increased after the supercritical water treatment, and the density of the FePt nanoparticles had a strong correlation with the crystallite size. Diffraction peaks from iron oxide were observed after the supercritical water treatment. Figure 3.17 shows magnetization curves of the FePt-nanoparticle/PDDA/silica core-shell particles and the porous hollow spheres fabricated by the supercritical water treatment measured at 300 K in applied magnetic fields from 9 to 0 T. The magnetization of the

core-shell particles after treatment at high magnetic field was higher than that of the untreated core-shell particles. The magnetization at 9 T of the porous hollow spheres was 12.4 emu/g, and the magnetic characterization revealed that porous hollow spheres exhibited superparamagnetic behavior at 300 K. This property should help to avoid the embolism of blood vessels during delivery of therapeutic agents to cancer lesions because the capsules do not have a spontaneous magnetization and do not coagulate without magnetic fields.

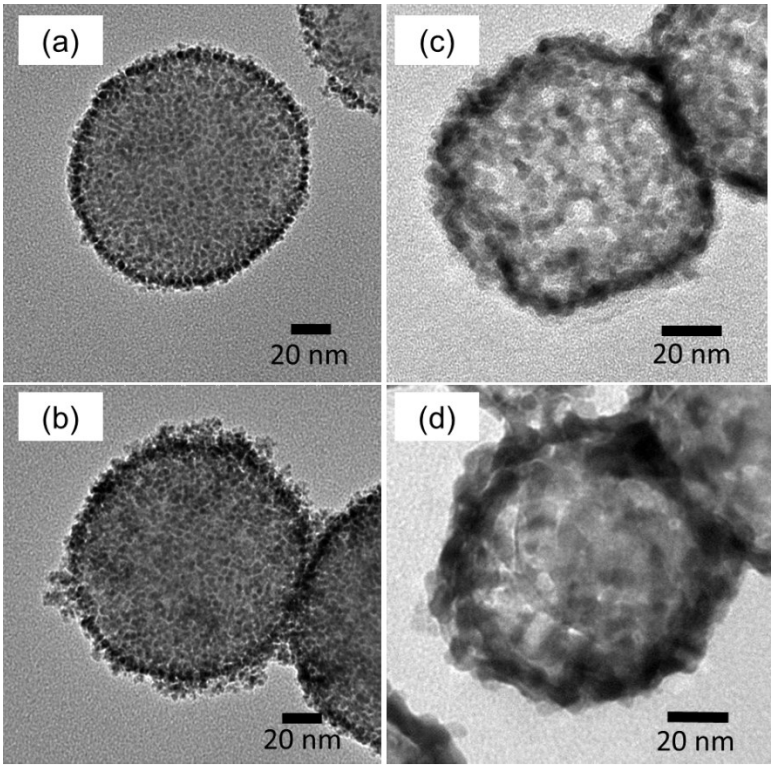

Figure 3.15 TEM images of FePt-nanoparticle/PDDA/silica composite particles fabricated with silica particles treated with 7 wt% of PDDA solution and a weight ratio of FePt precursors to silica particles of (a) 1 and (b) 4 and (c), (d) the porous hollow spheres with FePt netlike shell fabricated by supercritical water treatment at 673 K and 37 MPa in Ar/H_2 atmosphere for 3.5 h from (a) and (b) respectively.

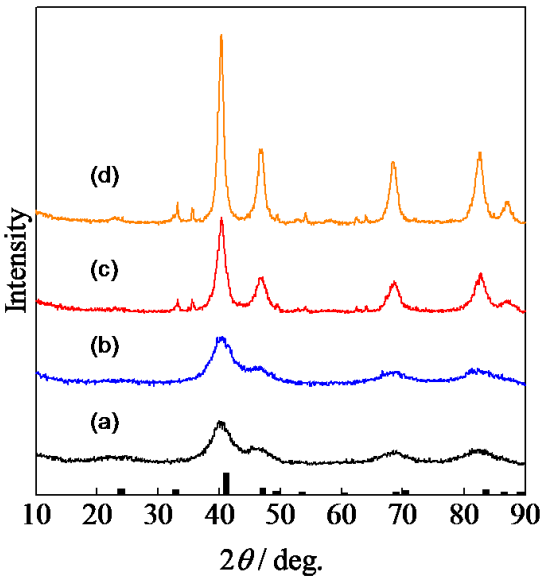

Figure 3.16 XRD patterns of FePt-nanoparticle/PDDA/silica composite particles fabricated with silica particles treated with 7 wt% of PDDA solution and a weight ratio of FePt precursors to silica particles of (a) 1 and (b) 4 and (c), (d) the porous hollow spheres with FePt netlike shell fabricated by supercritical water treatment at 673 K and 37 MPa in Ar/H_2 atmosphere for 3.5 h from (a) and (b) respectively.

Table 3.8 Crystallite size of FePt-nanoparticle/PDDA/silica composite particles fabricated with silica particles treated with 7 wt% of PDDA solution and a weight ratio of FePt precursors to silica particles of (a) 1 and (b) 4 and (c), (d) the porous hollow spheres with FePt netlike shell fabricated by supercritical water treatment at 673 K and 37 MPa in Ar/H_2 atmosphere for 3.5 h from (a) and (b) respectively.

sample	Crystallite size (nm)
(a)	2.0
(b)	2.0
(c)	5.5
(d)	8.1

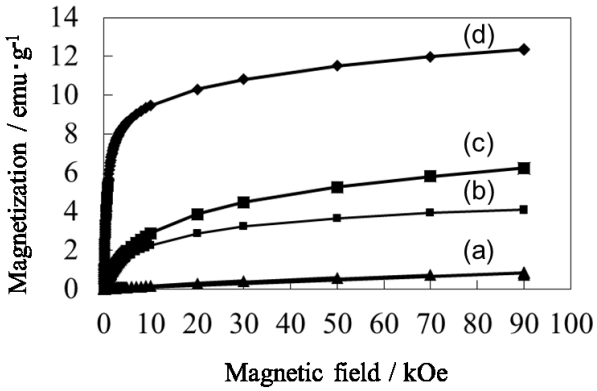

Figure 3.17 Magnetization curves of FePt-nanoparticle/PDDA/silica composite particles fabricated with silica particles treated with 7 wt% of PDDA solution and a weight ratio of FePt precursors to silica particles of (a) 1 and (b) 4 and (c), (d) the porous hollow spheres with FePt netlike shell fabricated by supercritical water treatment at 673 K and 37 MPa in Ar/H_2 atmosphere for 3.5 h from (a) and (b) respectively. These curves were measured at 300 K in applied magnetic fields from 9 to 0 T.

3.5 Supercritical ethanol treatment

In supercritical water treatment, FePt alloy was fused but the oxidization or dissolution of Fe was observed. Therefore, I tried to fabricate porous hollow spheres with FePt netlike shell by heat treatment using ethanol. For the supercritical ethanol (SCE) treatment, FePt-nanoparticle/PDDA/silica core-shell particles were fabricated using 320 nm of silica particles treated with 7 wt% of PDDA solution. The detail of the fabrication was described in chapter 2.

3.5.1 Dependence on treatment temperature

Figure 3.18 shows TEM images of the FePt-nanoparticle/PDDA/silica core-shell particles treated with subcritical or supercritical ethanol at 473-673 K and 10 MPa for 90 min. The pressure in the reaction cell was controlled by the volume of ethanol [14, 15]. After SCE treatment at 673 K, the ethanol was not remained in the reaction cell. Ethanol would be decomposed into acetaldehyde, diethyl ether and some gases during the treatment. The morphology of the FePt nanoparticles treated with subcritical ethanol at 473 K was not much different than that of the FePt nanoparticles before treatment. In contrast, morphology of FePt nanoparticles was changed after SCE treatment at 573 K

and 673 K. Silica particles were not dissolved by the SCE treatment. FePt nanoparticles were thermally fused together and the FePt netlike structures formed on the silica template particles. Increasing the treatment temperature from 573 to 673 K, the surface of FePt alloy became smooth and the pore size became large. Figure 3.19 shows TEM images of the FePt-nanoparticle/PDDA hybrid shell and the FePt netlike shell treated with ethanol at 473 K after dissolution of silica particles with NaOH aq. at 343 K. Before subcritical ethanol treatment, FePt nanoparticles were not fused. On the other hand, fused FePt nanoparticles were observed partially in the TEM results of the sample treated with subcritical ethanol treatment at 473 K as shown in Fig. 3.19. This result suggests FePt nanoparticles was fused by SCE treatment at 473 K which is lower temperature than synthesis temperature (503 K). Figure 3.20 shows TEM images of the sample treated with the SCE treatment at 573 K and 10 MPa for 90 min after dissolution of silica particles. Raptured capsules were partially observed. This results suggested the FePt nanoparticles were not completely fused in the SCE treatment at 573 K. Figure 3.21 shows TEM images of sample treated at 673 K and 10 MPa for 90 min after dissolution of silica particles. Most of capsules were not raptured. Figure 3.22 shows SEM image of the sample treated at 673 K and 10 MPa for 90 min after dissolution of silica particles. Pore size were evaluated to be 18.3 ± 8.3 nm. The porous hollow spheres with netlike shell were embedded to resin and cut by ion milling for evaluation of shell thickness. Figure 3.23 shows SEM images of cross-section surface of porous hollow spheres fabricated with supercritical ethanol treatment at 673 K and 10 MPa. Shell thickness was evaluated to be 10.5 ±3.0 from SEM images. I obtained porous hollow spheres with nano-sized shell by supercritical ethanol treatment.

Figure 3.24 show TG-DTA curves of silica particles modified with PDDA and the FePt-nanoparticle/PDDA/silica core-shell particles treated with SCE at 673 K and 10 MPa for 1.5 h. The decomposition of PDDA molecules shows endothermic peak in DTA curve at 573 K and weight loss in TG curves from 553 K. In the DTA curve of PDDA-modified silica particles as shown in Figure 3.24(A), endothermic peak was observed at 580 K. In contrast, there was no endothermic peak in the DTA of the FePt-nanoparticle/PDDA/silica core-shell particles treated with SCE as shown in Figure 3.24(B). These result showed PDDA molecules on the silica particles were completely decomposed by SCE treatment at 673 K and 10 MPa for 1.5 h, and the netlike structure was maintained only by FePt alloy.

XRD patterns of the core-shell particles treated with supercritical ethanol at various temperatures were shown in Fig. 3.25, and their crystallite size was summarized in Fig. 3.26. All of the samples showed a typical XRD pattern of FePt, and the diffraction from

iron oxide was not observed. The oxidation of FePt was not occurred in SCE treatment. Crystallite size of the sample treated with subcritical ethanol at 473 K was not much changed. The crystallite size was increased after SCE treatment at 573-673 K, and it was increased according to thermal fusion of FePt nanoparticles and increase of treatment temperatures. The intensities of the superlattice diffraction peaks at $2\theta = 24^{\circ}$ and 33° were increased with the increase of the reaction temperature. The XRD pattern of FePt netshell fabricated at 673 K clearly showed that the FePt netlike shell possessed an fct structure, which is the atomically ordered phase.

Figure 3.27 shows Magnetization curves of the capsules treated with supercritical ethanol at (a) 473 K and (b) 673 K. These curves were measured at 300 K in applied magnetic fields from 9 to -9 T. The magnetization at 9 T of the sample fabricated at 473 K was 9.5 emu/g, and the magnetic characterization revealed that the sample treated at 473 K exhibited superparamagnetic behavior at 300 K. In contrast, the porous spheres fabricated at 673 K had coercivity at 300 K. The porous hollow spheres fabricated at 673 K exhibited ferromagnetic behaviors at room temperature. The coercinity and magnetization at 9 T for the samples fabricated at 673 K was 8000 Oe and 26.2 emu/g, respectively.

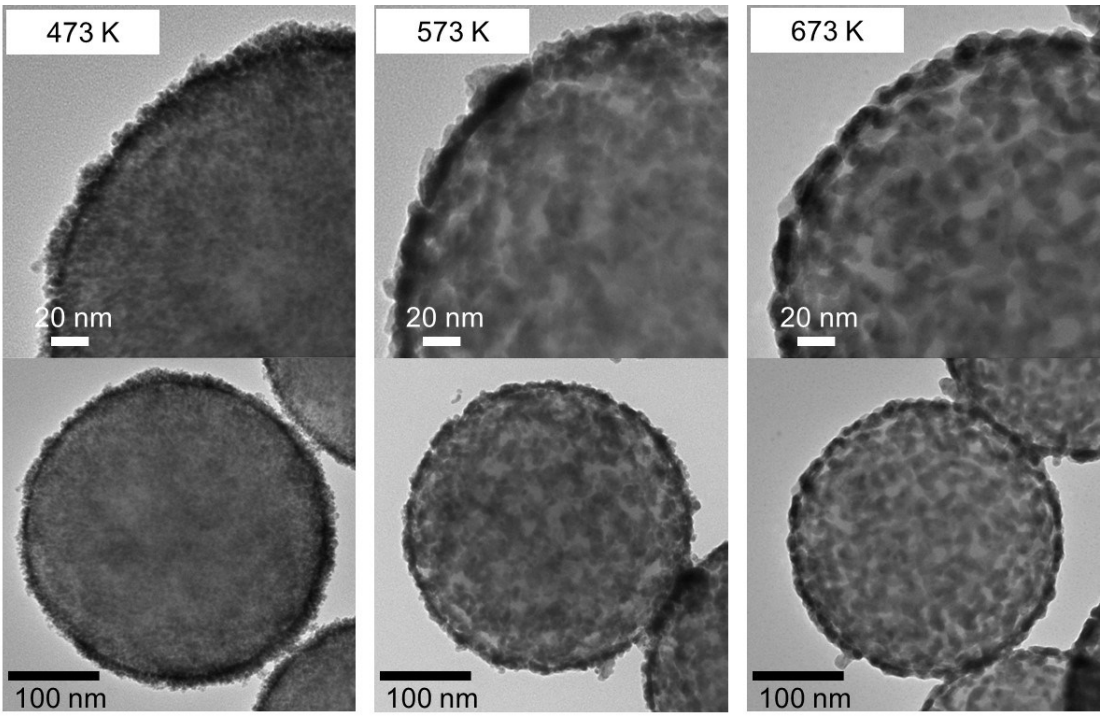

Figure 3.18 TEM images of the FePt-nanoaprticle/PDDA/silica core-shell particles treated with subcritical or supercritical ethanol at 473-673 K and 10 MPa for 90 min.

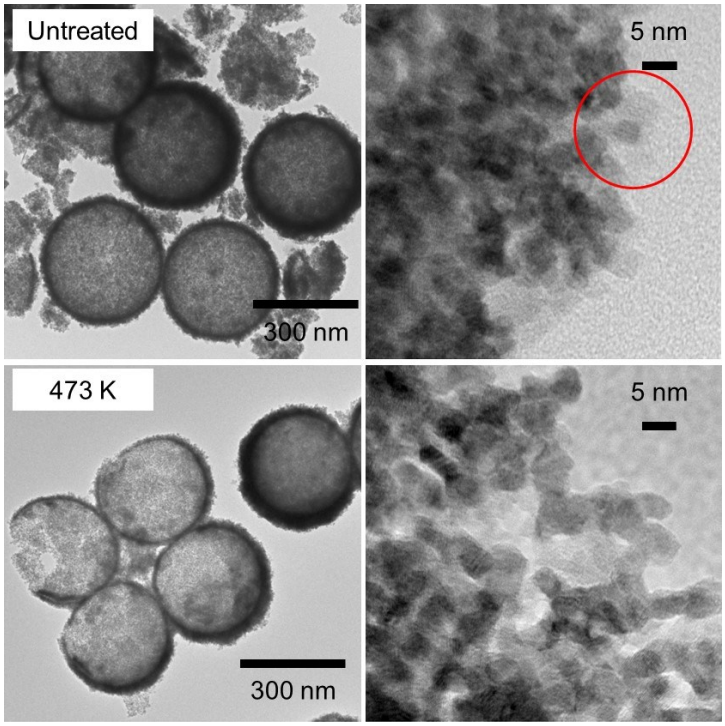

Figure 3.19 TEM images of the FePt-nanoaprticle/PDDA hybrid capsules and hollow spheres fabricated by SCE treatment at 473 K and 10 MPa for 90 min and dissolution of silica particles.

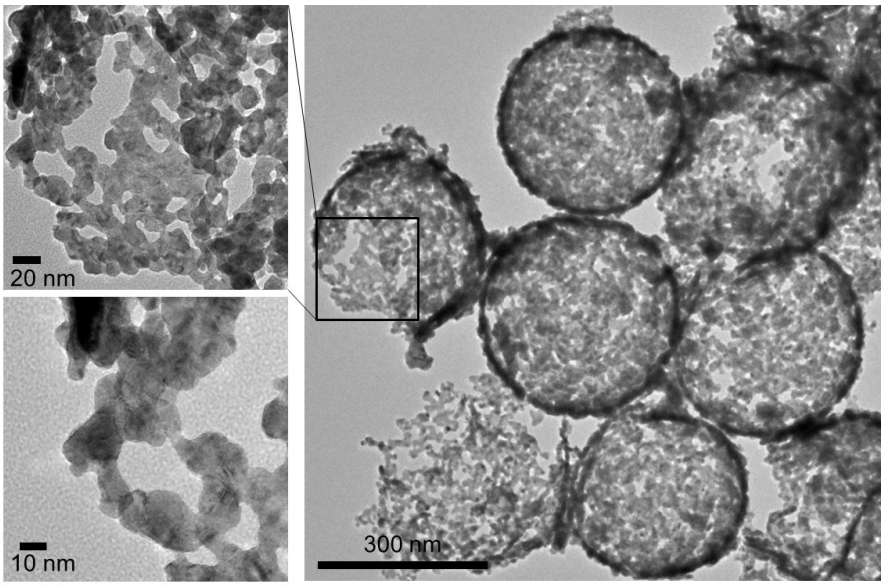

Figure 3.20 TEM images of the porous hollow spheres fabricated by SCE treatment at 573 K and 10 MPa for 90 min and dissolution of silica particles.

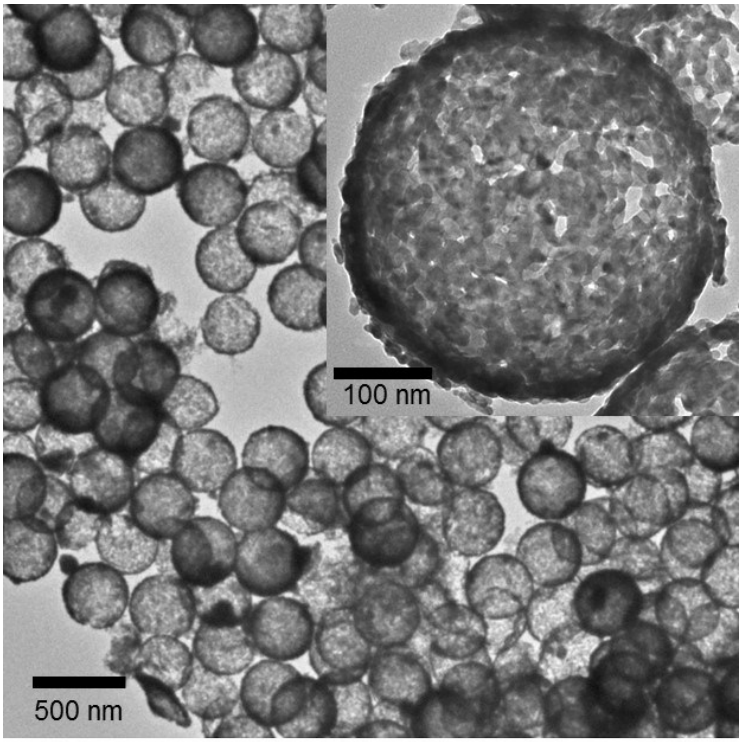

Figure 3.21 TEM images of the porous hollow spheres fabricated by supercritical ethanol treatment at 673 K and 10 MPa for 90 min and dissolution of silica particles.

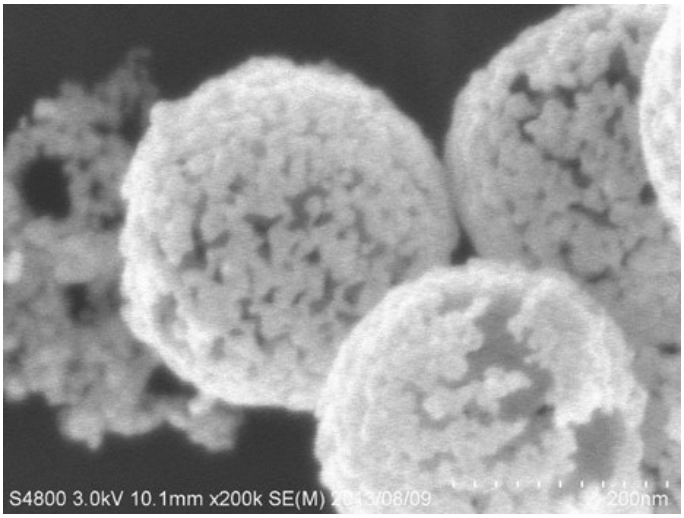

Figure 3.22 SEM image of the porous hollow spheres fabricated by supercritical ethanol treatment at 673 K and 10 MPa for 90 min and dissolution of silica particles.

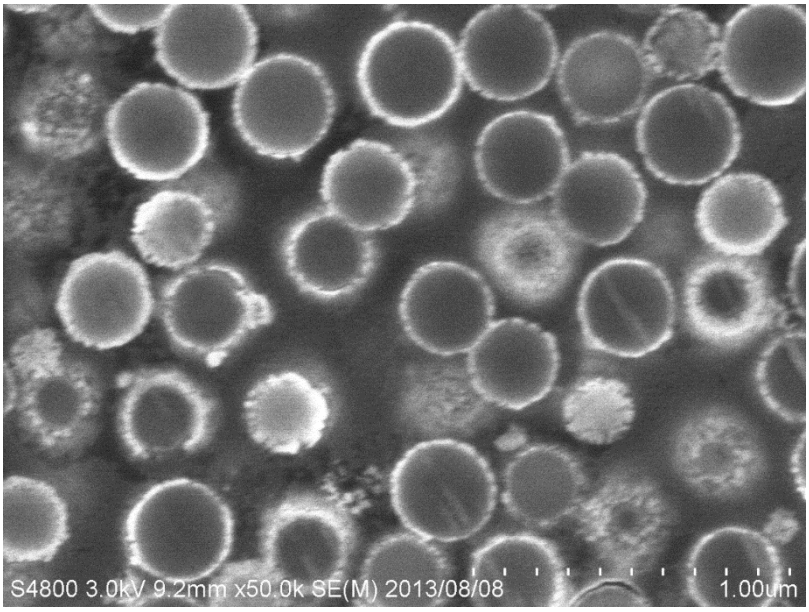

Figure 3.23 SEM image of cross-section surface of porous hollow spheres fabricated with supercritical ethanol treatment at 673 K and 10 MPa

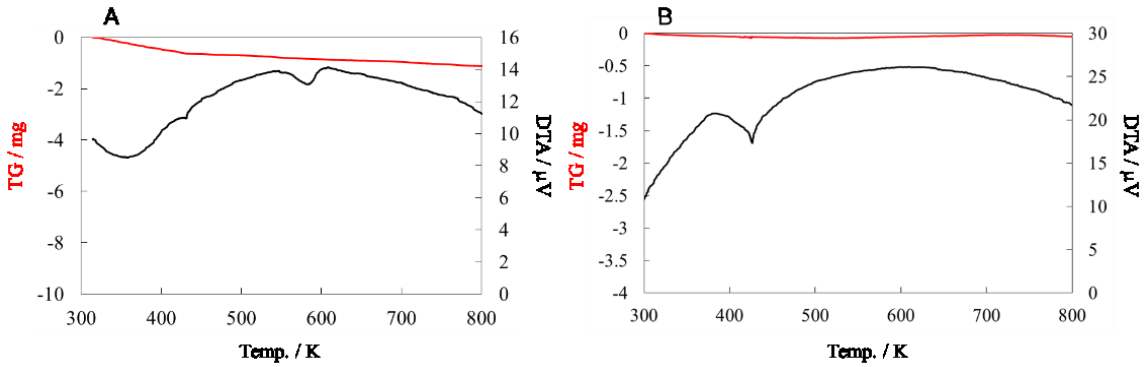

Figure 3.24 TG-DTA curves of (A) silica particles modified with PDDA and (B) the FePt-nanoparticle/PDDA/silica core-shell particles treated with SCE at 673 K and 10 MPa for 1.5 h.

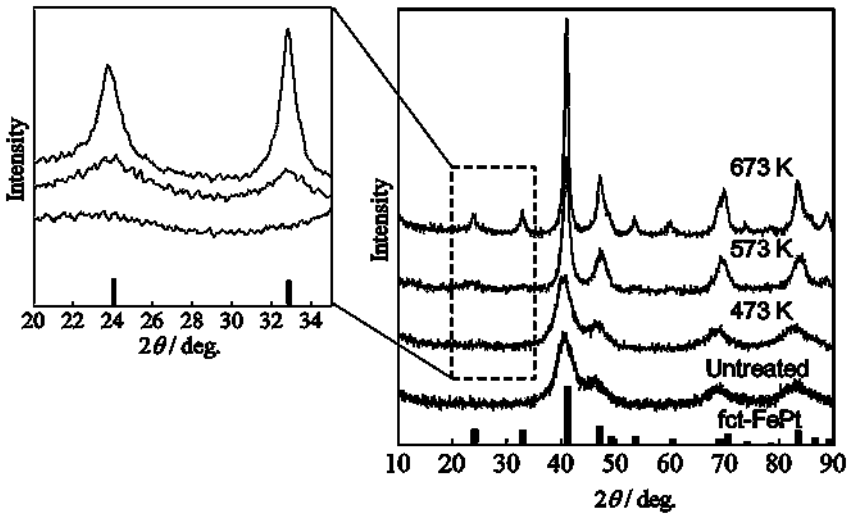

Figure 3.25 XRD patterns of the FePt-nanoaprticle/PDDA/silica core-shell particles and the FePt-nanoaprticle/PDDA/silica particles treated with subcritical or supercritical ethanol at 473-673 K and 10 MPa for 90 min.

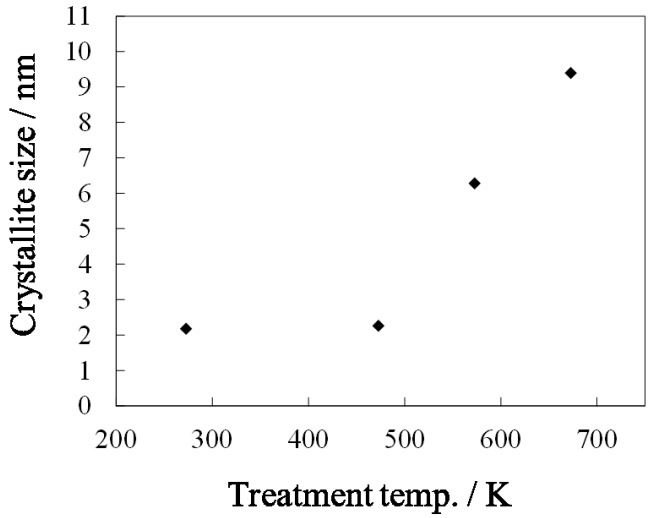

Figure 3.26 Crystallite size of the FePt-nanoaprticle/PDDA/silica core-shell particles and the FePt-nanoaprticle/PDDA/silica particles treated with supercritical ethanol at various temperatures vs. treatment temperature

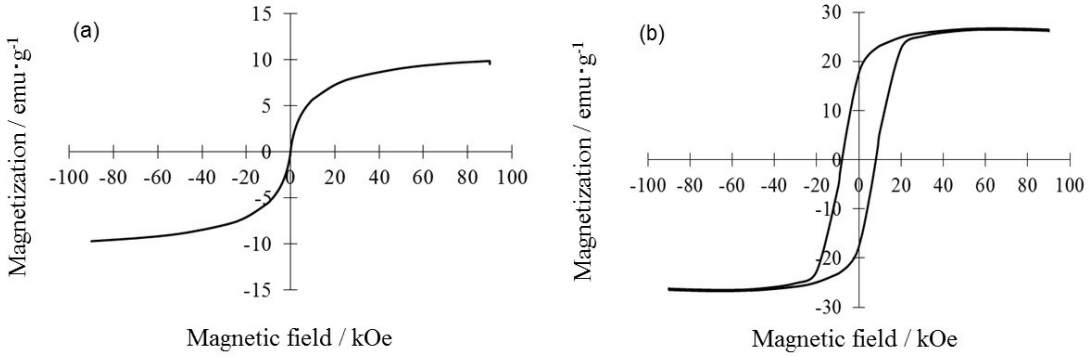

Figure 3.27 Magnetization curves of the porous spheres fabricated by SCE treatment at (a) 473 K and (b) 673 K. These curves were measured at 300 K in applied magnetic fields from 9 to -9 T. Silica particles were removed from the core-shell particles treated at 473 K and 673 K. Silica particles were remained in the sample treated at 573 K.

3.5.2 Dependence on treatment time

FePt-nanoparticle/PDDA/silica core-shell particles were treated by SCE treatment at 573 K and 10 MPa for 30-210 min. Figure 3.28 shows TEM images of untreated FePt-NPs/PDDA/silica core-shell particles and SCE-treated particles at 573K and 10 MPa by changing treatment time from 30 to 210 min. Fusion of FePt nanoparticles were observed in the sample treated for 60 min, there was no significant difference in their morphologies in the samples treated for 90-210 min. Figure 3.29 shows XRD patterns of untreated FePt-nanoparticle/PDDA/silica core-shell particles and SCE-treated particles at 573K and 10 MPa by changing treatment time from 30 to 210 min, and their crystallite size was summarized in Figure 3.30. Crystallite size was little increased after treatment for 30 min, and the crystallite size was increased with the increase of time. The intensities of the superlattice diffraction peaks at $2\theta = 24^{\circ}$ and 33° were increased with the increase of treatment time.

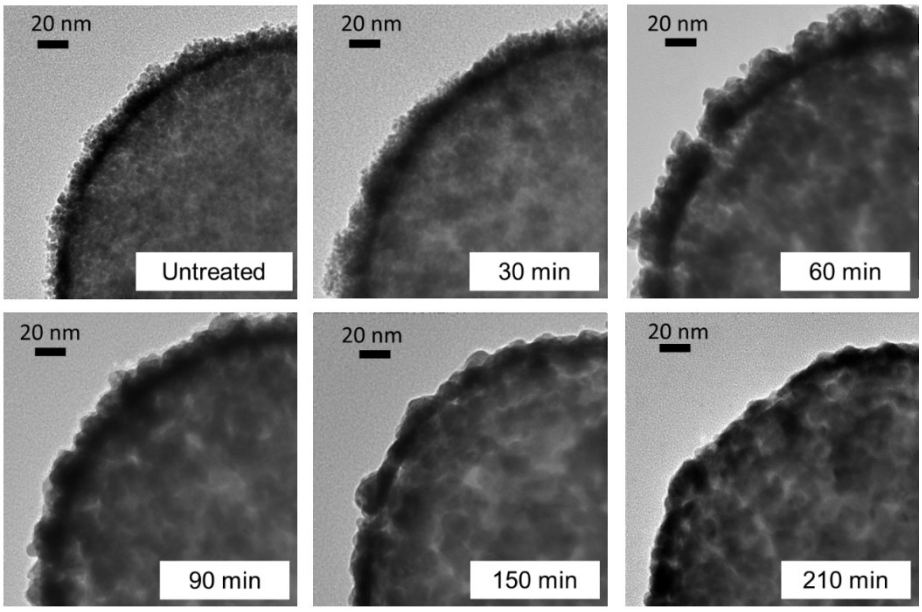

Figure 3.28 TEM images of untreated FePt-nanoparticle/PDDA/silica core-shell particles and SCE-treated particles at 573K and 10 MPa by changing treatment time from 30 to 210 min

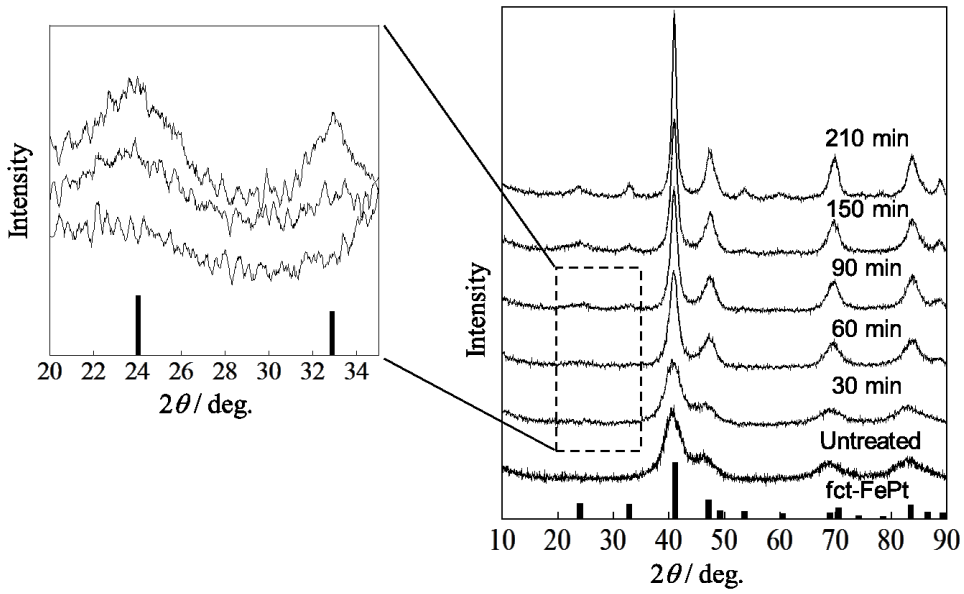

Figure 3.29 XRD patterns of untreated FePt-nanoparticle/PDDA/silica core-shell particles and SCE-treated particles at 573K and 10 MPa by changing treatment time from 30 to 210 min

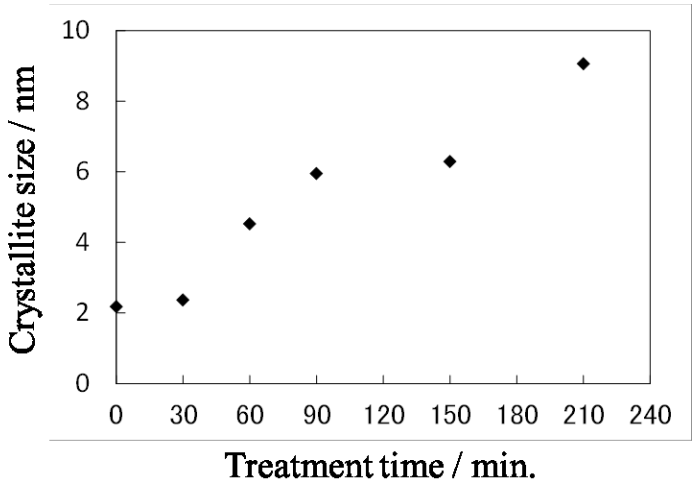

Figure 3.30 Treatment time dependence of crystallite size calculated from XRD patterns shown in Fig.3.29.

3.5.3 Dependence on pressure

FePt nanoparticle/PDDA/silica core-shell particles were treated with SCE at 573 K for 90 min. Reaction pressure was changed from 10 MPa to 31 MPa. Figure 3.31 shows TEM images of the netlike shell fabricated by SCE treatment at 10 MPa and 31 MPa. There was no significant difference between their morphology. XRD patterns of these samples were shown in Figure 3.32, and their crystallite size was summarized in Table 3.9. Two samples showed a typical XRD pattern of FePt and there was no difference between them. The crystallite size was slightly increased in the increase of the reaction pressure. These results suggests the increase of reaction pressure from 10-31 MPa does not have a significant effect on their morphology and structure in the fused shell.

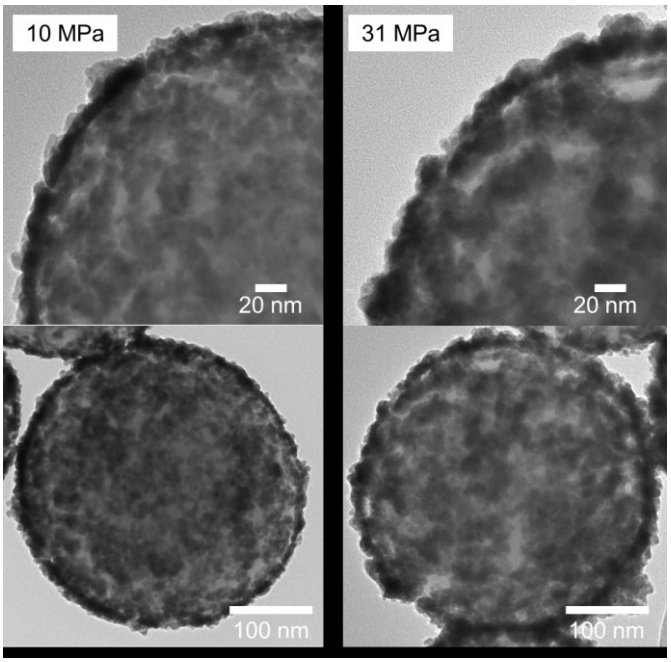

Figure 3.31 TEM images of the netlike shell fabricated by SCE treatment at 10 MPa and 31 MPa at 573 K.

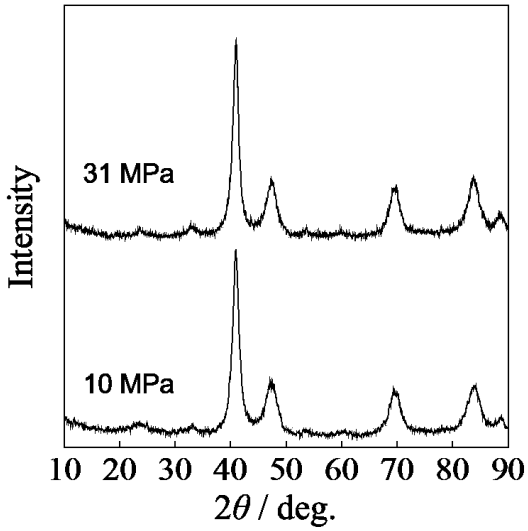

Figure 3.32 XRD patterns of the porous spheres fabricated by SCE treatment at 10 MPa and 31 MPa.

Table 3.9 Crystallite size of the porous spheres fabricated by SCE treatment at 10 MPa and 31 MPa calculated from their XRD patterns as shown in Fig. 3.32.

pressure	Crystallite size (nm)
10 MPa	6.3
31 MPa	6.7

3.6 Dry and liquid phase sintering of the FePt-nanoparticle/PDDA/silica particle

To get information for the formation of netlike shell, FePt-nanoparticle/PDDA/silica core-shell particles were put on a porcelain plate and sintered in electronic furnace at 573 K for 1.5 h under Ar/H_2 gas flow of 190 ml/min. Additionally, FePt-nanoparticle/PDDA/silica core-shell particles were heated in polyethylene glycol (PEG) at 573 K for 1.5 h. Figure 3.33 shows TEM images of the samples heated in various condition after dissolving silica template particles by NaOH (aq.). In all samples, FePt nanoparticles were thermally- fused. However, their morphologies were little different. Netlike structure was observed in FePt nanoparticles heated in supercritical ethanol and on a porcelain plate, and pore size of the netlike structure fabricated by supercritical ethanol treatment was larger than that of others. Figure 3.34 shows XRD patterns of FePt-nanoparticle/PDDA/silica core-shell particles heated in supercritical ethanol, PEG and on the porcelain plate at 573 K. All of the samples showed a typical XRD pattern of FePt, and superlattice diffraction peaks at $2\theta = 24^\circ$ and 33° were clearly observed in the samples heated in supercritical ethanol. The superlattice diffraction peaks in the XRD patterns of the samples sintered at 573 K was very week compared with the samples treated with supercritical ethanol at 573 K. These results suggested supercritical ethanol treatment promoted to the transformation of FePt alloy, and the thermal fusion of FePT nanoparticles.

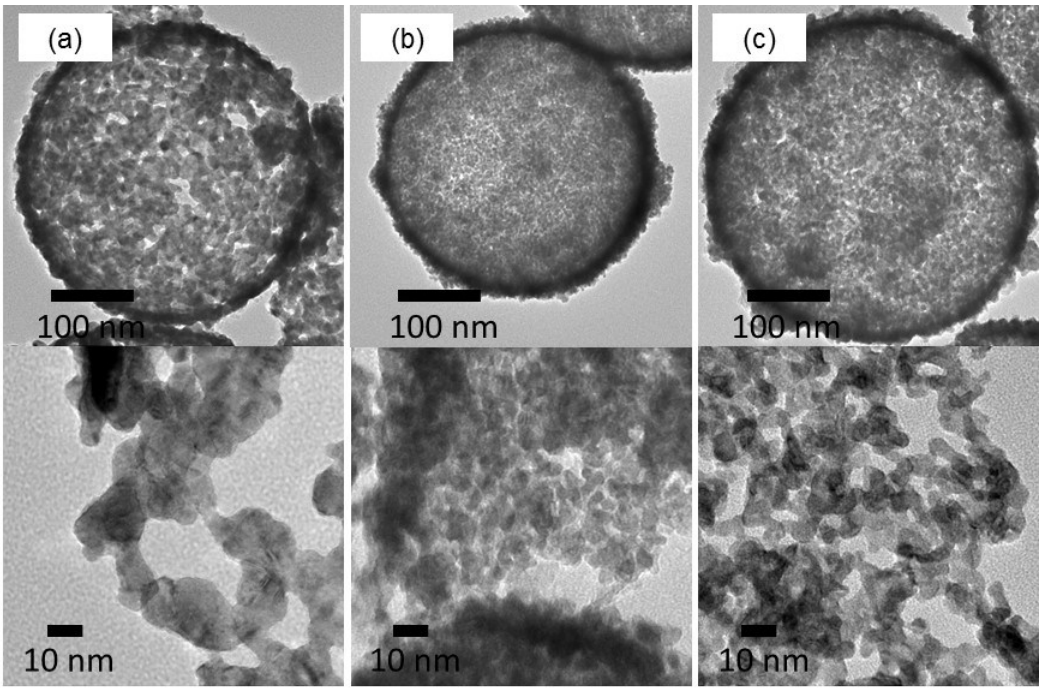

Figure 3.33 TEM images of FePt-nanoparticle/PDDA/silica core-shell particles heated in (a) supercritical ethanol at 573 K and 10 MPa (b) PEG at 573 K and (c) on the porcelain plate at 573 K in Ar/H_2 gas flow

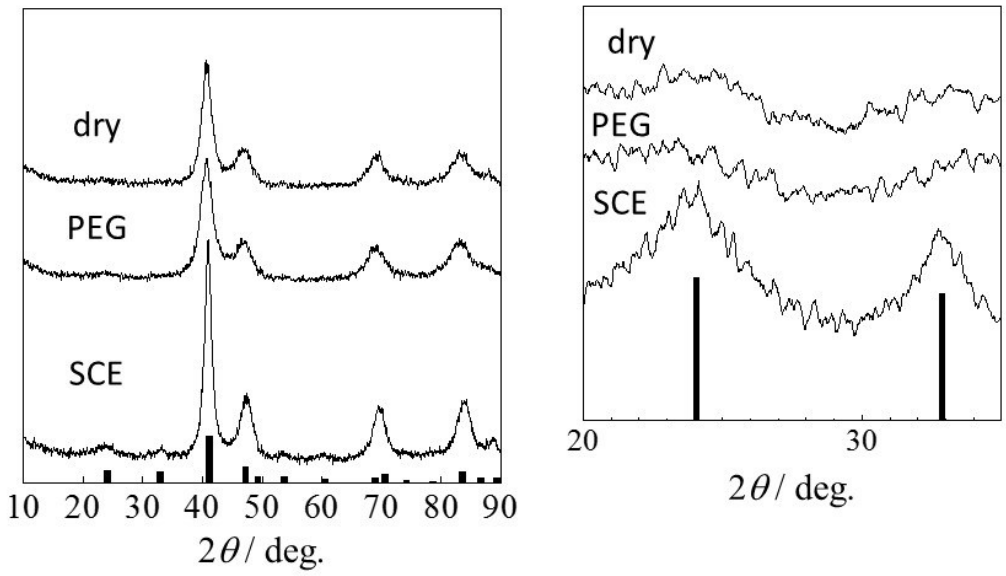

Figure 3.34 XRD patterns of FePt-nanoparticle/PDDA/silica core-shell particles heated in supercritical ethanol, PEG and on the porcelain plate at 573 K

Table 3.10 Crystallite size of FePt-nanoparticle/PDDA/silica core-shell particles heated in supercritical ethanol, PEG and on the porcelain plate at 573 K

	Supercritical ethanol	PEG	dry (Ar/H_2flow)
Crystallite size (nm)	5.9	3.5	4.0

3.7 Influence of occupancy of FePt nanoparticles on netlike structure

To investigate the influence of the occupancy of FePt nanoparticles on netlike structure in supercritical ethanol treatment, FePt-nanoparticle/PDDA/silica core-shell particles with various occupancy of FePt nanoparticles on the surface of silica template particles were treated with supercritical ethanol at 673 K and 10 MPa. Figure 3.35 shows TEM images of FePt-nanoparticle/PDDA/silica core-shell particles with various occupancy of FePt nanoparticles and FePt-nanoparticle/PDDA/silica core-shell particles treated with supercritical ethanol at 673 K and 10 MPa. The occupancy calculated by contrast in TEM images was summarized with the weight ratio of FePt precursors to silica particles in the synthesis of FePt-nanoparticle/PDDA/silica core-shell particles. The occupancy was over 100 %, pore was not observed on the shell. Netlike structure was obtained by supercritical ethanol treatment of FePt-nanoparticle/PDDA/silica core-shell particles which have 87 ± 8 % of the occupancy of FePt nanoparticles on the surface of silica particles. When the occupancy was 50 ± 10 %, FePt nanoparticles were thermally fused, but the most of FePt alloy was not connected. To investigate an influence of treatment time to the occupancy, FePt-nanoparticle/PDDA/silica core-shell particles which have 87 ± 8 % of the occupancy were treated with supercritical ethanol at 673 K and 10 MPa for 1.5 and 12.5 h. Figure 3.36 shows TEM images of FePt-nanoparticle/PDDA/silica core-shell particles which have 87 ± 8 % of the occupancy treated with supercritical ethanol at 673 K and 10 MPa for 1.5 and 12.5h. Netlike structure of FePt alloy was obtained by supercritical ethanol treatment for 1.5h. On the other hand, FePt alloy was not connected partially in the sample treated for 12.5h. This results shows the netlike structure is formed by stopping on the way to sintering of FePt nanoparticles. I think FePt nanoparticles are fused to decrease a surface energy like solid-state sintering. Therefore, for the last time, large spherical particles of FePt alloy is formed in supercritical ethanol treatment. Thus, when the occupancy of FePt nanoparticles on the surface of silica particles is low, netlike structure can be obtain by shorten the treatment time. Figure 3.37 shows TEM images of FePt-nanoparticle/PDDA/silica core-shell particles (fabricated using 100 nm of silica particles) which have 50 ± 10 % of the occupancy and the core-shell particles treated with supercritical ethanol at 673 K and 10 MPa for 0.5 and 1.5h. FePt nanoparticles treated for

0.5 h were connected in a netlike fashion. On the other hand, netlike structure of FePt alloy was not observed, and large spherical particles were formed on the surface of silica template particles in the sample treated for 1.5 h. This results suggest netlike structure can be obtained by control reaction time, even the occupancy was lower than 60 %.

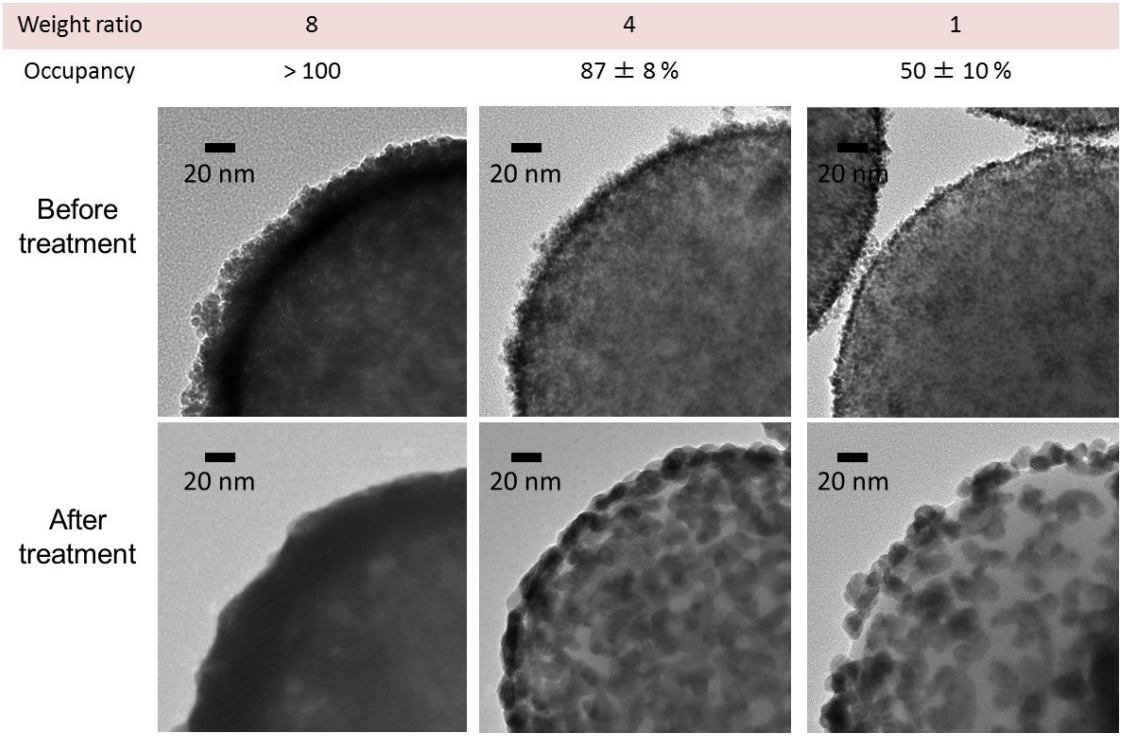

Figure 3.35 TEM images of FePt-nanoparticle/PDDA/silica core-shell particles with various occupancy of FePt nanoparticles and FePt-nanoparticle/PDDA/silica core-shell particles treated with supercritical ethanol at 673 K and 10 MPa. The occupancy calculated by contrast in TEM images was summarized with the weight ratio of FePt precursors to silica particles in the synthesis of FePt-nanoparticle/PDDA/silica core-shell particles.

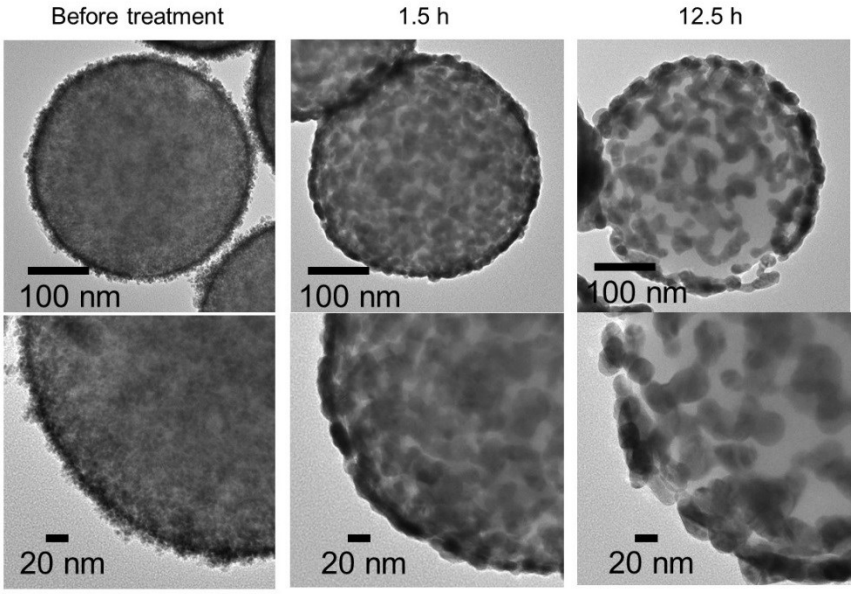

Figure 3.36 TEM images of FePt-nanoparticle/PDDA/silica core-shell particles which have 87 ± 8 % of the occupancy and FePt-nanoparticle/PDDA/silica core-shell particles treated with supercritical ethanol at 673 K and 10 MPa for 1.5 and 12.5h.

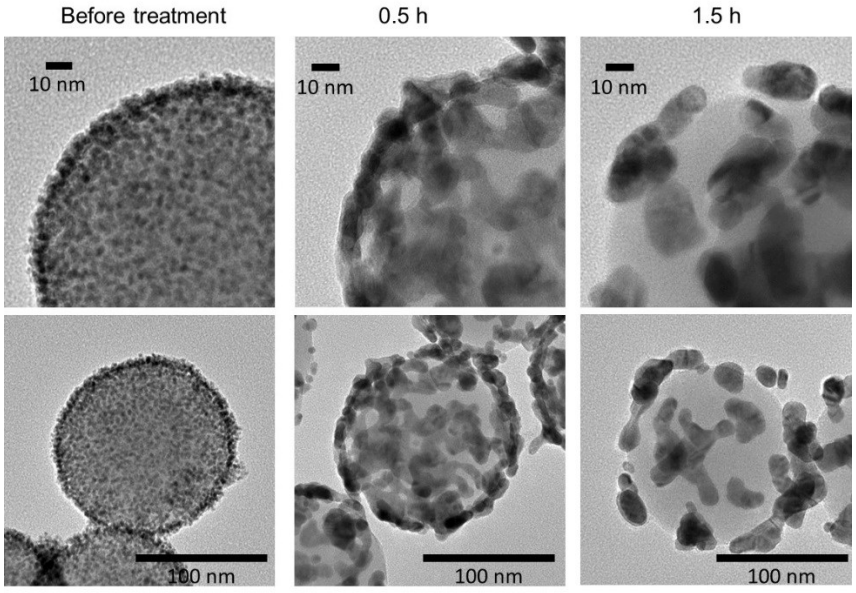

Figure 3.37 TEM images of FePt-nanoparticle/PDDA/silica core-shell particles (fabricated using 100 nm of silica particles) which have 50 ± 10 % of the occupancy and the core-shell particles treated with supercritical ethanol at 673 K and 10 MPa for 0.5 and 1.5h.

3.8 Influence of polymer layer on netlike structure of FePt alloy

To investigate the influence of polymer layer on the netlike structure, oleic acid (OAc) and oleylamine (OAm) were used for fabricating FePt-nanoparticle/silica core-shell particles, and FePt-nanoparticle/OAc/OAm/silica core-shell particles were treated with SCE. The FePt-nanoparticle/OAc/OAA/silica core-shell particles were fabricated in a manner similar to the fabrication of FePt-nanoparticle/PDDA/silica core-shell particles. Figure 3.38 shows TEM images of the FePt-nanoparticle/OAc/OAm/silica core-shell particles and FePt-nanoparticle/OAc/OAm/silica core-shell particles treated with SCE at 673 K and 10 MPa for 1.5 h. 3-5 nm of FePt nanoparticles were accumulated to silica particles modified with OAc and OAm as shown in Figure 3.38. The accumulation of FePt nanoparticles was not uniformly but the silica template particles were completely covered with FePt nanoparticles. After SCE treatment, FePt nanoparticles were thermally fused and large particles were observed on silica particles. Netlike structure was not obtained by SCE treatment of FePt-nanoparticle/OAc/OAm/silica core-shell particles. OAc and OAm would be adsorbed to the surface of silica particles and FePt nanoparticles by single point adsorption compared with PDDA molecules. FePt nanoparticles bound by OAc and OAm to the silica template particles are easily removable from the surface of silica particles in a process of SCE treatment. Therefore, FePt nanoparticles detached from the silica template particles were thermally fused in the fluid, and accumulated to the silica particles. In contrast, PDDA molecules are adsorbed to silica template particles and FePt nanoparticles with multiple point adsorption. FePt nanoparticles are not detached from the surface of silica particles in the process of SCE treatment, and PDDA molecules are decomposed after thermal fusion of FePt nanoparticles. Thus, netlike shell with FePt alloy can be obtained by SCE treatment of FePt-nanoparticle/PDDA/silica core-shell particles. I think that a stable adsorption between FePt nanoparticles and template particles is necessary to obtain the netlike structure of FePt alloy in SCE treatment, and a polymer layer play an important role in the formation of the netlike structure.

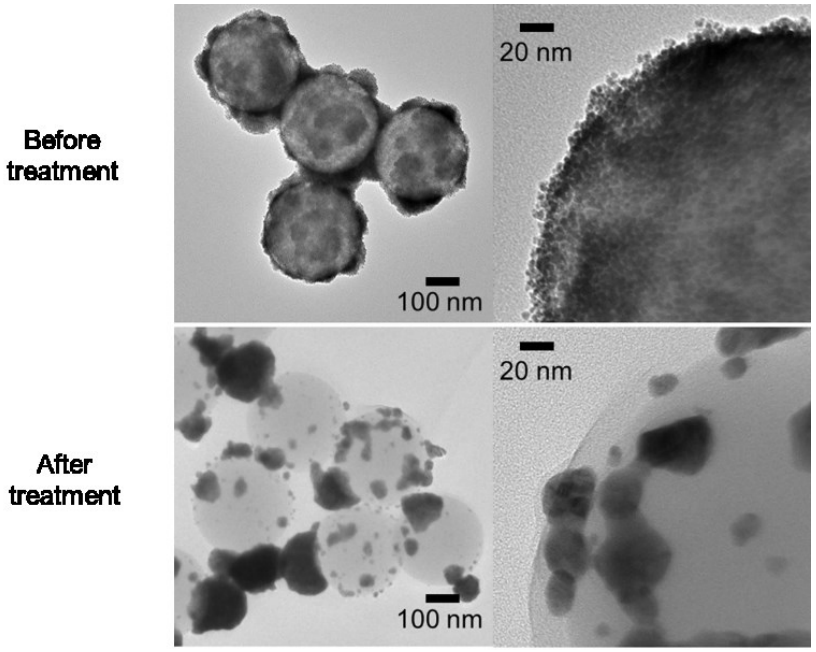

Figure 3.38 TEM images of the FePt-nanoparticle/OAc/OAm/silica core-shell particles and FePt-nanoparticle/OAc/OAm/silica core-shell particles treated with SCE at 673 K and 10 MPa for 1.5 h

3.9 Formation mechanism of netlike structure in supercritical ethanol treatment

Figure 3.39 shows schematic illustration of formation mechanism of netlike structure in supercritical ethanol treatment. FePt nanoparticles are fused to decrease surface energy between contacted FePt nanoparticles. Atomic diffusion occurs isotropically in the particles contacted in three dimensions. Therefore, the shell thickness depends on a shell thickness of FePt-nanoparticles/silica core-shell particles. FePt nanoparticles not contacted are not fused. So the pore on the FePt-nanoparticles/silica core-shell particles become larger. In the supercritical ethanol treatment, silica template particles are not dissolved. Since the motion of the FePt particles is suppressed on the template particles, netlike structure can not be maintained in progress of sintering. For long time treatment, FePt nanoparticles become one spherical particle so as to minimize the surface energy. I thought netlike structure was formed by stopping on the way to sintering of FePt nanoparticles.

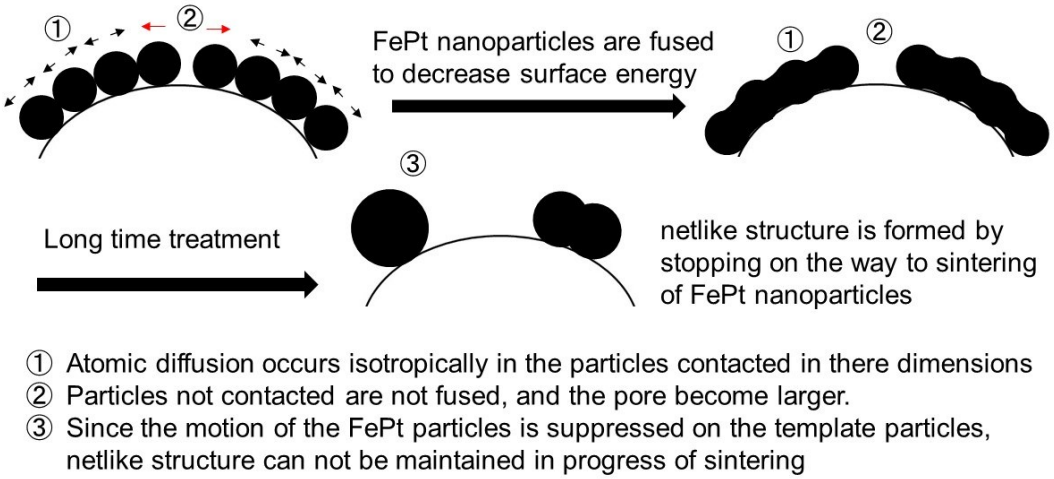

Figure 3.39 Schematic illustration of formation mechanism of netlike structure in supercritical ethanol treatment

3.10 Conclusion

In this chapter, I fabricated two types of porous hollow spheres. One was an inorganic-organic hybrid porous capsule composed of FePt nanoparticles and PDDA molecules fabricated by dissolution of silica template particles from FePt-nanoparticle/PDDA/silica core-shell particles by using NaOH aqueous solution. The shell thickness of the hybrid capsules was 10 nm at the maximum. These hybrid shells had many pores ($d < 6$ nm) and were stable in water. The amount of FePt nanoparticles accumulated on PDDA-modified silica particles could be easily controlled by changing the amount of precursors added to the synthesis of FePt-nanoparticle/PDDA/silica core-shell particles. FePt nanoparticles accumulated on the polymer molecules would anchor the polymer molecules resulting in the 3D structure being retained in the hybrid capsules. Therefore the decrease of the FePt nanoparticles resulted in a decrease of the mechanical strength of the hollow spheres, because the strength of their 3D structure depended on the binding force between PDDA and the FePt nanoparticles; thus, hollow spheres composed of FePt nanoparticles and PDDA molecules with a pore larger than 6 nm could not be obtained.

The second type of the hollow spheres was porous hollow spheres composed of FePt netlike structure fabricated by supercritical fluid treatment of the FePt-nanoparticle/PDDA/silica core-shell particles. FePt nanoparticles were thermally fused during the supercritical water treatment at 673 K, and porous hollow spheres with FePt netlike shell were obtained, but the magnetization was decreased because Fe was dissolved out into the supercritical water and then oxidized during the supercritical water

treatment. Despite the ratio of FePt precursors to silica particles being too low to obtain hybrid capsules after dissolution of the silica particles, and only a small amount of FePt nanoparticles being adsorbed on the PDDA-modified silica particles, the supercritical water treatment fused the FePt nanoparticles resulting in porous capsules with the 3D netlike structure of the FePt alloy. The total diameter of the porous hollow spheres with FePt netlike shell was about 90 nm and the shell thickness was about 3 nm. In addition, there were large pores in the shell of the porous hollow spheres with FePt netlike shell that had a diameter up to 10 nm. The magnetization at 9 T of the porous hollow spheres was 12.4 emu/g, and the magnetic characterization revealed that porous hollow spheres exhibited superparamagnetic behavior at 300 K.

Furthermore, I obtained porous hollow spheres with FePt netlike shell which shows ferromagnetic at 300 K treated by supercritical ethanol. FePt nanoparticles was fused by SCE treatment at 473 K which is lower temperature than synthesis temperature (503 K), and morphology and magnetic property were changed in the increase of treatment temperature and time. The porous hollow spheres fabricated by supercritical ethanol treatment at 673 K had a coercivity of 8000 Oe and the magnetization at 9 T of the porous hollow spheres was 26.2 emu/g. Pore size were evaluated to 18.3 ± 8.3 from SEM images, and shell thickness was evaluated to be 10.5 ±3.0 nm from SEM images of cross-section surface. The occupancy of FePt-nanoparticle to the surface of silica template particles is strongly effected to the morphology of the shell structure fabricated by supercritical ethanol treatment. The netlike structure would be formed by stopping on the way to sintering of FePt nanoparticles. Therefore, the morphology of shell can be tuned by control of treatment temperature and time.

Stable adsorption between FePt nanoparticles and template particles is necessary to fabricate the netlike structure of FePt alloy in a process of supercritical fluid treatment. PDDA layer in the FePt-nanoparticle/PDDA/silica core-shell particles play an important role in the fusion of FePt nanoparticles and formation of the netlike structure.

I also fabricated the FePt netlike shell by dry sintering on a porcelain plate in Ar/H_2 gas. FePt nanoparticles were thermally fused by sintering at 573 K in Ar/H_2 gas. The superlattice diffraction peaks in the XRD patterns of the samples sintered at 573 K was very week compared with the samples treated with supercritical water treatment at 573 K. These results suggest supercritical ethanol treatment promoted to the transformation of FePt alloy.

Reference

[1] A. Morozan, B. Jousselme, S. Palacin, Energy Environ. Sci., 4, 2011, 1238-1254
[2] J. Kim, Y. Lee, S. Sun, J. AM. CHEM. SOC. 9 VOL. 132, NO. 14, 2010 4997
[3] Zhang Y, Erkey C. J Supercritical Fluids 2006, 38, 252-67.
[4] Reverchon E, Adami R. J Supercritical Fluid 2006, 37, 1-22.
[5] Y. Kitamoto, J. He, Electrochim. Acta, 54, 2009, 5969–5972
[6] T. Fuchigami, et.al. Langmuir 2011, 27, 2923-2928
[7] T. Iwamoto, Y. Kitamoto, N. Toshima, Phys. B, 404, 2009, 2080–2085
[8] B. Jeyadevan, K. Urakawa, A. Hobo, N. Chinnasamy, K. Shinoda, K. Tohji, D. D. J.
[9] Matson DW, Petersen RC, Smith RD. J Mater Sci 1987, 22, 1919-28.
[10] Nakamura M, Katagiri K, Koumoto K. J Colloid Interface Sci 2010, 341, 64-68
[11] Abe M, Nishio N, Hatakeyama M, Hanyu N, Tanaka T, Tada M, et al. J Magn Magn Mater 2009, 321, 645-649
[12] Zhang C, Zhang H, Du B, Hou R, Guo S. J Colloid Interface Sci 2012, 368, 97-106
[13] Zhang Y, Huang Z, Tang F, Ren J. Thin Solid Films 2006, 515, 2555-2561
[14] A. R. Bazaev et al., International Journal of Thermophysics, Vol. 28, No. 1, 2007
[15] H. E. Dillon and S. G. Penoncello, Int. J. Thermophys. 25:321 (2004).

Chapter 4

Application to magnetically guided drug delivery system

4.1 Introduction

Magnetically guided drug delivery system (MG-DDS) is one of the active-targeted DDSs which have potential to effectively exert therapeutic effects on tumors with both pinpoint precision and minimal invasion. Among such systems, the use of magnetic materials as drug carriers is one of the most promising approaches [1-3]. Magnetic capsules are currently being developed in the field of biotechnology as carriers of therapeutic agents in MG-DDS because they have unique properties such as a hollow structure, low material density, and magnetism. The shells of these magnetic capsules are usually composed of magnetic inorganic and/or organic materials such as Fe_3O_4, $CoFe_2O_3$, block copolymers, silica or layer-by-layer assemblies of polyelectrolytes [4-16] In previous studies, the shells of these capsules have been too thick (> 20 nm) to afford sufficient internal space when applied to nano-scale drug delivery systems (nano-DDSs) targeting cancer lesions [17-20]. In nano-DDSs targeting cancer tissue, the size of the carrier must be between several tens of nanometers and 200 nm for avoiding the elimination of carriers after intravenous administration [17-20]. A thinner shell is therefore required to increase the loading capacity for biomedical agents and to decrease the amount of magnetic components administered to human bodies while still adhering to the size limitations applicable to nano-DDSs.

A shell structure which can load a drug agent to hollow space and release it from the internal space is needed to apply a magnetic capsule to MG-DDS. Typically, reagents are involved in capsules and release in response to an environmental trigger such as a change in pH, temperature, ionic strength and/or enzyme concentration [21-24]. Porous hollow spheres with a FePt netlike nanoshell (FePt capsules) fabricated in Chapter 3 have a lot of large pores in the nanoshell. The large pores will effectively work for loading and releasing medical agents. The drug agents can move from solution to the internal space by concentration diffusion as shown in Fig. 4.1. However, the drug agents easily come out from their internal space through the large pores. A lipid bilayer is used to avoid the leakage of drugs and the lipid membrane has a function for releasing the drug agents [25].

In this chapter, I fabricated lipid-coated capsules containing anti-cancer drug and demonstrated an applicability of porous hollow spheres with the FePt netlike nanoshell

to MG-DDS *in vitro* cytotoxicity assay using cancer cells. The cytotoxicity assay is used to investigate how toxic a chemical compound is to cells.

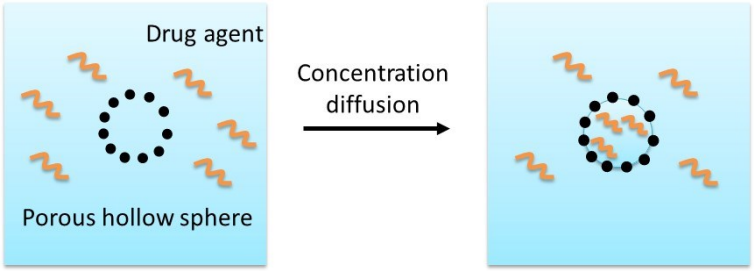

Figure 4.1 Schematic illustration of drug loading by concentration diffusion

4.2 Experimental

4.2.1 Fabrication of porous hollow spheres with FePt netlike nanoshell

FePt capsules were fabricated by the supercritical water treatment of the FePt-nanoparticle/PDDA/silica core-shell particles. The average size of the silica template particles was 100-200 nm or 250-350 nm. The aqueous dispersion (4 ml) of the core-shell particles was put into a reaction cell. The reaction cell of 11 ml was heated in an electric furnace and kept at 673 K for 3.5 h. The pressure in the reaction cell was about 37 MPa calculated from the volume of the aqueous dispersion and temperature. After rapid cooling to room temperature by putting the reaction cell into a large water bath, the FePt capsules were obtained as powder samples by centrifuging and drying procedures.

4.2.2 Preparation of lipid-coated FePt capsules containing anti-cancer drug

Lipid-coated FePt capsules containing doxorubicin (FePt-Dox) were fabricated in a manner similar to the fabrication of lipid-coated magnetic nanocrystals [1]. One milliliter of an aqueous solution of doxorubicin (5 mg/ml) was mixed with the FePt capsules (2 mg) in a pear shaped flask. Then this mixture was evaporated so as to remove the air in the FePt capsules and fill them with doxorubicin. The FePt capsules containing doxorubicin were mixed with 1 ml of egg phosphatidylcholine/chloroform (2 mg/ml). This mixture was stirred vigorously with a vortex-mixer, then, the mixture was stirred in an ultrasonic bath and the chloroform was evaporated. Finally, an aqueous dispersion of lipid-coated FePt-Dox was obtained by washing and dialysis with water.

4.2.3 Magnetic separation and fluorescence image of FePt-Dox

Doxorubicin can be fluorescently detected and quantified (excitation/emission wave length: 510 nm/550 nm). FePt-Doxs were dispersed in distilled water (1 mg/ml) and 200 μl of the dispersion were introduced into a well of a 96 well plate. After a NdFeB magnet (0.2 T) was directly attached under the well (magnet-attracted well) for 5 min, 100 μl of their supernatants were transferred to another well and the fluorescent intensity of these wells were compared.

4.2.4 *In vitro* cytotoxic assay

The cytotoxic effect of the magnetically guided FePt-Dox was investigated in cancer cell lines MKN-74 and RERF-LC-A1. Cells (1×10^4) were incubated with FePt-Dox or doxorubicin alone under a magnetic field (0.2 T). Four days after the initiation of the treatment, the antitumor effect was assessed by the colorimetric tetrazolium salt cleavage assay using 2-(2-methoxy-4-nitrophenyl)-3-(4-nitrophenyl)-5 5-(2,4-disulfophenyl)-2H-tetrazolium) (DOJIN, Kumamoto, Japan) [26,27].

4.2.5 Fluorescence image of magnetically guided FePt-Dox in cytotoxic assay

The accumulation of the FePt-Dox was investigated in the cancer cell line KATO-III. Cells (5×10^3) were cultured for 12 h in a well of a 96 well plate and then culture medium was removed. PBS containing FePt-Doxs (the final concentration of DOX: 1 mg/ml) were introduced into a well of a 96 well plate. Cells were incubated with FePt-Dox and a NdFeB magnet (0.2 T) was directly attached under the well for 5 min. Six hours after the initiation of the treatment, cells were washed with PBS and fixed with 10% formaldehyde/PBS. Ultimately, the cellular uptake of Dox was evaluated with fluorescent microscopy (excitation/emission wavelength: 510/550 nm).

4.3 Formation and morphology of lipid-coated FePt-Dox

Air and solvent were evacuated from the FePt capsules and their hollow space was filled with an aqueous anti-cancer drug, doxorubicin. Doxorubicin has been clinically used for the treatment of a wide range of cancers, however doxorubicin exerts dose- dependent adverse side-effects such as lethal cardiotoxicity. Therefore, DDS targeting actively tumors is a promising approach to minimizing the doxorubicin concentration in normal tissues. The surface of the FePt capsules containing doxorubicin was coated with egg phosphatidylcholine to prevent the leakage of doxorubicin. Figures 4.2 (a) and (b) show the lipid-coated FePt-Dox when the silica particles of 0.32 μm were used. The hollow space of the FePt capsules was not clearly observed, and an egg phosohatidylcholine

membrane of approximately 3 nm in thickness was observed on top of the FePt netlike shell as shown in Figs. 4.2 (a) and (b). To confirm incorporation of doxorubicin in the FePt capsules, I evaluated fluorescence of doxorubicin in magnetic capsules collected by a magnet with a fluorescence microscopy. The magnetically attracted well (A in Fig. 4.2 (c)) displayed strong fluorescence, however no fluorescence was detected in the supernatant (B in Fig. 4.2 (c)). This result clearly shows that FePt capsules were filled with doxorubicin and the FePt-Dox was attracted by the NdFeB magnet.

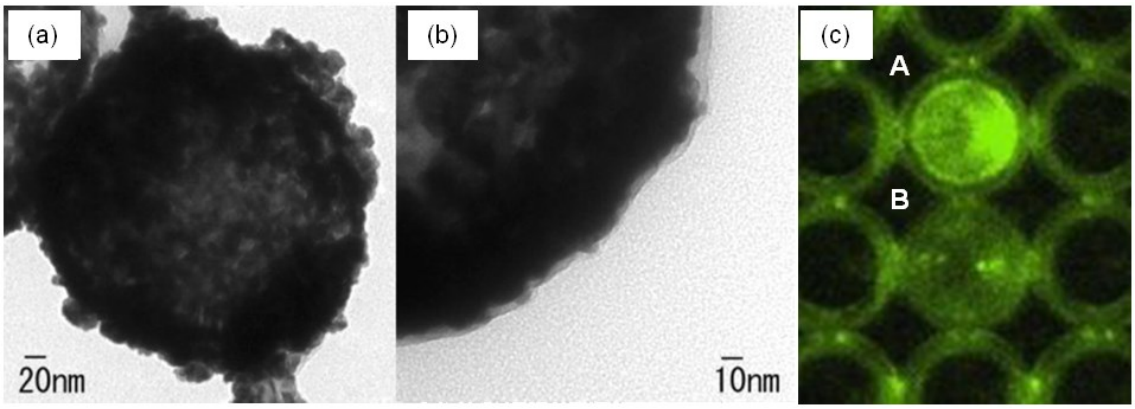

Figure 4.2 (a), (b) TEM images of a lipid-coated FePt capsule containing fluorescently detectable doxorubicin, which is aqueous fluorescence anti-cancer drug. (c) A fluorescence micrograph shows the magnetic attraction of the lipid-coated FePt-Dox.

4.4 *In vitro* anti-tumor efficiency

I further investigated the magnetically guided antitumor effect of FePt-Dox on the gastric cancer cell line MKN-74 and the lung cancer cell line RERF-LC-A1. The silica template size was 0.32 μm. The treatment and assessment schedules are summarized in Table 1. These cancer cells were incubated with doxorubicin alone or FePt-Dox as shown in Fig. 4.3. After these incubations for the indicated period, cells were washed twice with phosphate buffered saline (PBS) and fresh culture medium was introduced. Cells were cultured for a total of 4 days and the antitumor effect was measured using a cytotoxicity assay. Most importantly, magnetically guided FePt-Dox retarded 70.52% of the gastric cancer cell growth and 75.03% of the lung cancer cell growth (as shown as red bars, magnetic + in Fig. 4.3) compared with lipid capsules not containing doxorubicin. Additionally, when using lipid capsules containing the same amount of doxorubicin (1 mg/ml) (as shown by the yellow bar, magnetic (+) in Fig. 4.3) and magnetic capsules

without doxorubicin (as shown by the pink bar, magnetic (+) in Fig. 4.3), cell growth was not retarded. Furthermore, the group with FePt-Dox, but not magnetic field, did not display any antitumor effect (as shown by the red bar, magnetic (-) in Fig. 4.3). These results clearly show that the doxorubicin sealed in the FePt magnetic capsules could be magnetically guided to the targeted cancer cells and that this guidance induced the target-specific antitumor effect. These results suggest that doxorubicin was probably released from the capsules after the introduction of the FePt-Dox to the cancer cells. Overall, these FePt magnetic capsules are clearly useful as a magnetic carrier of aqueous anticancer drugs in magnetically guided DDS.

Table 1 The magnetically guided cytotoxic effect of the ferromagnetic capsules on a gastric cancer cell line, MKN-74, and a lung cancer cell line, RERF-LC-A1. MKN-74 cells and RERF-LCA1 cells were incubated with the lipid-coated FePt capsules or with the lipid capsules. These capsules contained various concentrations of doxorubicin in hollow spaces. The amount of doxorubicin entrapped in the FePt magnetic capsules was calculated from the fluorescent intensity after the lysis of the nanocomposite membrane with 0.3 N HCl-50% ethanol. The exitation/emission wave length was 510 nm/550 nm. FePt-Dox containing 1 mg/ml of doxorubicin was prepared (red) by dilution of the cell culture medium. Ten ml of this diluted FePt-Dox and 3 ml of chloroform were vigorously mixed and centrifuged to remove the outer lipid membrane and internal doxorubicin. The obtained sediment of empty magnetic capsules alone was washed with methanol three times and mixed with 10 ml of the cell culture medium (pink).

Group	Concentration of Doxorubicin (μg/ml)	Type of capsules	Treatment schedule (1×10^4 cell)
■	1	Lipid	4 days
□	0	Lipid	
■	1	Lipid	15 min
■	20	Lipid	
■	400	Lipid	
■	1	Magnetic	
■	0	Magnetic	

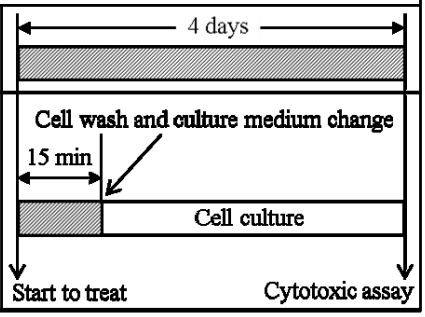

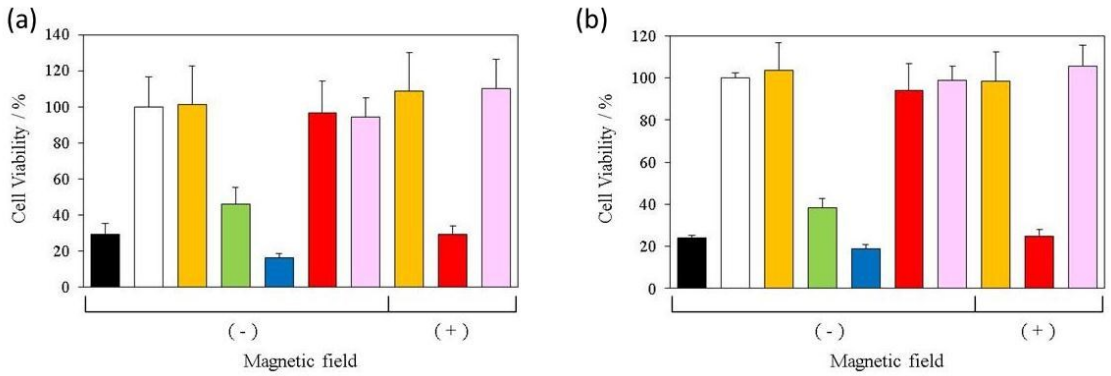

Figure 4.3 The magnetically guided antitumor effect of the ferromagnetic capsules containing doxorubicin (a) in a gastric cancer cell line, MKN-74, and (b) in a lung cancer cell line, RERF-LC-A1. Cells were incubated and cultured under the various condition summarized in Table 1. The viability of the cell lines cultivated putting NdFeB magnet was shown as "magnetic +". Percent cell viability compared with negative control was shown.

4.5 Fluorescence image of magnetically guided FePt-Dox in cytotoxic assay

Lipid-coated FePt capsules loaded with doxorubicin (FePt-Dox) were obtained using the FePt capsules fabricated by the hydrothermal treatment of core-shell particles fabricated with a weight ratio of FePt precursors to silica particles of 1. The silica template size was 0.10 μm. Figure 4.4 shows an optical micrograph and fluorescence micrograph of the cells incubated with FePt-Dox. The fluorescent micrograph was obtained in the same field of the optical micrograph. Fluorescence microscopy revealed that doxorubicin (Dox) was loaded into an internal space of FePt capsules. Dox was translated through their pores to their hollow space by diffusion, leading to the formation of FePt-Dox although the size of the internal space was 0.10 μm, which is the size of the silica template particles.. I found that the cells were dyed by FePt-Dox from the morphology change of the cells capturing FePt-Dox from the comparison between Figs. 4.4(a) and (b). FePt capsules without Dox were not toxic to the cells in this experiment. These results showed FePt-Dox had cellular toxicity to gastric cancer cells.

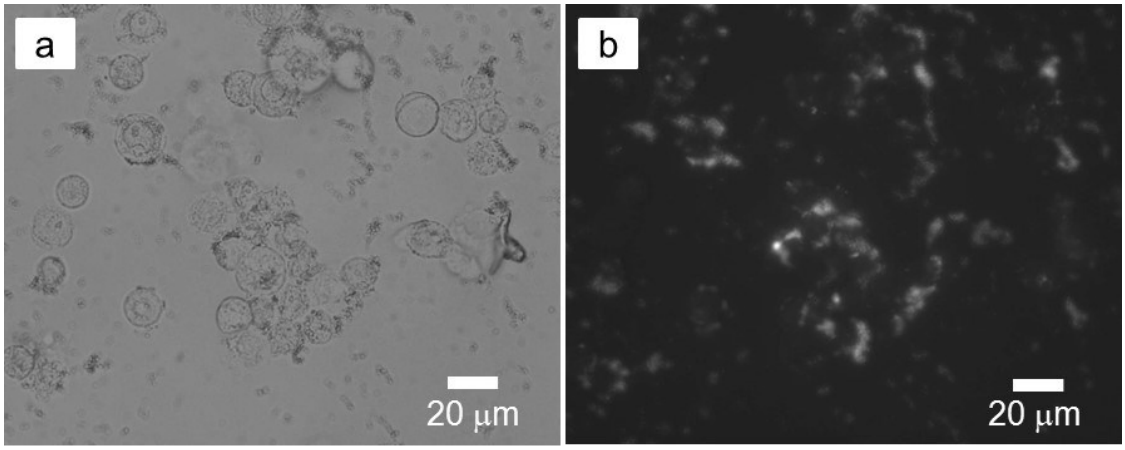

Figure 4.4 (a) Optical micrograph and (b) fluorescence micrograph of gastric cancer cells incubated with FePt-Dox. Fluorescent microscopy was investigated under the excitation/emission wavelength: 510/550 nm.

4.6 Conclusion

The porous hollow spheres with FePt netlike nanoshell were easily filled with an aqueous anti-cancer drug, doxorubicin, without external stimuli. The large pores are useful for loading an aqueous anti-cancer drug into their hollow space and then releasing it to cancer cells on cue. The drug-loaded magnetic capsules coated with a lipid membrane, egg phosphatidylcholine, were efficiently guided to the gastric cancer cells and lung cancer cells within 15 min using a NdFeB magnet (0.2 T), and more than 70% of the cancer cells were destroyed. Fluorescence microscopy showed water-soluble anti-cancer drugs could be loaded into the hollow space of FePt capsules, and optical microscopy revealed lipid-coated FePt capsules loaded with anti-cancer drugs showed cellular toxicity even the whole size was only 120 nm. The FePt capsules are thus clearly useful as the magnetic carrier for a target-oriented DDS.

Reference

[1] Namiki Y, Namiki T, Yoshida H, et al., Nat Nanotechnology 2009;4:598-606.
[2] Pankhurst QA, Connolly J, Jones SK, Dobson J., J Phys D Appl Phys 2003, 36, 167-81
[3] Hirota Y, Akiyama Y, Izumi Y, Nishijima S., Physica C 2009;469:1853-6.
[4] Zhang C, Zhang H, Du B, Hou R, Guo S., J Colloid Interface Sci 2012; 368:97-106
[5] Zhang Y, Huang Z, Tang F, Ren J., Thin Solid Films 2006; 515:2555-61
[6] Wang C, Yan J, Cui X, Wang H., J Colloid Interface Sci 2011; 354:94-9
[7] Yuan J, Zhang X, Qian H., J Magn Magn Mater 2010;322:2172-6
[8] Lu Z, Qin Y, Fang J, Sun J, Li J, Liu F, et al., Nanotech 2008; 19:055602
[9] Nakamura M, Katagiri K, Koumoto K., J Colloid Interface Sci 2010;341:64-8
[10] Abe M, Nishio N, Hatakeyama M, et al., J Magn Magn Mater 2009; 321:645-9
[11] Liu J, Deng Y, Liu C, Sun Z, Zhao D., J Colloid Interface Sci 2009; 333:329-34
[12] Shen S, Wu W, Guo K, Meng H, Chen J., Colloid Surf A 2007; 311:99-105
[13] Xia H, Foo P, Yi J., Chem Mater 2009; 21:2442-51.
[14] Lu X, Mao H, Zhang W., Polym Composites 2009; 30:847-54
[15] Wang C, Chen I, Lin C., J Magn Magn Mater 2006; 304:451-3
[16] Yang S, Liu H, Huang H, Zhang Z., J Colloid Interface Sci 2009; 338:584-90
[17] Miyata K, Christie RJ, Kataoka K., React Funct Polym 2011;71:227-34
[18] Yokoyama M, Satoh A, Sakurai Y, et al., J Control Release 1998; 55:219-29
[19] Nishiyama N, Bae Y, Miyata K, Fukushima S, Kataoka K., Drug Discov Today 2005; 2:21-6
[20] Litzinger DC, Buiting AMJ, van Rooijen N, Huang L., Biochim Biophys Acta 1994; 1190:99-107
[21]Tong, W.; Gao, C.; Mo¨hwald, H. Macromolecules 2006, 39, 335–340.
[22] Li, M. H.; Keller, P. Soft Matter 2009, 5, 927–937
[23] Akamatsu, K.; Yamaguchi, T.Ind. Eng. Chem. Res.2007,46, 124 –130.
[24] Sukhishvili, S. S. Curr. Opin. Colloid Interface Sci. 2005, 10, 37–44.
[25] K. Katagiri, M. Nakamura, K. Koumoto, Appl. Mater. Interfaces, 2010, 2, 3, 768–773
[26] Namiki Y, Namiki T, Yoshida H, Date M, et al.,Int J Cancer 2006;118:1545-55.
[27] Namiki Y, Namiki T, Date M, Yanagihara K, Yashiro M, Takahashi H., Pharmacol Res 2004;50:65-76.

Chapter 5

General conclusion

In this thesis, fabrication and characteristics of magnetic hollow spheres with a nanosized porous shell were investigated from the viewpoint of its application to magnetically guided drug delivery system (MG-DDS). I proposed two types of porous hollow sphere composed of FePt alloy. One was hybrid capsules composed of FePt nanoparticles and a single layer of water-soluble polymer. The other was porous hollow spheres with an FePt netlike nanoshell fabricated by thermal treatment of FePt-nanoparticle/polymer/silica core-shell particles in supercritical fluid, followed by the removal of silica template particles. The accumulation density of FePt nanoparticles onto the silica template particles modified with polymer and thermal treatment conditions were controlled for fabricating the nanosized porous shell. The formation mechanism of porous hollow structure was discussed. Principal results in the present study are summarized in the followings.

1. FePt nanoparticles were accumulated to five kinds of polymer-modified silica template particle, and FePt nanoparticles of 3-5 nm in size were accumulated uniformly onto the surface of the silica template particles modified with cationic polyelectrolyte. The cationic polyelectrolyte can be adsorbed uniformly to the negatively charged surface of silica particle, and the FePt nanoparticles are probably accumulated to the polymer layer.

2. Nanosized thin shells with pores were fabricated by controlling an accumulation density of FePt nanoparticles to polymer layer for the two types of porous hollow spheres. In a hybrid capsule composed of FePt nanoparticles and a polymer, the occupancy of FePt nanoparticles on the surface of silica template particles must be over 70 % to maintain the three-dimensional structure. Thus, I suggest that it is difficult to obtain the nanosized thin shell with pores larger than 5 nm. In the porous hollow spheres with the netlike nanoshell composed of fused FePt nanoparticles, the three-dimensional structure can be maintained by optimizing thermal treatment conditions of supercritical ethanol treatment such as time and temperature even when the occupancy is 50 ± 10 %, and the netlike nanoshell of 10 nm in thickness with larger pores was obtained.

3. I showed supercritical fluid treatment of nanoparticle-assembly is a novel method for fabricating magnetic porous hollow spheres with the netlike nanoshell and high magnetic response. I showed an accumulation density of nanoparticles strongly affect the netlike structure obtained after thermal treatment. To obtain the porous netlike structure, there must be gaps between FePt nanoparticles on FePt-nanoparticle/polymer/silica core-shell particles before the thermal treatment and the occupancy of FePt nanoparticles on the surface of template particles should to be less than 87 ± 8 %.

4. The thermal fusion between FePt nanoparticles was progressed preferentially in the plane direction on the silica template particles, not in the thickness direction. Thus, the crystallite volume of FePt alloy increased without the increase of the shell thickness. The FePt netlike nanoshell was fabricated by optimizing thermal treatment conditions such as time and temperature. When the treatment time is much longer than the optimized time to obtain the netlike structure, the island structure was obtained at the final stage of the treatment.

5. In a cell assay, I showed that the porous hollow spheres have functions of loading and releasing drug agents, and that the porous hollow spheres can be attracted by external magnetic fields. The drug-loaded magnetic capsules coated with a lipid membrane were efficiently guided to gastric cancer cells and lung cancer cells within 15 min using a NdFeB magnet (0.2 T), and more than 70% of the cancer cells were destroyed. The porous hollow FePt capsules with the netlike nanoshell exhibited the potential as carriers for MG-DDS.

In a typical condition (supercritical ethanol treatment at 673 K and 10 MPa for 1.5 h), I obtained porous hollow spheres with an FePt netlike nanoshell whose pore size was 18.3 ± 8.3 nm, shell thickness was 10.5 ±3.0 nm and magnetization at 9 T was 26.2 emu/g. Property of the magnetic porous hollow spheres with the FePt netlike nanoshell was compared with the property of typical porous hollow spheres composed of iron oxide from the viewpoint of its application to MG-DDS (Table 5.1). The porous hollow spheres with the FePt netlike nanoshell show higher magnetic response than the typical iron oxide hollow spheres even the FePt hollow spheres have a nanosized shell. However, it is not sufficient to apply the FePt hollow spheres to MG-DDS, the following issues must be solved in the further studies. Magnetic property of the porous hollow spheres with the FePt netlike nanoshell should be improved by controlling thermal treatment conditions to obtain the netlike structure and reaction conditions to synthesize FePt nanoparticles.

Regarding dispersibility of the hollow spheres, some of the FePt-nanoparticle/polymer/silica core-shell particles were agglomerated during accumulation of FePt nanoparticles to the polymer-modified silica particles, the synthesis process of the FePt nanoparticles must be modified based on the formation mechanism of the nanoparticles onto the template particles. I addition, surface modification of the FePt hollow spheres is required to improve biocompatibility for human body.

Table 5.1 Suitability of magnetic porous hollow spheres for MG-DDS

Hollow sphere	Loading capacity of medicine	Loading and releasing property	Magnetic response	Biocompatibility	Dispersibility
Typical porous hollow spheres with iron oxide shell	○	△	×	○	–
Porous hollow spheres with FePt netlike shell	○	○	△	△	×

Prospect

Using magnetic material with small magnetocrystalline anisotropy such as iron oxide, it was impossible to fabricate nanosized thin shells with high magnetic response. However, I showed the volume of magnetic crystallite that consist of the shell can be increased without an increase of the shell thickness by the supercritical fluid treatment of a nanoparticle-assembly. Therefore, I think that a magnetic material with small magnetocrystalline anisotropy can be used as a material for nanosized shell with high magnetic response by using the supercritical fluid treatment technique. Iron oxides are more suitable material as a drug carrier than FePt in view of biocompatibility. I expect porous hollow spheres with iron oxide netlike nanoshell are fabricated by my proposed technology and applied to biomedical devices in near future.

As another application for the porous hollow spheres with FePt netlike nanoshell, I propose a catalyst because the FePt has a catalytic ability and the FePt netlike nanoshell has a large surface area. FePt alloy has attracted attention in a fuel cell as low-platinum catalysts. Catalytic ability strongly depends on a surface area of particles. However, aggregation of catalytic particles is a problem, and a support such as carbon is required in the catalyst layer of the cells. If we use the FePt netlike nanoshell, catalyst layer without support can be fabricated by assembling the FePt porous capsules because the capsules composed of the FePt netlike nanoshell has porous hollow structure and large surface area. I expect the supercritical fluid treatment technique is widely applied to fabricate porous hollow structure as a carrier, marker and catalysts for biomedical and environmental applications.

Acknowledgments

I am grateful to my supervisors, Associate Professor Yoshitaka Kitamoto and Associate Professor Hiroyuki Wada for their guidance and support for whole my student life.

I am grateful to Medical doctor Yoshihisa Namiki for his advice and valuable discussion on bio-medical applications.

I am grateful to Professor Masaru Nakagwa for his advice and valuable discussion on sample synthesis.

I am grateful to Visiting Professor Masahiko Kaneko for his advice and valuable discussion on sample synthesis and magnetic measurement.

I wish to acknowledge the examination of degree with Professor Osamu Odawara, Professor Mamoru Yoshimoto, Professor Tomokazu Iyoda, Associate Professor Nobuhiro Matsushita and Visiting Professor Masahiko Kaneko.

I wish to acknowledge discussion and support for my experiment and support for my student life with Professor Quentin Pankhurst and all the other members of the Davy-Faraday Research Laboratory.

I wish to acknowledge discussion and support for my experiment and student life with all the other members of Kitamoto group.

I wish to acknowledge my parents and brother in the all aspects of my student life.

Teruaki Fuchigami
September 2013

Accomplishment

Philosophical papers

1. **T. Fuchigami**, R. Kawamura, Y. Yamazaki, Y. Kitamoto, M. Nakagawa and Y. Namiki, Fabrication of FePt/SiO_2 composite magnetic nanoparticles, Powder and Powder Metallurgy, Japan Society of Powder and Powder Metallurgy, 57, No.9 September, 636-641, 2010
2. **T. Fuchigami**, R. Kawamura, Y. Kitamoto, M. Nakagawa and Y. Namiki, Ferromagnetic FePt-Nanoparticles/Polycation Hybrid Capsules Designed for a Magnetically Guided Drug Delivery System, Langmuir, 27, 2923-2928, 2011
3. **T. Fuchigami**, R. Kawamura, Y. Kitamoto, M. Nakagawa and Y. Namiki, A magnetically guided anti-cancer drug delivery system using porous FePt capsules, Biomaterials, 33 1682-1687 2012
4. Y. Namiki, **T. Fuchigami**, N. Tada, R. Kawamura, S. Matsunuma, Y. Kitamoto and M. Nakagawa, Nanomedicine for Cancer: Lipid-based Nanosutructures for Drug Delivery and Monitoring, Accounts of chemical research, 44 1080-1093 2011
5. **T. Fuchigami**, Y. Kitamoto and Y. Namiki, Size-tunable drug-delivery capsules composed of a magnetic nanoshell, Biomatter, 2, 4, 313-320, 2012
6. Y. Kitamoto, **T. Fuchigami** and Y. Namiki, Growth of Fe-Pt Magnetic Nanoparticles on Silica Particles Modified with Organic Molecules, Japanese Journal of Applied Physics (accepted)

Presentations at International meetings

1. **T. Fuchigami**, R. Kawamura, Y. Kitamoto, M. Nakagawa, Y. Namiki, Assembly of FePt nanoparticles on a surface of silica microspheres covered with poly(diaryldimethylammonium chloride) and formation of magnetic soft-shell microspheres, International Symposium on Advanced Magnetic Materials and Applications (ISAMMA2010), Sendai, Japan, July 2010
2. **T. Fuchigami**, R. Kawamura, Y. Kitamoto, M. Nakagawa, Y. Namiki, FePt-nanoparticles/polycation magnetic capsules designed for magnetically guided drug delivery system, 55th Annual Conference on Magnetism and Magnetic Materials, Atlanta, GA, USA, November 2010
3. **T. Fuchigami**, R. Kawamura, Y. Kitamoto, M. Nakagawa, Y. Namiki, FePt-nanoparticles/polymer hybrid capsules designed for cancer therapy, IEEE International Magnetics Conference, Taipei, Taiwan, April 2011
4. **T. Fuchigami**, R. Kawamura, Y. Kitamoto, M. Nakagawa, Y. Namiki, FePt magnetic capsules and their applications for magnetically guided drug delivery system, 55th Annual Conference on Magnetism and Magnetic Materials, Phoenix, AZ, USA, July 2011

5. **T. Fuchigami**, R. Kawamura, Y. Kitamoto, M. Nakagawa, Y. Namiki, Magnetic nanoparticles/polymer porous magnetic capsule designed for cancer therapy, The 62nd Annual Meeting of the International Society of Electrochemistry, Niigata, September 2011
6. **T. Fuchigami**, Y. Kitamoto, M. Nakagawa, Y. Namiki, Size-controlled FePt/Polymer hybrid capsules and their application to magnetic drug carriers, The Asia-Pacific Interdisciplinary Research Conference 2011, Aichi, November 2011
7. **T. Fuchigami**, M. Nakagawa, Y. Namiki, Y. Kitamoto, Hybrid magnetic capsules composed of self-assembled monolayer of FePt nanoparticles and polymer designed for drug delivery system, IACIS2012, Sendai, Japan, May 2012
8. **T. Fuchigami**, M. Nakagawa, Y. Namiki, Y. Kitamoto, FePt Magnetic Hollow Sphere Designed for Nano-Scale Drug Delivery System Targeted to Cancer Tumor, PRiME2012, Honolulu, USA, October 2012

Presentation at Domestic meetings

1. 渕上輝顕，河村亮，北本仁孝，中川勝，並木禎尚、磁気誘導薬剤送達システム用 FePt/ポリマー複合磁性カプセル、第 35 回日本磁気学会学術講演会、新潟、2011 年 9 月
2. 渕上輝顕、北本仁孝、中川勝、並木禎尚、題目：水溶性抗がん剤を搭載した FePt 籠型カプセルによる磁気誘導薬剤送達システム、電気化学会第 79 回大会、静岡県浜松市、アクトシティ浜松、3 月、2012 年

Patent

特願２０１０－２５６６０
磁性粒子、及びその製造方法、並びに磁性粒子含有製剤. 発明者：並木禎尚、中川勝、北本仁孝、河村亮、渕上輝顕. 出願人：慈恵大学、東京工業大学、東北大学

Awards

1. 粉体粉末冶金協会論文賞、5 月 30 日 2011 年、粉体粉末冶金協会、Vol. 57 No. 9 September、636-641、2010
2. 第３５回日本磁気学会学術講演会、桜井講演賞、2012 年 10 月 3 日　講演番号 27aF‐3